MODE-LOCKED SEMICONDUCTOR TWO-PHOTON EXCITATION SOURCES

INVESTIGATION OF THE FEASIBILITY OF MODE-LOCKED SEMICONDUCTOR DEVICES AS EXCITATION SOURCES FOR TWO-PHOTON FLUORESCENCE

By

ANDREW STEPHAN LOGAN, B. Eng

A Thesis
Submitted to the School of Graduate Studies
in Partial Fulfillment of the Requirements
for the Degree
Master of Applied Science

McMaster University

MASTER OF APPLIED SCIENCE (2005) McMaster University
(Engineering Physics) Hamilton, Ontario

TITLE: Investigation of the Feasibility of Mode-Locked Semiconductor Devices as Excitation Sources for Two-Photon Fluorescence

AUTHOR: Andrew Stephan Logan, B. Eng. (McMaster University)

SUPERVISORS: Dr. H. K. Haugen and Dr. P. Mascher

NUMBER OF PAGES: xiii, 120

Abstract

The potential of a mode-locked semiconductor laser oscillator as a short pulse source for two-photon fluorescence microscopy is explored. Amplification of the 1075 nm laser is performed with a single pass semiconductor optical amplifier or a ytterbium-doped fibre amplifier. The mode-locked diode oscillator amplified by the Yb-doped fibre amplifier has been shown to produce uncompressed pulses of 4-10 ps with an average power of up to ~0.8 W. Compression with a single pass modified grating pair compressor reduces the pulse duration to as short as 860 fs. The output power level can be easily scaled to higher values.

The ability to tightly focus the Yb-doped fibre amplifier beam and semiconductor optical amplifier beam for the purpose of microscopy is studied. Results indicate that the fibre performs close to an ideal Gaussian laser beam source. The semiconductor optical amplifier beam does not focus as well. Measurements suggest that regions of the beam, when focused, do not significantly contribute to the generation of two-photon fluorescence.

The efficiency of two-photon fluorescence generation of the two amplifiers is compared to that of the conventional two-photon excitation source: the mode-locked titanium sapphire laser. Results illustrate the need to improve certain operating parameters of the laser oscillator and two amplifiers to be considered practical for two-photon fluorescence microscopy. The mode-locked semiconductor laser oscillator amplified by the Yb-doped fibre amplifier is deemed to be close to being ready for two-photon imaging applications.

Acknowledgements

I would like to thank the many people who, through their contributions, have helped me in this work. The design, fabrication, and characterization of the semiconductor devices used in this research was done by a number of former and current students. I would like to thank Mike Brennan for his direction early in my research and for the work he did designing and developing the long-wavelength lasers. The innumerable hours spent with my colleague, Andrew Budz, discussing and working on a great variety of subjects have been invaluable in both what I was able to achieve and what I learned while I was involved with this project. He is also responsible for the design and development of the semiconductor amplifiers used in the research. Thanks also go to Ben Doyle, Henry Tiedje, and Travis Crawford for their help and insight on practical research issues and other unrelated topics of discussion.

I would like to thank my primary supervisor, Harold Haugen, for the direction, suggestions, and patience he showed me while I was under his tutelage. As well, I would like to thank my other supervisor, Peter Mascher, who made the funding available for my research. Thank you to the funding agencies who supported this work: the Ontario Photonics Consortium and the Natural Sciences and Engineering Research Council. Also, indirect support was provided by the Canadian Institute for Photonic Innovations through the funding of existing equipment and the work of Andrew Budz and Mike Brennan.

Finally, I would like to express my infinite gratitude to my parents and Michelle Clausi. Without their endless support and patience I would not have made it this far in my academic career

.

Table of Contents

List of Figures

List of Tables

Chapter 1 Introduction

1.1 Outline

This section provides a brief outline of the material covered in this thesis. In Chapter 1 the motivation behind this work is included as well as recognition of the contributions other people have made toward it.

The second chapter presents the relevant background pertaining to fluorescence microscopy and more specifically two-photon fluorescence microscopy (TPFM). The theory describing two-photon excitation and the advantages of TPFM over other types of optical imaging are also discussed.

Chapter 3 outlines the design and operational characteristics of the three two-photon excitation sources used in the experiments. The design properties of a passively mode-locked semiconductor diode laser and a semiconductor optical amplifier are described in detail. Background information concerning the operation of an ytterbium-doped fibre amplifier and a titanium sapphire laser are discussed. Some selected results from the hybrid master-oscillator power-amplifier system (mode-locked diode amplified by the doped Yb-fibre) are included.

A detailed description of the experimental apparatus is described in Chapter 4. Included is an overview of the equipment used in the experiments as well as some of diagnostic tools used to analyze the performance of the pulsed laser sources.

In Chapter 5 the measurement of the focused beam spot size of the three excitation sources, as well as a helium neon laser, is discussed and analyzed. Included is a discussion of the methods used to retrieve the beam waist from the knife edge scans. Given the difference in the mode profiles, different techniques are used to estimate the beam waist of the different sources. A discussion is included addressing the agreement, or lack thereof, between prediction and observation.

The results of absolute two-photon fluorescence measurements are presented in Chapter 6. Given the different operating conditions of the excitation sources, estimates were made of the different fluorescence signals that would be measured. These were compared to what was obtained by experiment. An explanation of the observed differences is included.

The last chapter summarizes the key results of the thesis as well as puts them into the overall context of the goals of the project. Specifically, an in-depth look at the prospects of the mode-locked diode laser, amplified by either the semiconductor optical amplifier or a Yb-doped fibre amplifier, as an excitation source for TPFM is discussed. An outline of future work is also included.

1.2 Motivation

The motivation behind the work reported here is to determine the suitability of compact, tunable mode-locked semiconductor lasers and amplifiers as sources for two-photon excitation. Experiments with these sources have been on-going successfully for a number of years within this group. Development of a source for non-linear optical applications has been one of the prime motivators of the research done in this lab. Potential non-linear applications include two-photon fluorescence microscopy, two-photon photodynamic therapy and second harmonic generation among others (this thesis will focus on its potential as a two-photon fluorescence microscope excitation source). An ideal source for two-photon work is one that can generate pulses of light shorter than 10 picoseconds with repetition rates below 1 GHz and which is wavelength tunable. The group has demonstrated laser devices that generate pulses of several picoseconds at a repetition rate of ~600 MHz with average powers of approximately 1 mW with a tuning range of greater than 50 nm in some cases [1], [2]. Concurrently, there have been studies on semiconductor optical amplifiers (SOAs) to increase this power to a more usable level. The maximum average power attained with a 980 nm laser/SOA combination has been approximately 90 mW and a 1075 nm source combination achieved an average power of approximately 50 mW [3], [4]. At these power levels there is sufficient pulse energy to be able to efficiently drive two-photon absorption processes.

A novel amplification approach being undertaken within the group is to amplify the diode signal with an ytterbium doped fibre amplifier (YDFA). This hybrid approach can generate much higher powers (in a first attempt, hundreds of milliwatts in our group and over 10 watts with a gain switched diode and pre-amplifier in another group [5]) than the SOAs. They also have a better beam quality which makes them potentially ideal excitation sources for fluorescent dyes with single photon absorption ranges of ~500-600 nm as the tuning range is from 970-1200 nm. The use of a mode-locked diode as a seed source for a YDFA has not been reported in the literature to the author's knowledge.

Two-photon microscopes typically use a titanium sapphire (Ti:Sapphire) laser (though other sources such as Nd:YAG and dye lasers are sometimes used) as an excitation source. A mode-locked Ti:Sapphire laser is easily capable of generating sub 100 fs pulses at a repetition rate of 80 MHz with pulse energies greater than a nanojoule, which is more than sufficient for two-photon work. The tunable range of a Ti:Sapphire laser equipped with the proper mirrors is 660-1050 nm which makes it suitable for a broad range of biological dyes. However these lasers are bulky and expensive which opens a niche for the lower power semiconductor sources. The semiconductor devices can be designed to have tuning ranges of ~50 nm. They are also cheap enough that multiple devices could be included in a package to allow access to a large range of the spectrum (from the visible to the NIR). This can all be done while still being more cost effective and smaller in size than a Ti:Sapphire laser.

A mode-locked diode laser amplified with either the SOA or Yb-doped fibre amplifier should yield a sufficiently high peak power and pulse energy to make it an attractive alternative to the expensive Ti:Sapphire as a two-photon fluorescence excitation source. With this is mind, work was performed to explore the feasibility of replacing the Ti:Sapphire with a diode based system and what changes need to be made to accomplish this goal.

1.3 Project Contributors

The results presented in this thesis have been obtained directly as a result of the author's efforts. This includes data fitting routines, design, implementation, performing experiments as well as the analysis of the results. Outlined below are the significant contributions other individuals have made to the project.

- The material for the semiconductor lasers and amplifiers was grown by Brad Robinson using the molecular beam epitaxy facility at McMaster University.
- Most of the design features of the diode laser were a product of the work of Michael Brennan as a part of the research completed for his PhD degree. Mike was also involved in the design and implementation of the autocorrelator and grating pair compressor.
- Andrew Budz designed, tested and characterized the flared semiconductor optical amplifiers while working toward his PhD. He was intimately involved in the Yb-doped fibre project as well as the day to day operation of the semiconductor excitation sources. He contributed to numerous technical discussions regarding experimental work.
- Insight into the error function fitting routine used to analyze the knife edge data was provided by Ben Doyle.
- Assistance regarding the operation of the Ti:Sapphire laser as well as technical discussions on measurement techniques was provided by Henry Tiedje.

Chapter 2 Microscopy

2.1 Introduction

Optical imaging is an invaluable tool in science as well as in many other disciplines. The advantages of optical imaging over other types, such as MRI, ultrasound and x-rays, are the high resolution (≤100 nm with near-field microscopy [8], 4pi fluorescence microscopy [9]-[12]), reasonable cost and the (essentially) non-damaging nature of the radiation. Two important fluorescence based optical imaging techniques, confocal and two-photon fluorescence microscopy (TPFM), are discussed below to highlight their similarities as well as the advantages that TPFM offers.

2.2 Conventional fluorescence microscopy

In fluorescence microscopy a fluorophore, either endogenous (produced from within) or exogenous (developed externally), is localized in various regions of a sample. It can absorb a photon (or multiple photons) in a certain wavelength range and be excited to a higher energy state. When it relaxes, it emits a photon at a longer wavelength after a period of time, typically in the pico to nanosecond regime. A laser source is commonly used to excite the fluorescent specimen in a point-wise manner to allow efficient generation of fluorescence and a high signal to noise ratio; it also mitigates the need to bathe the entire sample in high intensity light for extended periods of time [13]. Exposures to high intensities can lead to damage of the sample and the destruction of the dye. The point-wise generation of fluorescence requires a raster scanning technique to create an image. The scanning is typically done by a set of galvanometric mirrors that raster scan the excitation beam across the sample, though it is also sometimes done by keeping the beam stationary and moving the sample stage [13]-[15]. Fluorescence is collected by a focusing lens (in an arrangement called epi-fluorescence illumination) and separated from the excitation light by a dichroic mirror. A schematic of a standard laser scanning fluorescence microscope is shown inFigure 2-1. Scanning efficiency can be greatly increased by generating multiple parallel foci by methods such as a Nipkow disk or a microlens array [18].

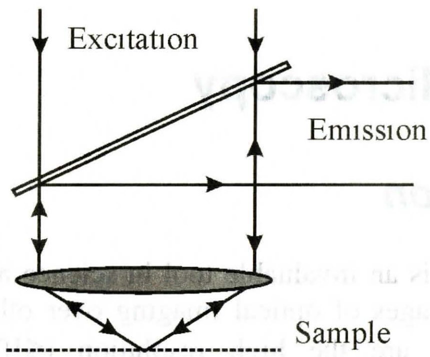

Figure 2-1: Standard epi-fluorescent illumination for fluorescence microscopy Generated fluorescence is separated from the excitation signal by a dichroic mirror

2.3 Confocal fluorescence microscopy

In a conventional fluorescence microscope arrangement, a significant amount of signal is generated in the cones of light that extend above and below the focus (see Figure 2-2) This has the effect of reducing the contrast of an image because the out of focus region can be generating as much fluorescence as the object of interest. A common technique to eliminate this problem is to use a confocal aperture to reject light from outside the focal region [16] Through this approach, collected fluorescence is imaged onto the plane containing the pinhole. Light that was emitted from the focal plane will pass through the aperture and be detected. Light from an out-of-focus plane will be collected but imaged onto a plane in front of or behind the pinhole. The majority of it will not pass through the aperture and is rejected from the final image [17]. A simple schematic illustrates the basic principle in Figure 2-2. The depth discrimination that the pinhole achieves leads to a natural optical sectioning of the sample. In an actual microscope the imaging depth is selected by raising or lowering the sample stage along the optical axis, usually by a stepper motor or piezoelectric stage [20] By stacking a number of sections it is possible to build a three-dimensional image of the sample. Three-dimensional imaging is important for *in-vivo* investigations where reactions occur below the surface and minimal disruption to the cellular processes is required. The axial resolution of the slice becomes better as the aperture becomes smaller; however the amount of signal declines as the pinhole is constricted and it is therefore necessary to increase the excitation intensity This increase leads to one of the inherent problems of a confocal microscope - the increased possibility of photodamage to the entire sample. The regions above and below the plane of interest absorb much of the light even when they are not contributing to the image. Another drawback, that relates to the use of single photon absorption, is that important endogenous fluorophores such as tryptophan and NAD(P)H as well as some exogenous ones, which require a blue or UV excitation light, cannot be easily excited [19] Blue and UV light is strongly attenuated in tissue and this limits the depth at which imaging is possible. The higher energy photons of short wavelength light also more readily cause damage to biological samples [20]

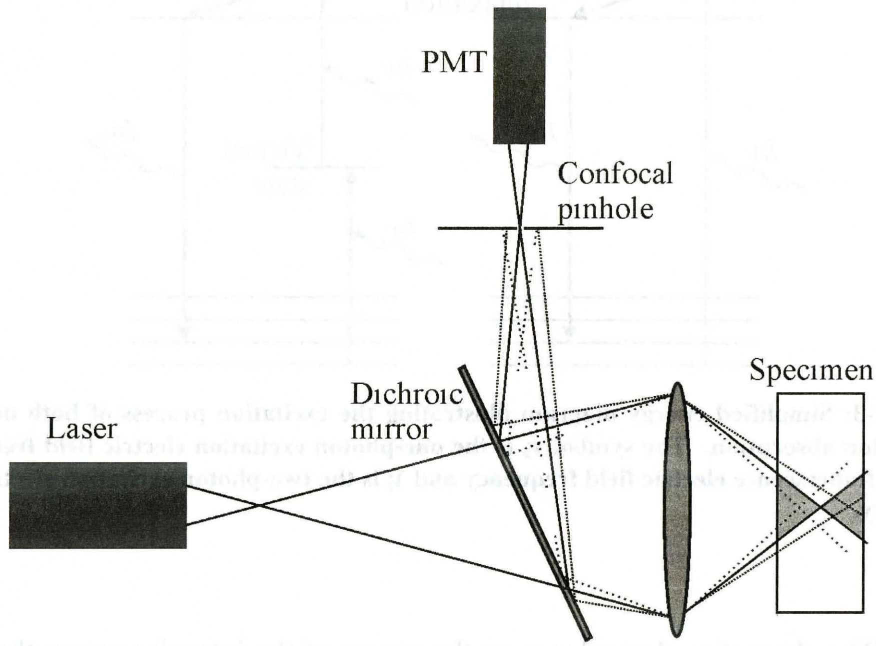

Figure 2-2: Schematic illustrating the rejection of out-of-focus fluorescence by the confocal aperture in a confocal microscope. The scanning mirrors are absent.

2.4 Two-photon fluorescence microscopy

A number of the shortcomings of confocal fluorescence microscopy can be addressed by the non-linear imaging technique known as two-photon fluorescence microscopy (TPFM) First demonstrated by Denk in 1990, in TPFM two photons are simultaneously absorbed to provide the equivalent energy of one shorter wavelength photon [21] Single-photon excitation occurs when a photon of sufficient energy to elevate the fluorophore from its ground state to an excited state is absorbed. It then relaxes and emits a photon of less energy In the case of two-photon fluorescence, two photons, whose combined energy is sufficient to excite the fluorophore, are absorbed essentially simultaneously The time frame in which both photons must arrive at the same molecule to be considered simultaneous is determined by the uncertainty principle and is on the order of 0 1 femtoseconds [22] The excited fluorophore, when it relaxes, emits a photon of a shorter wavelength which may be detected. A simplified energy diagram showing excitation in both the one and two-photon absorption case is given in Figure 2-3 The simultaneity requirement is the source of the well known square dependence of fluorescence power with excitation intensity

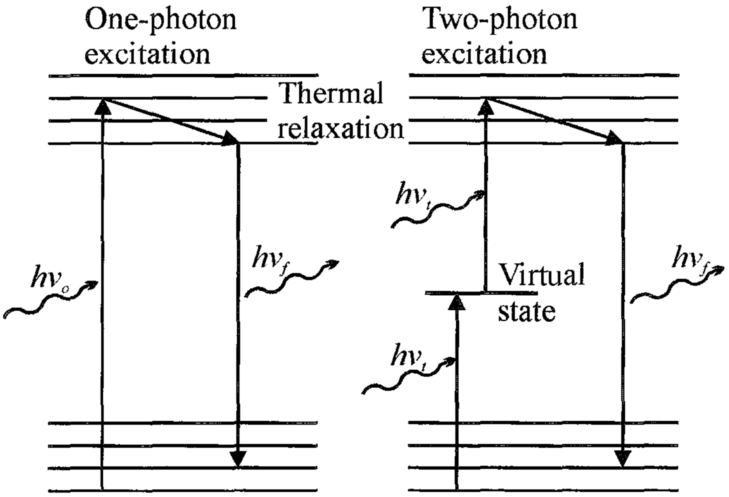

Figure 2-3: Simplified energy diagram illustrating the excitation process of both one- and two-photon absorption. The symbol ν_o is the one-photon excitation electric field frequency, ν_f is the fluorescence electric field frequency and ν_t is the two-photon excitation electric field frequency.

The absorption dependence on the square of the intensity means that there is no significant signal coming from regions other than the focal spot where the intensity is highest. This selectivity is the source of the inherent optical sectioning properties of a two-photon fluorescence microscope [23]. Figure 2-4 provides a schematic of a typical TPFM. Normally, excitation sources emit in the NIR so that they are compatible with most commonly used fluorophores whose emission wavelengths are typically in the visible region of the spectrum. For a given intensity, the probability of a two-photon absorption event is much lower than that of a single photon absorption and so for there to be a reasonable likelihood of two-photon excitation transitions very high illumination intensities (on the order of GW/cm^2) are required. These types of intensities are best achieved by tightly focusing a picosecond or femtosecond laser beam. These lasers can provide a very high photon flux without depositing large amounts of energy which could damage the sample. A typical two-photon fluorescence source generates about 10 mW of average power, with a pulse width of ~100 fs and a repetition rate of 80 MHz [23].

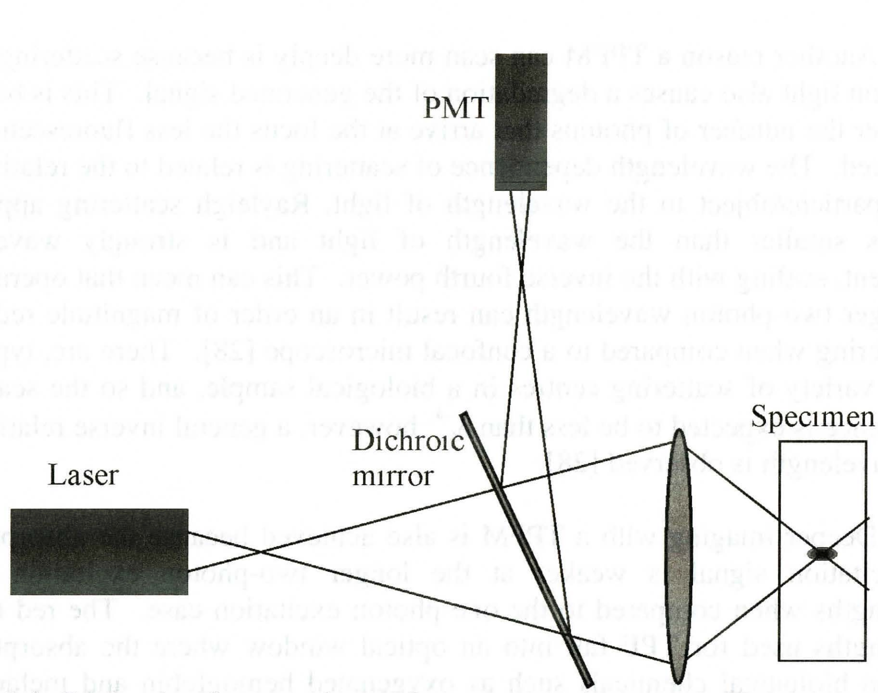

Figure 2-4: Schematic of a two-photon fluorescence microscope. Fluorescence is only generated in the focus, eliminating the need for a pinhole. Scanning mirrors are not shown.

2.4.1 Advantages of TPFM

A two-photon fluorescence microscope has a number of advantages over a conventional confocal microscope. Because fluorescence is only generated near the focal region in a TPFM a confocal pinhole is not necessary. This simplifies the setup and operation of the microscope. In a confocal system it is necessary to adjust the diameter of the aperture in order to achieve a balance between the desired depth resolution and reduced signal, this is not the case with a TPFM [25] Also, in confocal microscopy it is necessary for the fluorescence to return through the scanning mirrors (de-scan) in order to properly pass through the confocal aperture, this is another source of loss that is not present in a TPFM.

A two-photon fluorescence microscope is able to image more deeply into a turbid sample than a confocal microscope for a few reasons. First, because fluorescence that is generated deep (hundreds of microns) within a specimen can be scattered multiple times and still contribute to the measured signal, whereas in a confocal system only unscattered fluorescence photons are detected [24]. Scattered photons are blocked by the pinhole because the photon appears to be originating from somewhere other than the focus, this is not as issue in TPFM. The improved collection efficiency means less fluorescence is being wasted, reducing the required excitation power [26], [27] Another reason a TPFM can scan more deeply is because scattering of the excitation light also causes a degradation of the generated signal. This is because, the fewer the number of photons that arrive at the focus the less fluorescence will be emitted. The wavelength dependence of scattering is related to the relative size of the particle/object to the wavelength of light. Rayleigh scattering applies to particles smaller than the wavelength of light and is strongly wavelength dependent, scaling with the inverse fourth power. This can mean that operating at the longer two-photon wavelength can result in an order of magnitude reduction in scattering when compared to a confocal microscope [28]. There are, typically, a large variety of scattering centres in a biological sample, and so the scattering dependence is expected to be less than λ^{-4}; however, a general inverse relationship with wavelength is observed [28].

Deeper imaging with a TPFM is also achieved because the absorption of the excitation signal is weaker at the longer two-photon excitation (TPE) wavelengths when compared to the one-photon excitation case. The red to NIR wavelengths used for TPE fall into an optical window where the absorption of common biological chemicals such as oxygenated hemoglobin and melanin are decreasing and the absorption of water has not yet risen dramatically [19]. The combination of reduced scattering and reduced absorption makes it possible to image more deeply (hundreds of microns deep) than with a confocal microscope [27], [30], [31].

Another primary benefit of a TPFM is the reduced photobleaching that occurs outside the focal region. When the image of a sample is being constructed, absorption is largely occurring only in the focal region. The rest of the sample is essentially transparent. This is in contrast to a single photon laser scanning system where the entire hour-glass shaped region above and below the focus is absorbing energy (see Figure 2-2) [23]. The increased absorption can lead to irreversible bleaching of the fluorophore and it can also contribute to unwanted heating and damage of the sample. There is some debate as to whether two-photon fluorescence microscopy is more or less phototoxic to the sample than single-photon fluorescence [21], [32] . There appears to be an intensity threshold above which the amount of damage increases more rapidly than the squared dependence of the fluorescence, though there seems to be a strong dependence on the fluorophore [33]-[36].

A two-photon fluorescence microscope gives researchers better access to dyes that are excited in the deep blue and UV part of the spectrum. At these wavelengths there can be severe damage to samples with prolonged exposure. Using TPFM, the dyes can be excited by sources in the visible region of the spectrum which means the amount of time the bulk of the sample is exposed to the equivalent of high energy photons is reduced. There is also a reduction in the need for expensive UV optics [29].

Finally, the separation of the excitation and fluorescent light is easier to accomplish with a TPFM due to the large difference in the excitation and emission wavelengths. The spectral separation is generally several hundred nanometers while in the single photon case it is only tens of nanometers [23]. In the confocal setup the dichroic mirror that is used to separate the excitation and emission light must be made to a tighter tolerance, which is likely to reduce transmission/reflection efficiency while increasing the cost.

In addition to two-photon fluorescence excitation, there has also been some investigation into three-photon fluorescence excitation (3PE) [37]-[39]. 3PE can further reduce the excitation volume when compared to TPE [38], [40]. It also provides access to dyes further into the ultraviolet [37]. However, the likelihood of a three-photon absorption event is generally much lower than that of the two-photon case. The absorption cross-section is on the order of 10^{-82} $cm^2(photons/cm^2s)^{-2}$ for three-photon absorption versus 10^{-50} $cm^2(photons/cm^2s)^{-1}$ for the two-photon case [41]. Higher intensities are required for 3PE to generate a sufficient fluorescence signal. Given the same laser properties (i.e. pulse duration, repetition rate, and beam quality) it would require roughly about a factor of 10 greater intensity to generate the same amount 3PE as TPE at a moderate power level (10 mW) [37], [42].

2.4.2 TPE theory

Two-photon absorption (TPA) was first predicted by Maria Göeppert-Mayer in 1930 [45], and first demonstrated by Kaiser and Garrett in 1961 [46]. A simplified description of the two photon absorption process is given here; a more detailed one can be found in Nakamura [43] or Esposito *et al* [44]. Two-photon excitation is a non-linear process that depends on the third-order susceptibility tensor of the fluorophore [25]. It occurs when two photons excite a fluorophore into an allowed excited state via a forbidden virtual state [47]. Since the virtual state is forbidden, the two photons must arrive within a time frame determined from the uncertainty principle. In order to not violate energy conservation the transition time frame is on the order of 10^{-15}-10^{-16} seconds [22]. A rough estimate of the likelihood of this occurring can be made by looking at what is the likelihood of a pair of photons passing through a sufficiently small area within the allowed interaction time. An estimation of the interaction area can be derived from the one photon absorption case where the electronic interaction area is on the order of 10^{-16}-$10^{-17}cm^2$ [23], [41], [48]. A somewhat intuitive expression that neglects some of the physics involved but provides roughly the right order of magnitude of the TPA cross-section is:

$$\delta_2 = \sigma_1 \sigma_1 \tau_{\text{int}} \tag{2.1}$$

where σ_1 is the one photon cross-section and τ_{int} is the time frame within which the two photons must be absorbed for the transition to occur [41]. Evaluating Equation (2.1) with the input values indicated above yields a two-photon cross-section on the order of 10^{-50} cm^4s (which is defined as one GM – in honour of Maria Göeppert-Mayer) which is confirmed to within a couple of orders of magnitude through a number of reported measured values [48]-[50]. There is ongoing work to create fluorophores with much higher cross-sections [51], [52]. In reality the likelihood of absorption is also governed by parity rules, which are not addressed here [28].

When imaging a thin sample (less than the Rayleigh range for a Gaussian beam) with CW excitation the time averaged two-photon fluorescence intensity can be approximated with

$$\langle I_{f,cw} \rangle \propto \delta_2 C P_{avg}^2 \left[\frac{NA^2}{2\text{h}c\lambda} \right]^2 \tag{2.2}$$

where δ_2 is the two-photon cross-section (which includes the absorption cross-section as well as the quantum efficiency for radiative emission), P_{avg} is the average excitation power, λ is the excitation wavelength, c is the speed of light in a vacuum, C is the dye concentration in the illuminated volume, $\hbar$ is Planck's constant divided by 2π (1.055×10^{-34} J·s), and NA is the numerical aperture of the objective lens [22]. Imaging a thin sample with a pulsed laser, the time averaged two-photon fluorescence intensity is approximated with

$$\langle I_{f,pulse} \rangle \propto \frac{g_p \delta_2 C P_{avg}^2}{\tau_p f_p} \left[\frac{NA^2}{2\text{h}c\lambda} \right]^2 \tag{2.3}$$

where τ_p is the FWHM of the pulse width, f_p is the repetition rate of the laser system and g_p is a correction factor that is described below [22]. A study of these equations shows why a pulsed laser system is much preferred when imaging with two-photon fluorescence. Given a pulse duration of 1 ps, a repetition rate of 100 MHz and an average power of 10 mW a CW source would require 1 W of average power to generate the equivalent fluorescence signal. At these powers sample heating would be an issue even though the sample is relatively transparent at the wavelengths being used.

When discussing the scaling of the fluorescence with the square of the intensity it is important to note that it is the square of the laser pulse intensity and not the square of the average intensity that is being discussed, or, in other words

$$\langle I^2(t)\rangle \neq \langle I(t)\rangle^2 \tag{2.4}$$

Most measurement devices give the average power, $\langle I(t)\rangle$, so a correction, g_p, must be made to account for the discrepancy [49]. This factor g_p depends only on the shape of the laser pulse and the pulse duration.

$$g_p = \frac{\tau_p \int_{-1/(2f_p)}^{1/(2f_p)} I^2(t)\,dt}{\left[\int_{-1/(2f_p)}^{1/(2f_p)} I(t)\,dt\right]^2} \tag{2.5}$$

For the sake of simplicity the temporal shape of the laser pulse will be assumed to be Gaussian in all cases. This is not in fact known, however, it will be sufficient for the comparisons to be performed. Evaluating Equation (2.5) yields a correction factor of 0.664 for a Gaussian shaped pulse, however, because all the sources are assumed to be Gaussian, the correction factor will get cancelled when relative comparisons are made.

When generating fluorescence from a bulk sample (where the thickness is much greater than the focal depth/ Rayleigh range) it is necessary to integrate over the full volume of the focal region. As has been shown by Xu and Webb in [49], the time averaged *generated* fluorescence no longer depends on the numerical aperture of the focusing lens or beam waist. The approximate equation governing the time-averaged fluorescence generated in a bulk sample excited by a pulsed beam with a Gaussian mode profile is

$$\langle I_{f,pulse}\rangle \propto \frac{g_p \delta_2 C n P_{avg}^2}{\tau_p f_p \lambda} \tag{2.6}$$

where n is the index of refraction of the medium (Xu and Webb also present a similar equation for uniform illumination of the lens). This can be understood by appreciating that while the intensity of the fluorescence generated at the focal spot is lower for a larger beam waist than for a smaller one, the fluorescence is generated in a larger volume. Integrating over the entire illuminated volume exactly compensates for the reduced fluorescence at the beam waist. Of course in a practical measurement situation the ability to collect the fluorescence is as important as generating it. For an ideal TEM_{00} Gaussian beam, ~87% of the fluorescence is generated within ten Rayleigh ranges (related to the beam waist and defined in more detail in Section 5.4) centered on the focal spot. This length can be expected to be less than 25 μm for a microscopy situation. Modest changes in the beam waist should not significantly impact the fluorescence collection efficiency of the measurement system.

The likelihood of two-photon absorption is partially governed by the degree of alignment of the absorption dipole of a fluorophore molecule with the polarization of the excitation light [53]-[55]. This dipole is fixed with regard to the orientation of the molecule. Depending on the nature of the experimental setup, this relationship could influence observations. Similarly, the emission polarization is dependent on the orientation of the emission dipole of the molecule. The emission anisotropy is a measure of the degree to which the emission polarization is parallel to the excitation polarization [53]. In the case of a fluorophore dissolved in a liquid the molecule can freely rotate. The anisotropy is then largely a function of the ease with which the molecule can rotate and the fluorescence lifetime. Given enough time, the free molecule will rotate in a sufficiently random manner to make the emitted fluorescence essentially isotropic and unpolarized. In experiments described in Chapter 6 the fluorescent dye Rhodamine 6G is used. It has a fluorescence lifetime of ~ 4 ns [56], and is dissolved in a non-viscous solvent (methanol) at room temperature. Given the lifetime and the solvent the molecules will rotate sufficiently during the fluorescence lifetime to make the emitted light isotropic. This qualitatively agrees with observations where the generated fluorescence signal was independent of the input linear polarization.

There has been much work on trying to determine the ideal pulse regime to minimize photodamage and maximize the fluorescence signal. At moderate excitation intensities the damage appears to be driven by a quadratic process [26], [57]. In other words it scales as P^2/τ, the same as the fluorescence. This means that at moderate excitation rates a short pulse and low average power is equivalent to a longer pulse and higher average power in terms of photodamage and fluorescence signal [26], [57]. This is important in determining what types of criteria are required for a two-photon excitation source.

2.4.3 Resolution

A common method of comparing the performance of optical microscopes is to study their point spread functions (PSF). A PSF is an image of the ideal spot which can be generated with an optical system [58]. A thorough derivation of the three-dimensional field intensity at the focus of a well corrected lens with uniform illumination can be found in Born and Wolf [59]. The PSF can also describe the probability of an emitted photon being recorded by a point detector (such as a confocal pinhole) on the image plane of the microscope. The theoretical resolution of a microscope can be defined as a combination of the illumination PSF and the detection PSF. In a conventional laser scanning fluorescence microscope (i.e. no confocal pinhole) there is no PSF associated with the detector since there is no point-wise detection. In the case of a two-photon microscope the fluorescence intensity is proportional to the square of the excitation intensity and so the illumination PSF is the square of the illumination PSF of the one-photon case. It can also be advantageous to use a confocal aperture when using a two-photon excitation source. The illumination and detection PSFs are independent of one another and so the overall PSF of the microscope is the product of the two [60].

$$\begin{aligned}&\textit{Conventional one-photon microscope } PSF = PSF_{ill}\\&\textit{Confocal one-photon microscope } PSF = PSF_{ill}PSF_{det}\\&\textit{Conventional two-photon microscope } PSF = PSF_{ill}\,PSF_{ill}\\&\textit{Confocal two-photon microscope } PSF = PSF_{ill}\,PSF_{ill}\,PSF_{det}\end{aligned} \tag{2.7}$$

Table 2-1 lists some example theoretical resolutions for the different types of microscopes [58]. The sample being imaged is a point-like sample of the commonly used biological probe - enhanced fluorescent green protein (eGFP). The system characteristics were defined as the following: one-photon excitation wavelength of 488 nm, two-photon excitation wavelength of 900 nm, and an emission wavelength of 520 nm.

Table 2-1: Theoretical axial and lateral resolution of different microscopes when imaging a point-like eGFP dyed specimen [58].

Microscope	Lateral Resolution (μm)	Axial Resolution (μm)
Conventional 1-p	0.23	0.88
Confocal 1-p	0.16	0.65
Conventional 2-p	0.28	1.07
Confocal 2-p	0.18	0.72

In a thicker sample, where confocal and two-photon configurations would be used, the conventional single-photon setup would offer no axial discrimination. In the ideal case it is clear that a one-photon confocal setup provides superior resolution than both types of two-photon setups. The difference is not likely to be as large in reality because the axial resolution depends strongly on the diameter of the confocal pinhole [20]. In a confocal setup it cannot normally be reduced to its ideal size due to the corresponding reduction of signal [61]. In a turbid sample the effect is even more pronounced [62]. However, the loss of lateral resolution is the cost of the longer wavelength being used to excite the sample and image deeper within it. Two-photon confocal microscopy improves the resolution of the microscope but with a corresponding loss of imaging depth as the confocal pinhole eliminates the ability to detect scattered fluorescence photons. A confocal pinhole is not normally used with a TPFM as there is not an abundance of signal that can be sacrificed. However, with increased integration time it can improve the signal to noise ratio over conventional TPFM [63]-[65]. As in many other aspects of science there are tradeoffs to be made when selecting a type of microscope to use. The single-photon approach provides greater resolution but the two-photon system gives access to greater depth.

There has been work on improving the resolution performance of a two-photon microscope. One technique with the most dramatic results, 4Pi-confocal microscopy has yielded an axial resolution of 80 nm while lateral resolutions of 100 nm have been achieved [9]-[12]. This is at the cost of increased complexity of the imaging system.

2.5 Conclusion

Two-photon microscopes offer a number of advantages over single-photon confocal microscopes such as simpler fluorescence collection arrangements, potentially reduced phototoxicity and photobleaching, improved imaging depth and easier access to shorter wavelength dyes. However, it lacks the ideal resolving power that a single-photon confocal microscope can provide. In practice the resolution difference is not likely to be large due to mitigating factors in the implementation of the microscope.

Chapter 3 Excitation Sources

3.1 *Introduction*

For the majority of the experiments performed in this work there were three principal optical sources used: a mode-locked titanium sapphire (Ti:Sapphire) laser and a mode-locked semiconductor diode laser amplified by either a semiconductor optical amplifier (SOA) or a ytterbium-doped fibre amplifier (YDFA). The Ti:Sapphire laser is generally the source of choice for two-photon applications and is considered the bench mark against which the two amplified sources are compared. Though the physics of operation of the Ti:Sapphire laser, diode laser, the SOA and the fibre amplifier were not a focus of this research, some general information will be presented in this chapter.

3.2 *Mode-locked semiconductor laser oscillator*

In this section the pulse generation technique and design properties of the mode-locked semiconductor laser will be discussed. The oscillator described here is used to seed both the SOA and the YDFA.

3.2.1 Mode-locking

Diode lasers as a source of short pulses of light have been explored to a great degree [66]. The advantages of this technology over other short pulse sources such as solid state and dye lasers are their much lower cost, smaller size, tunability, efficiency and simpler operation when high powers and sub 500 femtosecond pulses are not required. (Shorter pulses have been demonstrated but are not easily achieved.)

There are a number of techniques to generate short pulses of light from a semiconductor source, including gain-switching, Q-switching and mode-locking. Each offers some advantages. Gain-switched devices are easy to fabricate, Q-switched devices can generate high pulse energies, and mode-locked devices generate shorter pulses with a more stable pulse train [67], [68]. Here the principles of mode-locking will be briefly described.

A standard Fabry-Perot laser will tend to lase on a number of wavelengths that correspond to the standing wave modes within the device. The spacing of these modes is governed by the length of the device as well as its refractive index

$$\delta\omega = \frac{\pi c}{nL} \tag{3.1}$$

where $\delta\omega$ is the frequency spacing, c is the speed of light, L is the device length and n is the group refractive index of the device. The number of modes on which the device will lase depends on the gain bandwidth. The modes will exist where the gain exceeds the loss. The output electric field, $E(t)$, of the device consists of the sum of each of the lasing modes and is given by

$$E(t) = \sum_m A_m e^{i[(\omega_0 + m\delta\omega)t + \phi_m]} + cc \tag{3.2}$$

where A_m is the mth mode amplitude, ω_0 is the center frequency, and ϕ_m is the phase of the mth mode. Typically, the phases between modes are random and the output is approximately constant. If, however, the relative phases can be locked together such that

$$\begin{gathered} \phi_{m+1} - \phi_m = \delta\phi \\ A_m = A_0 \end{gathered} \tag{3.3}$$

then the output will be a series of short pulses of light described by the equation:

$$E(t) = A_0 \frac{\sin\left[(M+1)\delta\omega t_1 / 2\right]}{\sin(\delta\omega t_1 / 2)} e^{i\omega_0 t} + cc \tag{3.4}$$

where M is the number of locked longitudinal modes and $t_1 = t + \delta\phi/\delta\omega$ [67]. If we assume 20 locked modes the electric field squared as a function of time of the laser would resemble Figure 3-1. The time between pulses is dictated by the cavity round trip time given by

$$T = \frac{2Ln}{c} \tag{3.5}$$

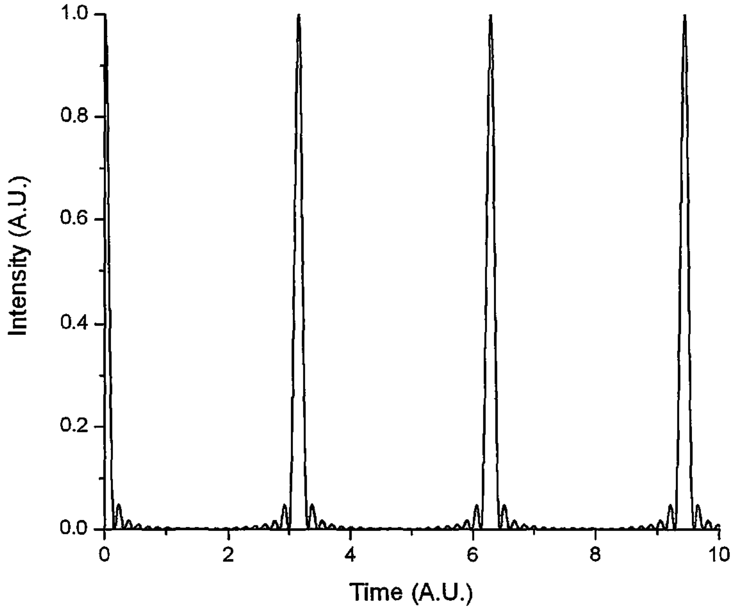

Figure 3-1: Simulated mode-locked pulse train with 20 locked modes.

3.2.2 Methods of mode-locking

There are three principal ways to mode-lock a diode laser: active, passive and hybrid. Active mode-locking is achieved by applying an external RF source in conjunction with a base DC signal to the gain region of the device. By modulating the signal at the frequency corresponding to the round trip cavity time, side bands are produced for each of the Fabry-Perot modes. As a consequence of this the phases of the different modes are locked together. Due to the small size of the typical semiconductor devices, ~300-1000 μm, the required modulation frequency is greater than 100 GHz which is not trivial to achieve in practice. In order to reduce the repetition rate, the diode laser can be coupled to an external cavity to reduce the required driving frequency to something more manageable [69].

A passively mode-locked device, as the name suggests, is a device that achieves mode-locking in the absence of an external modulation source. Typically, a saturable absorber is placed within the laser cavity and provides the means to modulate the loss of the entire resonator. In the absence of an optical pulse, the loss exceeds the gain. When a pulse does pass through the absorber section the leading edge experiences loss and saturates the absorber. In passive mode-locking it is necessary for the absorber to saturate and recover more quickly than the gain. The fast recovery prevents the build up of spontaneous emission between pulses. The loss experienced by the leading and trailing edges of the pulse ensures that only the region near the peak of the pulse experiences gain, resulting in shorter pulses. In the steady state condition this shortening is limited by pulse stretching phenomenon such as self-phase modulation, the gain response of the laser and dispersion [70]. A final requirement is that the unsaturated gain of the device needs to be greater than the unsaturated loss. This allows laser action to begin upon startup.

Hybrid mode-locking is a combination of both active and passive mode-locking. A saturable absorber is incorporated into the device and an external RF field is applied to the gain region. Here the device benefits from the stable pulsing of active mode-locking as well as the pulse shortening effect of passive mode-locking

3.2.3 Diode design

The semiconductor sources used in this work were developed by Mike Brennan and Andrew Budz. The development and performance of the devices has been reported in previous work [2], [71]. The devices used in experiments are ridge waveguide single quantum well devices operating in the 1065-1090 nm regime. The devices are grown lattice matched on a GaAs substrate with a 6 nm thick InGaAs quantum well, 110 nm GaAs barriers and 1370 nm InGaP cladding layers using the gas source molecular beam epitaxy facility at McMaster University. The devices were processed using photolithography and chemical wet-etching. The ridge width was between 3 and 4 μm.

To allow for passive mode-locking a saturable absorber is monolithically incorporated onto the semiconductor chip. The two-contact device allows for a positive bias to be applied to a large gain section of the device while a negative bias is applied to the smaller section such that it operates below its transparency regime and functions as the saturable absorber. It is clearly necessary that there be strong electrical isolation between the gain and absorber sections. This is achieved by wet etching a gap in the ridge and having the material below the etch stop behave as the insulating material. Larger gaps in the ridge provide greater electrical isolation but reduce the mode confinement of the light within the waveguide. Essentially, under the gap there is no optical confinement in the lateral direction and if the gap is too large the loss in the cavity will inhibit lasing. An etched gap of 10 μm provides a compromise between the two requirements. The gain section has a length of 800 μm while the absorber section has a length of 90 μm.

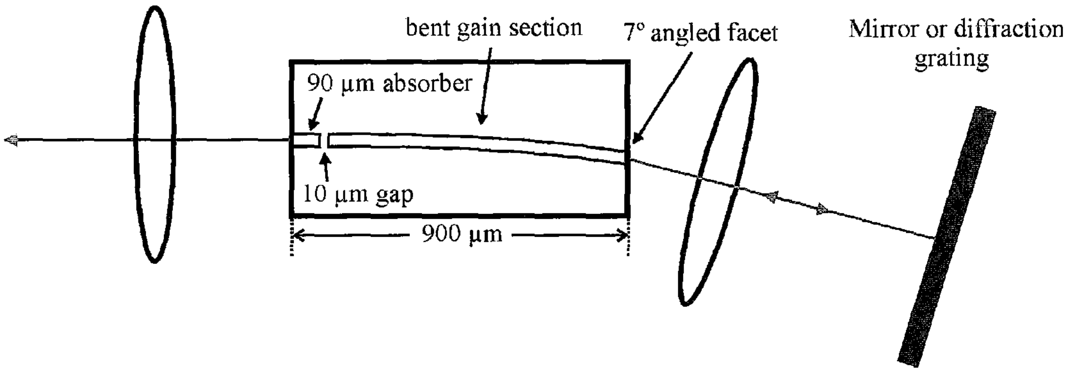

Figure 3-2: Schematic of two-contact single 1075 nm quantum-well oscillator with bent waveguide and angled facet.

3.2.4 Waveguide and facet

As mentioned previously, mode-locking a 900 µm device results in very high repetition rates. In order to reduce this to below 1 GHz an external cavity is used. Operating issues arise when coupling the light from the diode chip into an external cavity. In the simplest configuration a cleaved device is setup such that light that is emitted from the rear facet is reflected back into the diode by an external mirror or diffraction grating that is placed some distance away (about 25 cm in this case). The inherent reflection from a rear diode facet is 30%; the result would be that the mode-locked device would operate as if it had two rear reflectors and therefore a number of cavities, which would cause a hybrid operation between the high repetition rate chip cavity and lower repetition rate external cavity. Steps must be taken to attenuate the reflection from the rear facet of the diode.

A first step is to apply an anti-reflection coating. The reflectivity must be reduced to below 10^{-4} to suppress the Fabry-Perot modes of the chip [73]. Using a single layer SiO_xN_y anti-reflection (AR) coating the practical minimum achievable reflectivity is ~10^{-4}. However, the bandwidth over which the low reflectivity applies is typically smaller than what is required to allow for wavelength tunable mode-locking. It is possible to apply multiple layer AR coatings to further broaden the bandwidth. However, these are difficult to grow and suffer from greater variability between devices. Another straightforward approach to reduce the facet reflectivity is to angle the facet such that the light that reflects off it is not coupled back into the waveguide. An angled facet can reduce the modal reflectivity to 10^{-2} on its own [72]. A straightforward method of achieving an angled facet is to modify the design of the device so that the waveguide is not normal to the cleaved facets. This approach is not attractive in this case because having an angled front facet would require both ends of the laser to be coupled to an external cavity which increases the complexity of the device while reducing its robustness. The chosen solution in this situation is to implement a bent-waveguide design. This allows for an angled facet at one end and a normal facet at the other. This can be seen in Figure 3-2. The angle the back facet makes with the normal is 7°, which corresponds to a radius of curvature of 5700 μm. A single layer AR coating is added to the angled end to suppress the reflectivity to the desired level.

3.2.5 External cavity

As stated previously, an external cavity was used to reduce the operating frequency of the oscillator and provide the ability to tune the wavelength. The external cavity was approximately 25 cm in length. This was short enough so the device could operate at the fundamental frequency (~600 MHz) when passively mode-locked and long enough to allow hybrid mode-locking. If the cavity length was made much longer the devices tended to operate at higher harmonics of the fundamental round-trip frequency. The external cavity reflector could either be a mirror or a diffraction grating. In general, when a mirror was used, greater bandwidths would be observed along with shorter pulses. However, due to the large bandwidth being coupled back into the device it would lase on multiple wavelengths as well as make the output less stable; it would tend to jump between harmonics and appear to 'restart' the mode-locking process frequently. For most experiments a 600 lines/mm grating was used in the external cavity. This provided enough feedback to produce pulses of approximately 5 ps in duration while still forcing operation at one wavelength. The grating also seemed to produce the most stable outputs. A 1200 lines/mm grating was also tested. However, the reduced bandwidth yielded pulse durations that were too long for TPF work and the average output power suffered due to the increased loss of the external cavity.

3.2.6 Typical operating conditions

Typical operating parameters for the ~1075 nm oscillator are mode-locked pulses of duration between 1 – 10 ps with a fundamental repetition rate of ~550 – 700 MHz (and multiples of this when operating at higher harmonics). Observed bandwidths are between 2-5 nm, the average mode-locked output power is between 0.25 – 1.5 mW, and the operating wavelength ranges from 1070 nm to 1085 nm.

During the time over which the measurements reported in this thesis were made, a single laser oscillator was used for the majority of the work. The performance of this device degraded with time. While performing earlier measurements, it was relatively easy to obtain good quality mode-locking with pulse durations of 2-3 ps and an average power of 1 mW. When later measurements were made it was much more difficult to obtain quality mode-locking. Pulse durations were longer (6-10 ps) and the average power was reduced to less than 0.5 mW. This is why, in work described later in this thesis, sometimes very good results are presented and at other times it is stated that good quality mode-locking could not be achieved.

Selected results from the mode-locked oscillator can be found in Appendix A.

3.3 Semiconductor optical amplifier

The peak power and pulse energy of a mode-locked oscillator is too low to be reasonably able to perform any two-photon experiments; it is therefore necessary to amplify the signal. A straightforward method to achieve power gains is to employ a semiconductor optical amplifier. An SOA is advantageous over other types of optical amplification due to its small size, ease of fabrication, easy matching of gain peak with that of the oscillator and the fact it is electrically, as opposed to optically, pumped. This last advantage is important as it simplifies the operation of the device by reducing the number of components required for operation. The SOA is fabricated with the same material structure as the oscillator. The device operates in a single pass manner such that internal reflections must be suppressed at both the input and output ends to eliminate Fabry-Perot modulation of the amplified signal. To achieve this, 5° angled facets and a single layer SiO_xN_y AR coating are applied to both ends with similar results to those obtained for the oscillator.

To increase the amount of power that can be extracted from the SOA it is necessary to increase the gain volume. To maintain its suitability as a source for two-photon excitation the volume needs to be increased without significantly diminishing the mode quality of the beam. A common method of achieving this is by incorporating a flare into the active region [74], [75]. In the devices used in experiments there is a 310 μm long narrow section followed by a 1390 μm long 2° flared section. The width of the waveguide in the narrow stripe region is 3 μm and is 52 μm at the flared end. A schematic is shown below in Figure 3-3.

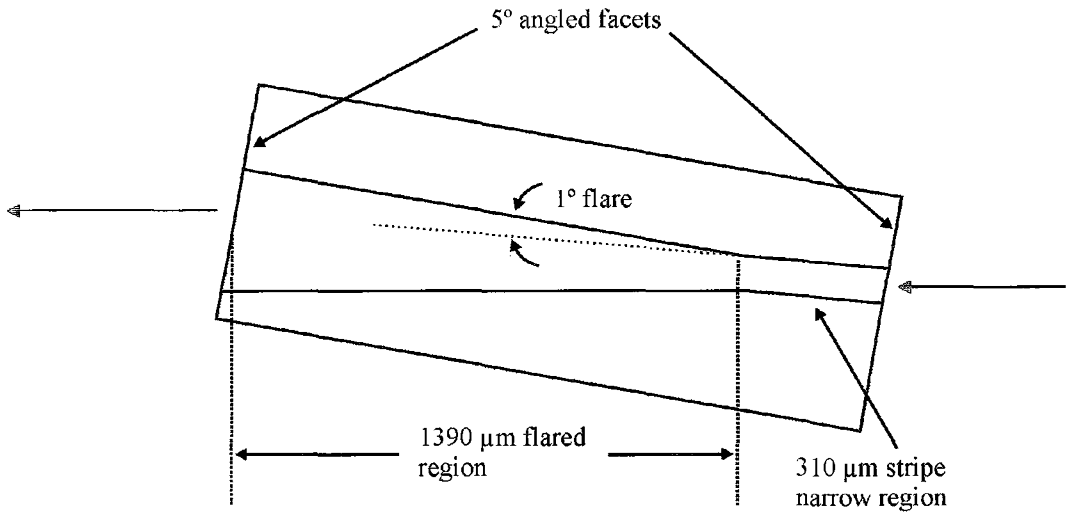

Figure 3-3: Top down schematic of the flared semiconductor optical amplifier.

Typical amplified powers were ~35 mW. The amplification had minimal effect on the duration or wavelength of the pulse [4]. However, there was some degradation of the beam quality, especially in the lateral (flared) direction but it was still sufficient for the desired applications.

3.4 Ytterbium-doped fibre amplifier

Ytterbium-doped fibre amplifiers (YDFAs) have been receiving a great deal of interest recently as a means of generating and amplifying short optical pulses. Indeed the interest in the YDFA was a driving force in the group's development of the 1075 nm oscillators and SOAs.

3.4.1 Introduction

The core of a silica glass fibre is doped (hundreds to thousands of parts per million by weight) with Yb atoms which become triply ionized in the glass matrix. The ions are optically pumped into an excited state where they will typically radiatively decay either by spontaneous or stimulated emission back down to the ground state. The gain from Yb-doped fibres ranges, for practical purposes, from 970 – 1200 nm which makes them well suited as sources for two-photon applications. Part of the attractiveness of the Yb-doped fibres over other rare-earth doped fibres such as erbium, neodymium and praseodymium is the simple electronic structure that consists of two manifolds, the ground $^2F_{7/2}$ and excited $^2F_{5/2}$ that are separated into four and three Stark levels respectively. The two manifolds are separated by ~10 000 cm^{-1} which precludes a number of undesirable effects that reduce the quantum efficiency of the medium. Examples of such effects are non-radiative multiphonon decay into the silica host, excited state absorption and concentration quenching [76]. The lack of concentration quenching allows the fibre to be highly doped, which permits higher gain in shorter lengths of fibre. The small energy defect between the pump and emission wavelengths of the Yb-doped fibre reduces heating of the host media and increases the energy conversion efficiency. The wide absorption and emission spectra make Yb-doped fibres suitable for short pulse amplification and the high saturation fluence permits high peak powers [77]. The absorption and emission spectra are both dominated by a prominent peak at 975 nm. A broader secondary absorption peak is centered at ~920 nm and a secondary broad fluorescence peak is centered at ~1030 nm [76], [77]. When amplifying beyond the primary 975 nm emission peak, it is still possible to obtain substantial amplification by increasing the interaction length, i.e. using a longer fibre.

The straightforward approach to achieving the necessary population inversion for amplification is to couple the pump light into the core at one end of the fibre and the laser seed signal at the other end. At pump powers below 1 W this direct approach works well because the guided pump signal largely overlaps with the doped core of the fibre. The strong overlap yields the benefit of reducing the required interaction length as the pump will be efficiently absorbed. Above 1 W there is an increased likelihood of damage to the facet of the fibre due to the tight focus required to couple into the small core of a single-mode fibre. A solution to this problem is the so called double-clad fibre, whereby the core is surrounded by an inner and outer cladding. Only the core is doped with Yb ions and the signal wave is coupled into it and amplified. The pump beam is coupled into the larger multimode inner cladding which has a diameter of >100 μm. The modes of the inner cladding overlap to a degree with the doped core where the pump can be absorbed by the Yb ions. In this configuration it is possible to couple in much higher pump powers which allows for much greater amplified signals. The required interaction length is much longer than for a single cladding fibre because the absorption per unit length is reduced by roughly the ratio of the inner cladding to the core areas [76]. Aside from the greater available amplification other advantages of the double-clad fibres include the ability to pump with multimode diode bars, improved launch efficiency and reduced alignment sensitivity.

In the amplifier configuration sub-picosecond pulses as short as 80 fs [7] have been amplified to greater than 75 W average power with peak powers of greater than one megawatt [6], and pulse energies of several millijoules [78]. Another group has demonstrated the amplification of a 1060 nm gain-switched diode to an average power of 11.1 W with a post-compression pulse duration of 20 ps at a repetition rate of 1 GHz [5].

3.4.2 Selected Yb-doped fibre amplifier results

The results discussed in this thesis were obtained from an 18 m double clad Yb-doped fibre. The fibre was end pumped with a diode laser delivering a maximum of 2.5 W at ~971 nm which is close to the peak absorption wavelength for an Yb-doped fibre. The fibre was seeded with the mode-locked diode laser described in Section 3.2, operating at ~1075 nm where there is low absorption but relatively strong gain. With a fibre as long as 18 m the gain spectrum of the fibre shifts to the red as a result of re-absorption and the gain peak should be close to the operating wavelength [79]. A 2 m long single-mode fibre was spliced to the non-pumped end of the Yb-doped fibre to facilitate coupling of the mode-locked diode seed into the amplifier and to prevent the unabsorbed pump light from being coupled back into the mode-locked diode laser. Both ends of the spliced fibre were cleaved at an angle of 8° to reduce facet reflectivity. This minimized the likelihood of unwanted lasing at low seed powers. The amplified signal was obtained from the pump end of the fibre and was separated by a dichroic mirror.

Over the time during which the Yb-doped fibre amplifier measurements were being made, the average output power of the mode-locked oscillator declined from approximately 1 mW to 300 μW. This had a marginal impact on the amplified output powers. Also, at some point in time it appears that the fibre was damaged. The maximum achievable average output power declined from 650 mW to 450 mW. The damage mechanism is not well understood. A seed coupling efficiency of ~40% into the single mode fibre was observed. A typical average available pulsed power (pre-damage) was ~650 mW with post-amplification pulse durations of between 4 and 10 ps. Pulse stretching can be observed on the output pulses due to normal group velocity dispersion within the fibre. The dispersion of the fibre as well as some of the initial chirp on the pulse can be compensated with a modified single pass grating pair compressor. A compressed pulse duration of 860 fs was observed. Because the fibre induced dispersion can be compensated, the duration of the final compressed pulse is largely dependent on the characteristics of the pre-amplified pulse. With this is mind compressed pulse durations closer to 500 fs should be with a more typical laser oscillator. Obtained results are illustrated in Figure 3-4. Taking into account the loss of the compressor the peak power of the 860 fs pulse is ~750 W. The coupling efficiency of the pump beam into the double clad fibre was measured to be ~70%. Losses to the amplified signal from the collimating lens as well as a dichroic mirror were measured to be approximately 15%. With these effects taken into account a plot of amplified power as a function of pump power is given in Figure 3-5. It is clear from the graph that given more pump power it would be possible to generate more amplified signal. However, there is a limit to this due to the low average powers from the mode-locked diode and the somewhat low coupling efficiency (~40%). A significant increase in the pump power will prevent the seed from suppressing the amplified spontaneous emission (ASE).

The ASE will reduce the gain available to amplify the seed pulse while at the same time generate an unwanted broadband (essentially) CW signal. With the system operating at its best, the ASE was fully suppressed when ~ 1 mW of average power was used to seed the fibre and the maximum available ~ 1.4 W was used to pump the fibre. When the seed power was reduced to ~250 μm the ASE on the output signal started to become an issue. Therefore, given a mW of seed power it should be possible to scale up the output power by a factor of 3 before the ASE is no longer suppressed (provided a more powerful pump diode is available). To go beyond that, a more powerful seed or pre-amplification would be required, either from an SOA or a low power Yb-amplifier. However, for the purpose of the two-photon experiments performed here, there is sufficient power in the current setup.

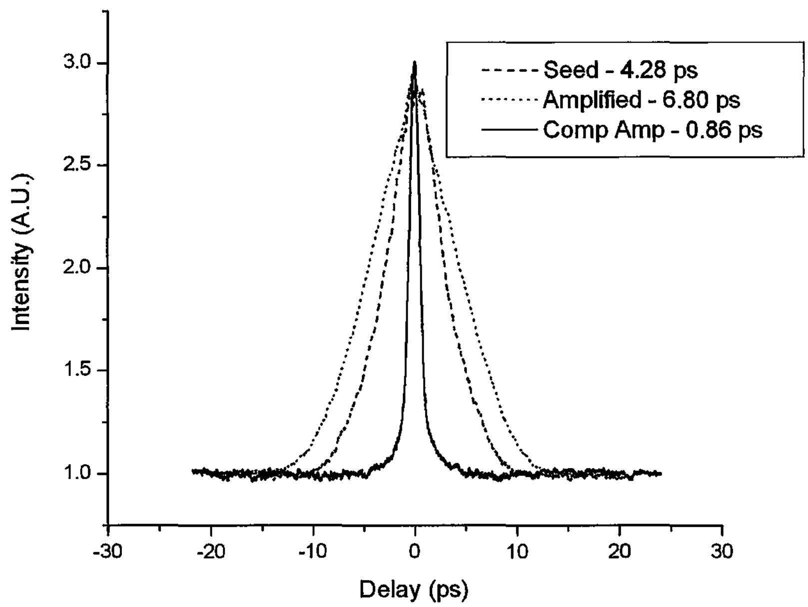

Figure 3-4: Second order intensity autocorrelation traces of the mode-locked oscillator pulse (Seed), seed pulse amplified with a Yb-doped fibre (Amplified) and the amplified pulse compressed (Comp Amp) with a modified single pass grating pair compressor. Stated pulse durations assume a Gaussian temporal profile.

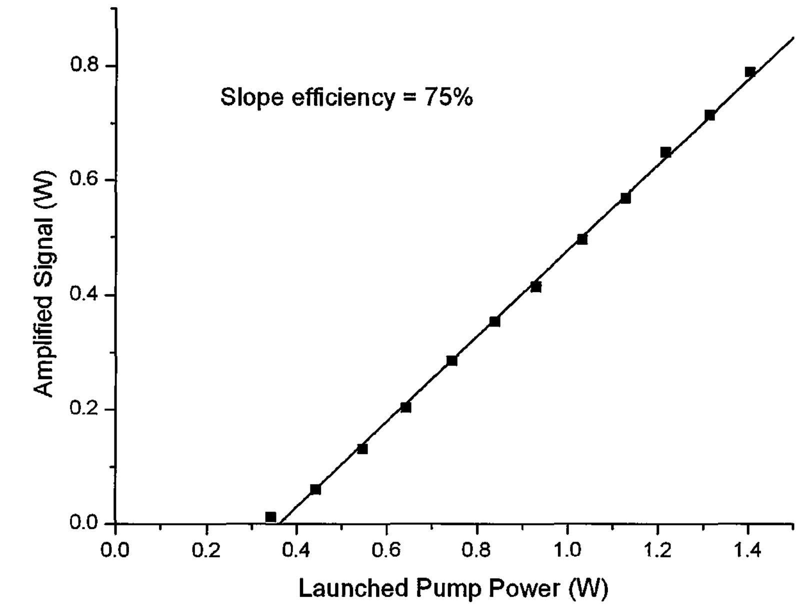

Figure 3-5: Output power as a function of launched pump power for Yb-doped fibre amplifier seeded with a passively mode-locked diode oscillator operating at 1077 nm with a repetition rate of 690 MHz and an average power of 930 μW. Pump power is the estimated energy coupled into the fibre. The line is a linear least squares fit to the data.

3.5 Titanium sapphire laser

The titanium sapphire laser is a popular laser source for work requiring tunable short pulses of light such as micro-machining, atomic spectroscopy and non-linear applications. The gain medium is a sapphire (Al_2O_3) crystal doped with titanium ions. The Ti^{3+} ions are responsible for the lasing mechanism in the crystal. The crystal is grown by introducing Ti_2O_3 into the Al_2O_3 melt. A small number of the aluminum ions are replaced with Ti^{3+} [80]. Titanium ion concentrations are on the order of 2-10 x 10^{19} cm^{-3} [81]. The sapphire crystal host field splits the electronic ground state of the titanium ions into two broadened levels, the ground and excited bands [82]. The crystal exhibits a relatively broad absorption (400-650 nm) and emission range (600-1050 nm) [82]. The available tuning range is limited to 650-1050 nm due to overlap of the absorption and emission spectra between 600 and 650 nm.

The population inversion of the Ti:Sapphire crystal in the Spectra-Physics Tsunami laser used in these experiments is achieved by focusing a frequency doubled neodymium vanadate pump laser into the Ti:Sapphire crystal. The tight focal region generates a localized inversion within the crystal which is easier to maintain than pumping of the entire crystal. Wavelength tuning is achieved by spectrally dispersing the beam with a pair of prisms and selecting the desired wavelength range with a movable slit. The light is then collimated after another identical prism pair. All wavelengths not able to pass through the slit experience significant loss and are therefore absent from the emission spectrum of the laser. The width of the slit can also be adjusted to change the emission bandwidth (and also the temporal width of the pulse) of the laser. The prisms also compensate for group velocity dispersion that is introduced by the other optical elements as well as the Ti:Sapphire crystal allowing pulse durations as short as 80 fs to be obtained.

Pulse generation is achieved by a variation of active mode-locking known as regenerative mode-locking [83]. The active element used in the Tsunami Ti:Sapphire laser is an acousto-optic modulator (AOM). A standing acoustic wave perpendicular to the optic axis is maintained within a quartz crystal at a frequency corresponding to twice the round trip time of the laser cavity (in this case ~80 MHz). The standing wave creates a time dependent index change within the quartz. Light that encounters the grating is diffracted out of the laser cavity creating the required periodic loss for active mode-locking. In the absence of the acoustic grating, light passes directly through the quartz crystal and is partially reflected by the output coupler on the other side of the AOM. It either returns through the crystal into the laser cavity or is not reflected and becomes the output beam. The difference between regenerative and active mode-locking is the inclusion of a feedback element. During the course of operation the cavity length can change by small amounts due to various effects such as temperature changes. This will negatively impact the quality of the pulses because unless the length changes are compensated for the cavity length will not match the standing wave frequency of the AOM thereby degrading the mode-locking. Feedback of the cavity length is achieved by splitting part of the output beam to a photodiode where the measured pulse frequency is used to drive the AOM and keep it synchronized with the laser cavity length. This will allow the system to maintain the quality of the output.

Chapter 4 General Experimental Setup

In this section the layout of the various components with respect to the diagnostic and measurement equipment will be described.

4.1 Oscillator and SOA

The configurational basics of both the oscillator and SOA have been laid out briefly in previous sections. A more detailed description will be made here.

4.1.1 Device mounting

The laser and the SOA are bonded to separate copper blocks with Epotek H20E silver epoxy. This ensures good electrical and thermal contact of the devices with the temperature controlled mounting base. The copper blocks are about the same thickness as the devices are long; this provides the greatest mechanical stability while minimizing interference of the block with the emitted light. Temperature is controlled by a thermoelectric cooler mounted to the fixed base. A more detailed description can be found in the PhD thesis of Michael Brennan [71].

4.1.2 Oscillator – SOA configuration

In Figure 4-1 the operational layout of the oscillator-seeded SOA is shown. The diode laser is coupled to an external cavity where either a mirror or diffraction grating is used as the reflector. The bent waveguide is used to minimize the coupling of light reflected at the back facet into the waveguide. Light emitted from the oscillator passes through an optical isolator to the flared semiconductor amplifier. The isolator (a Conoptics Model 715, with the 730 compensator) is necessary to prevent the amplified spontaneous emission of the SOA from being coupled back into the oscillator and disrupting the mode-locking or damaging the device. The facets of the SOA are angled and anti-reflection coated at both ends to increase the single pass efficiency of the device and to minimize any lasing. The flared waveguide increases the gain of the SOA without greatly changing the mode structure of the beam. The lateral dimension of the output end of the SOA is ~50 μm while in the transverse dimension it is ~3 μm; this causes the divergence angle in the transverse direction to be much larger than in the lateral direction. A cylindrical lens is used in conjunction with the collimating aspheric lens to correct for most of the astigmatism caused by the difference in the exit waveguide dimensions [84].

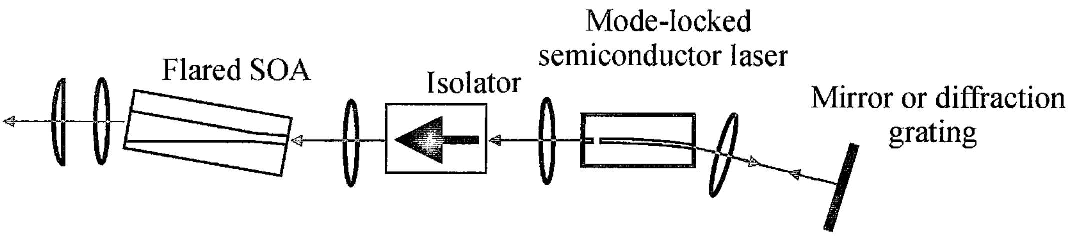

Figure 4-1: Schematic of oscillator and SOA setup used in experiments. The cylindrical lens after the SOA is to correct for astigmatism.

4.1.3 Equipment

Light was coupled into the SOA by an AR coated aspheric Thorlabs C330TM-B lens. The output lens of the SOA and both lenses of the oscillator were AR coated aspheric Thorlabs C230TM-B. Contact with the oscillator was made with two long fine-tipped probes. The bias to the absorber section was provided from a Keithley LV-2400 Source Meter while the current to the gain section came from an ILX Lightwave LDC-3724 Laser Diode Controller. The temperature of the oscillator was controlled with an ILX Lightwave LDT-5412 Temperature Controller. The current and temperature control of the SOA was provided by an ILX Lightwave LDC-3900 Modular Diode Controller.

4.2 Oscillator and Yb-doped fibre amplifier

The layout for the oscillator and Yb-doped fibre amplifier is similar to that described in Section 4.1.2. Much of the equipment for the Yb-doped fibre amplifier was provided by Donna Strickland of the University of Waterloo as part of the ongoing collaboration between our two groups.

4.2.1 Oscillator - Yb-doped fibre configuration

Figure 4-2 gives a layout of the YDFA setup. The layout of the oscillator is the same as is described in Section 4.1.2. The maximum average amplified optical powers generated by the YDFA in this setup are more than an order of magnitude greater than those obtained for the SOA. As such, care must be taken to ensure that back traveling light (toward the oscillator) is strongly attenuated. Two isolators (Conoptics Model 715, one has the 730 compensator) are used in this arrangement because attenuation of these isolators is wavelength dependent and there are two separate wavelength regimes that must be minimized. The first is the broad bandwidth spontaneous emission from the pumped fibre which peaks at around 1070 nm. The second is the backwards traveling amplified signal which has a wavelength of ~1075 nm. Depending on the quality of the cleave at the pump end of the fibre, the back traveling signal can be substantial and both isolators are needed to reduce the power to an acceptable level.

The necessary population inversion in the core was generated by counter-directionally pumping with a laser diode. It is capable of producing 2.5 W at 970 nm. It was observed that approximately 10% of the pump is lost at the microscope objective and 70% of the light incident on the fibre is coupled into the inner cladding. The power supply was a Laser Drive Inc. LDI-820. The left-most dichroic mirror in Figure 4-2 reflected light at the 1075 nm amplified signal wavelength and allowed the 970 nm pump beam through. The right-most dichroic mirror in Figure 4-2 was put in place to further minimize the amplified signal that might travel back into the pump diode and damage it.

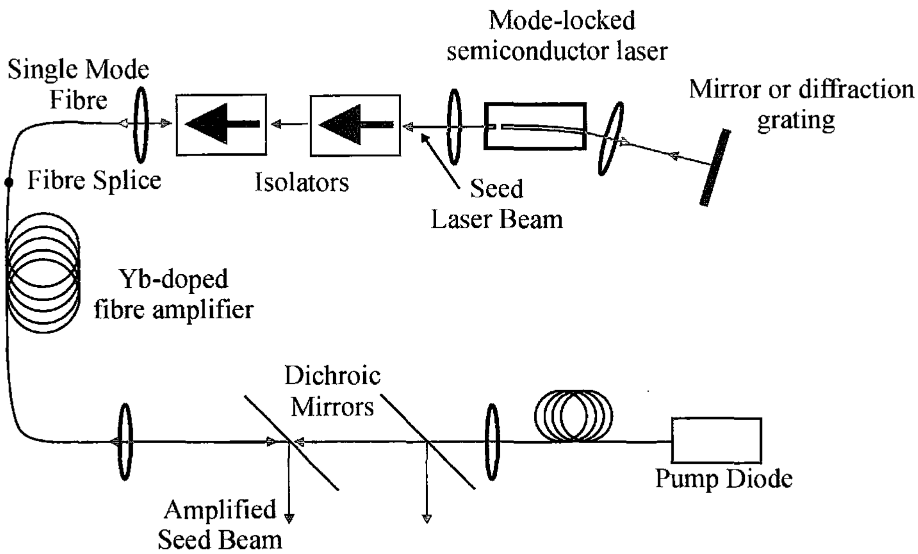

Figure 4-2: Schematic of oscillator and Yb-doped Fibre amplifier layout used in experiments. The single mode fibre facilitates the coupling of the mode-locked laser into Yb-fibre core.

4.2.2 Fibre description

The doped fibre is a Nufern SM YDF-5/130 single-mode ytterbium-doped double clad fibre and is approximately 18 m long. With this type of fibre the pump laser beam is coupled into the 130 μm diameter inner cladding of the fibre while the seed beam is coupled into the 6.5 μm mode field diameter single-mode core. In practice, it can be difficult to couple the seed beam into the core (where the fibre is doped) and not into the cladding. A Thor Labs single-mode fibre of similar core diameter was fused to the oscillator end of the Yb-fibre. In this way efficient coupling can be achieved by maximizing the amount of seed beam power emitted from the pump diode end of the fibre. It also serves a secondary purpose: pump power that is not absorbed by the Yb-doped fibre is scattered away at the splice because there is no waveguiding counterpart to the inner cladding in the single-mode fibre. The loss at the splice for the seed beam was around 0.2 dB. The ends of the single-mode and Yb-doped fibres were cleaved with an 8° angle to minimize reflections at the facets. With a normal cleave the fibre has sufficient gain that it would lase with the 4% reflection of the facet ends and a moderate pump power. Seed laser light was coupled into the single-mode fibre with a Thor Labs TM230-B AR-coated aspheric lens. The pump signal was coupled into the fibre with a 10x microscope objective.

4.3 System characterization equipment

A generalized layout of the various optical sources and diagnostic equipment is given in Figure 4-3. The titanium sapphire laser used in the experiments described in the following sections was a Spectra Physics Tsunami laser pumped with a Spectra Physics Millennia pump laser. The Ti:Sapphire laser generates an output of about 600 mW of average power at a repetition rate of 80 MHz and pulse duration of ~80 fs. A portion of the beam is tapped to an amplifier which reduces the available power. The beam also passes through an optical isolator which further reduces the power and stretches the pulse in time. After the beam splitter and optical isolator, the beam properties have changed such that the average power has been reduced to approximately 220 mW and the pulse duration has been stretched to ~200 fs. Each junction in the different optical paths of Figure 4-3 are switched by either a removable or articulated mirror mount.

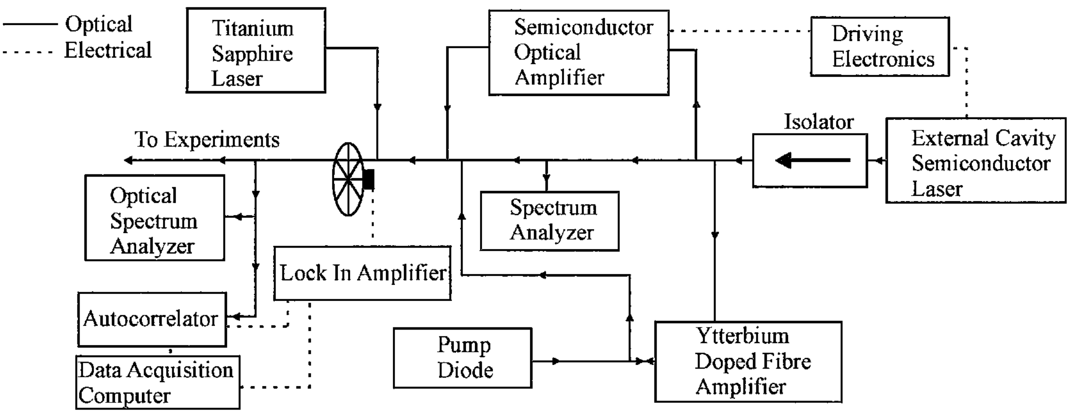

Figure 4-3: Generalized experimental setup for pulse diagnostics of the three principal sources. Optical junctions are switched by removable or articulated mirror mounts.

4.3.1 Autocorrelator

Pulse durations were measured with a standard Michelson interferometer autocorrelator setup [85]. A diagram of the schematic is presented in Figure 4-4. The beam is split by a Newport 50/50 beam splitter. One path is reflected by a fixed retroreflector and the other retroreflector is on a movable Oriel Encoder Miocrometer, model 18254. The recombined beam is focused through a 1 mm thick beta barium borate crystal that has been cut for a wavelength of 1000 nm. Anti-reflection coatings have been applied to the crystal for wavelengths of 1000 nm and 500 nm. The re-collimated second harmonic beam passes through a short-pass filter to remove the fundamental wavelength signal. The second harmonic signal is detected with a 1P28 Hamamatsu photomultiplier tube. The signal is amplified in a Stanford Research Systems SR510 Lock-In Amplifier where it passes to a data acquisition computer. The movable interferometer arm and data acquisition is controlled by in-house software written in Visual C++ 6.0 by Michael Brennan. More details of the physics and limitations of this measurement technique can be found in Vasil'ev [85].

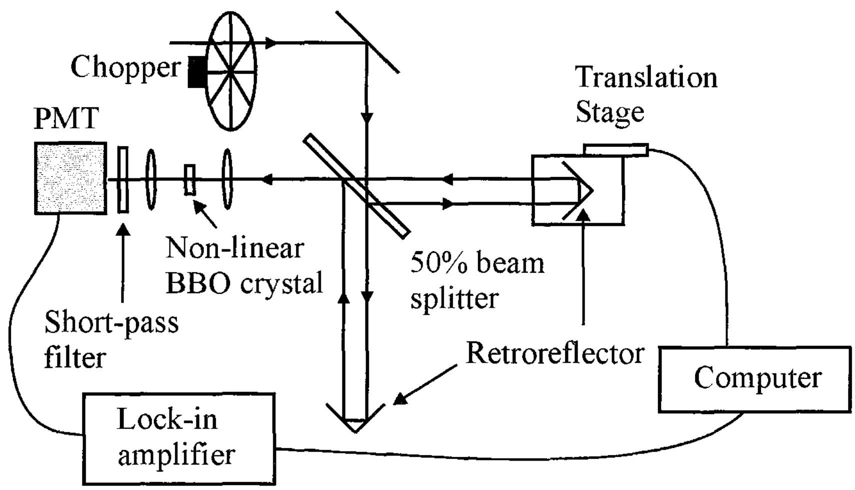

Figure 4-4: Schematic of autocorrelator used for short pulse measurements. The top-right side of the beam splitter has an anti-reflection coating in this diagram.

Chapter 5 Beam Profile Measurements

5.1 Introduction

In order to compare the generation of two-photon fluorescence (TPF) signals, three excitation sources were used. The titanium sapphire laser was considered the standard because it is a well understood commercial device that can be expected to generate a reproducible and reliable train of short pulses with good beam quality. The other two sources are the SOA and the YDFA, both seeded with the output of the diode oscillator. The mode profiles of these three sources are different and can be expected to affect the focal spot size which in turn can change the TPF generation efficiency and/or resolution in a microscopy application. Characterization of the focal region of a helium neon laser was performed alongside the three two-photon sources in order to provide assurances that the values measured were of adequate resolution. A HeNe laser has a nearly perfect Gaussian beam profile that allows some confidence in using a model to predict its focal spot size.

A standardized method of assigning a value to the quality of a laser beam is the M^2 (read M-squared) parameter. It is essentially the ratio between the beam waist – divergence angle product of a real laser beam and an ideal one. The parameter is defined as

$$M^2 = \frac{w_0\theta}{w_{ideal}\theta_{ideal}} = \frac{w_0\theta\pi}{\lambda} \tag{5.1}$$

where w_{ideal} is the beam waist of a perfect TEM_{00}, θ_{ideal} is the divergence angle of the ideal beam, w_0 is the waist of the real beam, and θ is the divergence angle of the real beam [88]. An ideal laser beam is purely TEM_{00} with a Gaussian mode profile. This situation corresponds to an M^2 value of one. Real world lasers do not have purely a TEM_{00} mode structure. Invariably some of the energy is carried in higher order modes and as such, these beams have M^2 values greater than one [86]. Certain lasers, such as the helium neon laser, can come quite close to this ideal with an M^2 value close to one. An M^2 value greater than 1 has a negative impact on the ability to focus the beam tightly. The exact M^2 value for the three sources is unknown, though it is assumed to be one for both the helium neon laser and the YDFA. In the case of the Ti:Sapphire laser beam, Spectra-Physics quotes the M^2 value as being ≤ 1.2 out of the laser [87]. The M^2 value of the SOA is not known but is expected to be significantly greater than one. An estimate of the M^2 value will be made from the data obtained in the beam waist measurements.

5.2 Experimental setup

Spot size measurements were made by having a razor blade scan through the focal region using a computer controlled Oriel Encoder Micrometer, model 18254. The micrometer has a position resolution of 0.1 μm. Light was focused using a Thor Labs C230TM aspheric lens with a focal length of 4.5 mm, an NA of 0 55, and a working aperture of 4.95 mm. In order to locate the minimum spot size, a number of measurements on slices through the focal region were made by moving the razor blade in the direction of light propagation in ~2.5 μm sized steps near the beam waist and in 10 μm steps further from the waist using a Newport 460A linear stage. Optical power measurements were made with an Ophir PD-300-3W with a detector size of 10mm x 10mm. The photodiode was approximately 6-7 mm from the razor blade to capture most of the light and minimize diffraction effects of the blade. The signal was fed directly into a data acquisition computer via an analog to digital converter A diagram of the setup is given in Figure 5-1.

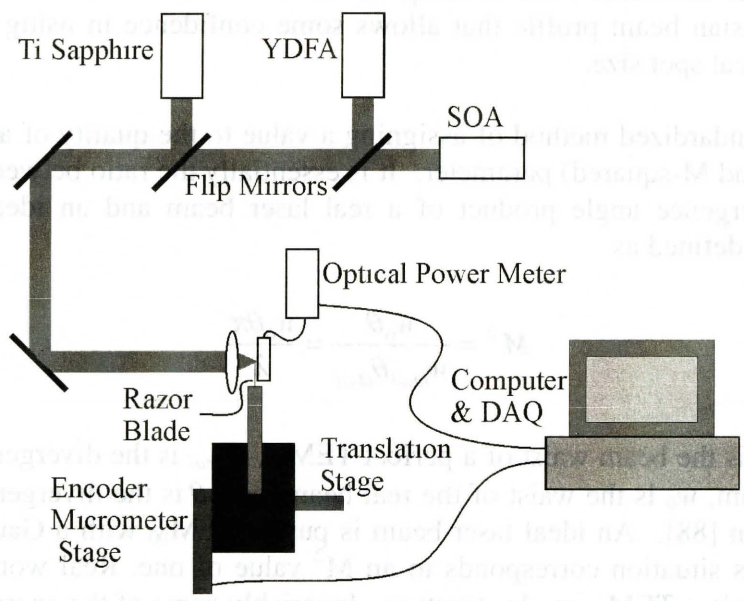

Figure 5-1: Schematic of spot size determination setup to make measurements in the lateral direction. Details of the individual source arrangements can be found in figures from Chapter 4.

A razor blade was initially chosen due to its durability and availability. The smoothness of the edge is not expected to be a large contributor of error to the measurements. The edge of the blade must be straight over only 10 μm sections for the overall smoothness to not be a factor Qualitatively inspecting the blade under an optical microscope showed smooth sections punctuated by rougher areas. Using different parts of the blade to occlude the beam did not significantly alter the measured results. In the future, however, it would likely be wise to use a cleaved wafer of InGaAs or Ge which has a more uniformly smooth and sharp edge.

Assuming the optical axis is the z-direction, measurements were made in both the x- (lateral) and y- (transverse) directions. This enabled the investigation of the lateral and transverse focal spot properties. The data acquisition system was setup such that the blade traveled (perpendicular to the z-axis) at either 2 or 5 μm/s and ~75 measurements were taken per second. Due to the nature of the acquisition system, a fixed sampling rate was unachievable. Instead the distance the stage traveled between acquired data points was recorded. Beam profile measurements were made with an Ophir BeamStar FX-66 CMOS beam profiler. The profiler has a maximum resolution of 1280 x 960 pixels with a pixel spacing of 7.5 μm. The area of the CMOS array is 9.6 mm x 7.7 mm. The spectral response is considered good from 350-1100 nm.

5.3 Measurement of spot size

To recover the focal point spot size and shape from the knife edge data a differentiation method was used. The differentiation method is susceptible to noise and smoothing techniques must be performed to obtain useful data. A program was written to take a subsection of data points (usually five) and average them to generate a new data point. A three-point differentiation was also performed to further smooth the data and regenerate the beam profile. Spot size measurements were taken to be the half-width at $1/e^2$ of the maximum intensity value, w. The minimum beam radius at the focus is referred to as the beam waist, w_0. Also, some of the beam profiles are not circular but instead are elliptical or asymmetric. It will be assumed that the x- and y- dimensions are independent of one another, meaning that the beam waist in the x- dimension can be predicted by considering only the width of the input beam in the lateral dimension. The same rationale applies to the y- dimension. In general this approach was successful in reconstructing the spot shape, especially in the focal region where the slope (and therefore the signal to noise ratio of the derivative) is largest. To confirm a reasonable accuracy of the retrieved beam waist, the values were compared to those generated when the measured data was fitted to an error function and the corresponding Gaussian shape was retrieved. This comparison was performed with the helium neon laser, the Ti:Sapphire laser, and the Yb-doped fibre amplifier where all the beam profiles are reasonably Gaussian in shape.

5.3.1 Error function fitting

A common method of determining the beam waist of a Gaussian beam from a knife edge scan is to fit an error function to the measured data. The error function is related to the Gaussian function by the following relationship

$$erf\left(z\right)=\frac{2}{\sqrt{\pi}}\int_{0}^{z}e^{-x^{2}}dx \tag{5.2}$$

where e^{-x^2} generates the normal distribution. In reality a Gaussian other than the standard normal distribution (i.e. $\mu = 0$ and $w = 1$) is required to fit to the acquired knife edge data. A more general form of the distribution would be

$$\frac{A}{w}\int_{0}^{z}e^{-\frac{2(x-\mu)^{2}}{w^{2}}}dx \tag{5.3}$$

where A is a normalizing value, w is the $1/e^2$ radius and μ is the spatial position of the Gaussian function peak. The mean can be assumed to be at the position x where the knife-scan signal drops to half of its maximum value. This is reasonable because the Gaussian function is symmetric. Knowing μ, it is possible to find w relatively easily using a simple search algorithm. Minimizing the least squares difference between the data and $erf\,(\sqrt{2}\,(x\text{-}\mu)/w)$ yields the correct width because the numerator in the error function expression can be considered a constant (say m) in the fitting routine and so the expression $erf(m/w)$ gives

$$A\int_{0}^{\frac{m}{w}}e^{-x^{2}}dx=\frac{A}{w}\int_{0}^{m}e^{-\left(\frac{x}{w}\right)^{2}}dx \tag{5.4}$$

So, by minimizing the squared difference between the data and the left side of Equation (5.4) the width of the beam at a given slice is correctly retrieved by varying w using a search algorithm. The error function fitting method is less sensitive to noise than the differentiation method, though a Gaussian must be a reasonable approximation of the beam profile. As will be seen with the SOA, it is not reasonable to assume a Gaussian profile. In that case the differentiation method will need to be used.

5.4 Helium neon laser beam waist measurement

The beam profile of a helium neon laser approximates very closely an ideal Gaussian and so it would be a good case to test the spot size measurement system. The helium neon laser (Melles Griot 05-LLR-811 - 632.8 nm) source was placed close to the measurement apparatus (~65 cm) and the beam interacted with few optical (two mirrors before lens) elements which preserved the integrity of the mode profile. An image of the HeNe profile taken ~10 cm from the lens aperture is given in Figure 5-2 (the profiler is ~55 cm from the laser aperture) Structure within the beam is interference associated with the neutral density filters on the beam profiler

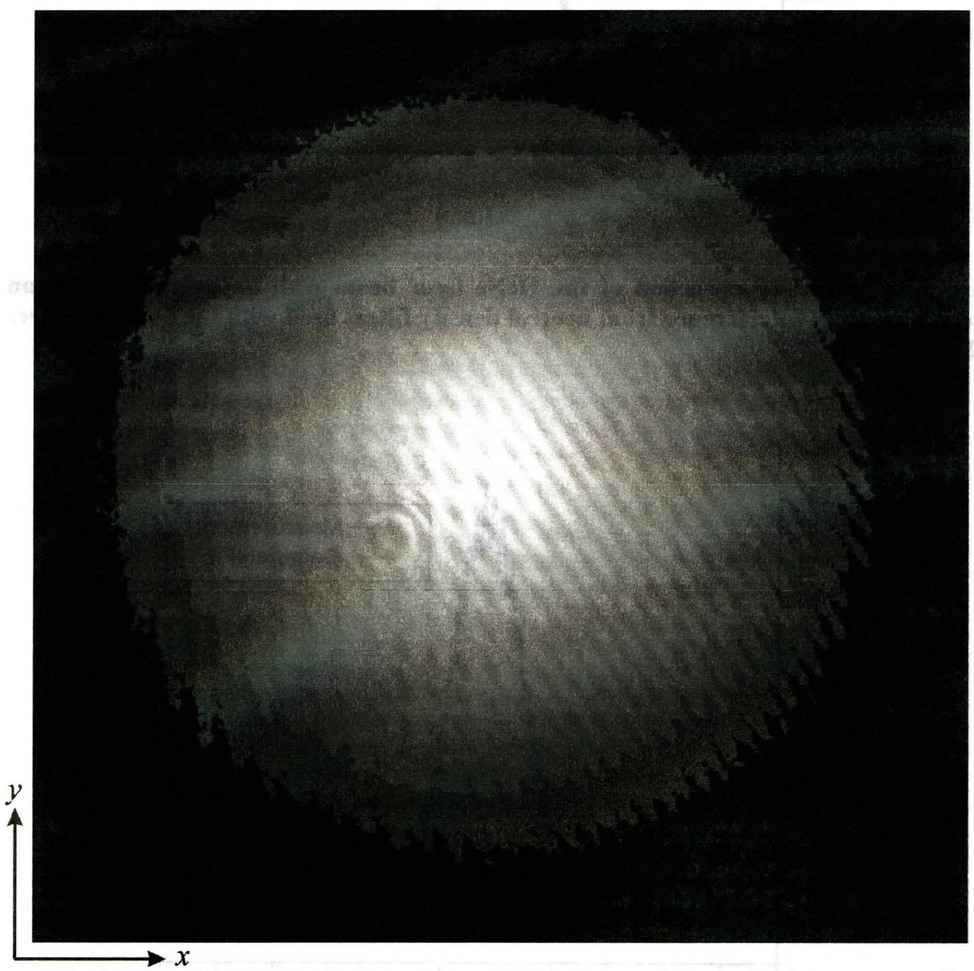

Figure 5-2: Profile of helium neon laser beam. Fringe patterns and ripples are an artifact of neutral density filters.

Cross-sections through Figure 5-2 indicate that the mode quality is good in the lateral and transverse directions as can be seen in Figures 5-3 and 5-4, respectively The profiles are essentially Gaussian.

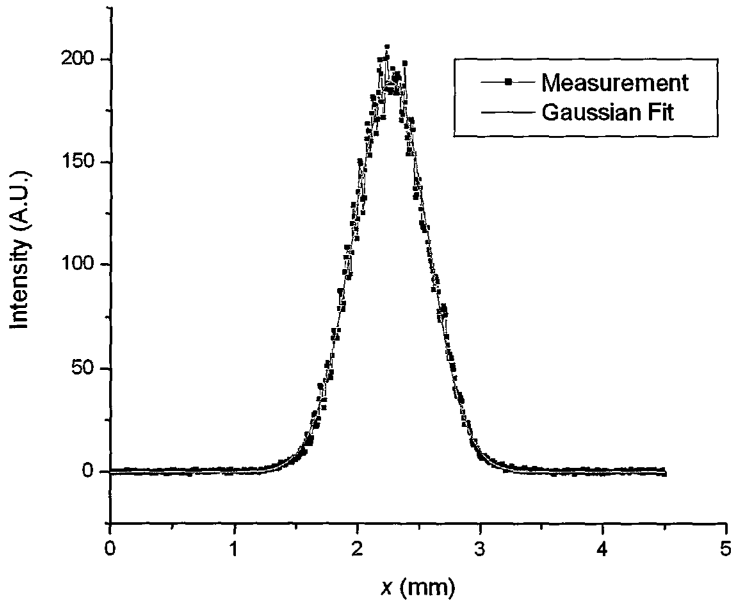

Figure 5-3: Lateral cross-section of the HeNe laser beam with an overlaid Gaussian fit. Noise is a result of interference from neutral density filters used with the beam profiler. 2w = 1.2 mm.

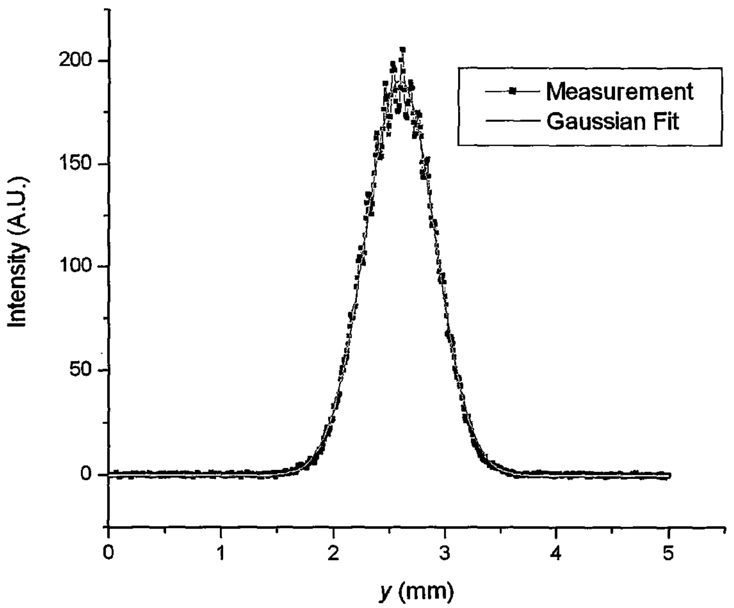

Figure 5-4: Transverse cross-section of the HeNe laser beam with an overlaid Gaussian fit. Noise is a result of interference from neutral density filters used with the beam profiler. 2w = 1.3 mm.

Gaussian fits performed on the cross-sections by the beam profiler software yields $1/e^2$ diameters in the lateral and transverse directions of 1.2 mm and 1.3 mm respectively. Because the diameters are much less than the diameter (4.95 mm) of the lens it is reasonable to assume that the lens aperture is not the diffraction aperture. The thin lens approximation of the predicted spot size radius for an untruncated Gaussian beam is given by:

$$w_0 = \frac{w_i}{\sqrt{\left[\left(1-\frac{s}{f}\right)^2 + \left(\frac{z_R}{M^2 f}\right)^2\right]}} \tag{5.5}$$

where w_0 is the radius of the spot size after focusing, f is the focal length of the lens, w_i is beam waist of the input beam, s is the distance from the input waist to the lens and z_R is the Rayleigh range of the input beam [88], [89]. The Rayleigh range is the distance from the beam waist to the position where the beam has expanded to $\sqrt{2}$ times the beam waist. The equation for the Rayleigh range is given by

$$z_R = \frac{\pi w_i^2}{\lambda} \, . \tag{5.6}$$

To predict the focused spot size it is therefore necessary to know the input waist of the beam. The specifications provided for the helium neon laser state that the nominal divergence angle, 2θ, is 1.70 mrad and the output beam diameter is 0.47 mm. Given the divergence angle, it is possible to determine the beam waist of the laser beam with the equation

$$w_i = \frac{\lambda}{\pi\theta} \tag{5.7}$$

The calculated beam waist from the specified data is 0.237 mm (diameter of 0.474 mm). Therefore, the calculated beam waist of the laser is very close to the nominal beam radius at the output of the laser. It will therefore be reasonable to use the measured beam radius at the output aperture of the laser as the actual beam waist for this source. The output beam $1/e^2$ diameter is measured to be 0.45 mm (w_0 = 0.23 mm), which agrees well with the laser specifications. The measured output diameter translates to a Rayleigh range of 25 cm. The focal length of the lens is 4.51 mm and the distance from the laser to the lens was approximately 65 cm. Therefore the predicted $1/e^2$ beam waist (w_0) after the focusing lens is 1.47 μm if we assume an M^2 value of 1. The measured values in the x and y direction are 1.50 μm and 1.44 μm, suggesting reasonable agreement. This gives an indication of the measurement accuracy available with the knife edge system. The difference between the expected and measured spot size is small. This suggests that the knife edge scan and resulting analysis can provide a reasonable measure of the beam spot size near the focus. Using the beam waist and divergence angle obtained from the knife edge scans, an estimate of the M^2 can be made for both dimensions. In the lateral dimension the M^2 value is measured to be ~1.1, while in the transverse direction it is ~0.99. This supports the assumption that the M^2 value of the HeNe laser is very close to 1.

Figure 5-5 demonstrates the smooth convergence and divergence of the HeNe laser beam near the focal region. Data is given from 50 μm on either side of the minimum diameter in ~2.5 and 10 μm steps. The error in the propagation distance of Figure 5-5 is a couple of microns for the 10 μm steps due to the limitation of the stage used to move the blade along the optical axis. Near the focus the step size was reduced to ~2.5 μm. This step size is an approximation because the markings on the z-axis translation stage translate to a 10 μm movement. In essence, three measurements were taken between the 10 μm resolution markings of the micrometer. As a result there is likely an error of 1-2 μm in the stated z position. This may explain the lack of smoothness of the measured widths near the focus. Note that, in Figure 5-5 it is illustrated that the beam waist minima of the lateral and transverse directions are occurring at the same spatial position. While this is expected, it could not be confirmed with the measurement setup used. The results are presented as such for aesthetic purposes. Plots of the recovered profiles of the beam waists for the lateral and transverse directions are given in Figures 5-6 and 5-7, respectively. The plots indicate a smooth profile in both dimensions.

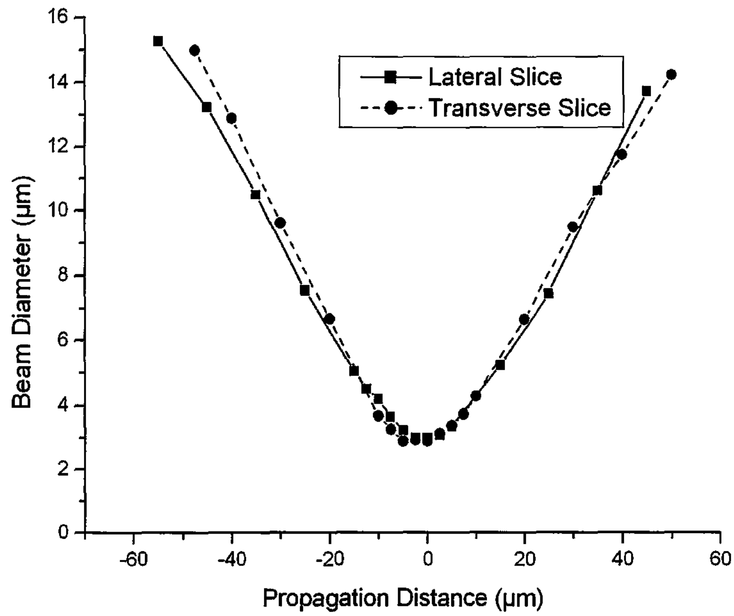

Figure 5-5: Plot of HeNe laser beam 1/e² diameters in the lateral and transverse directions near the focal point.

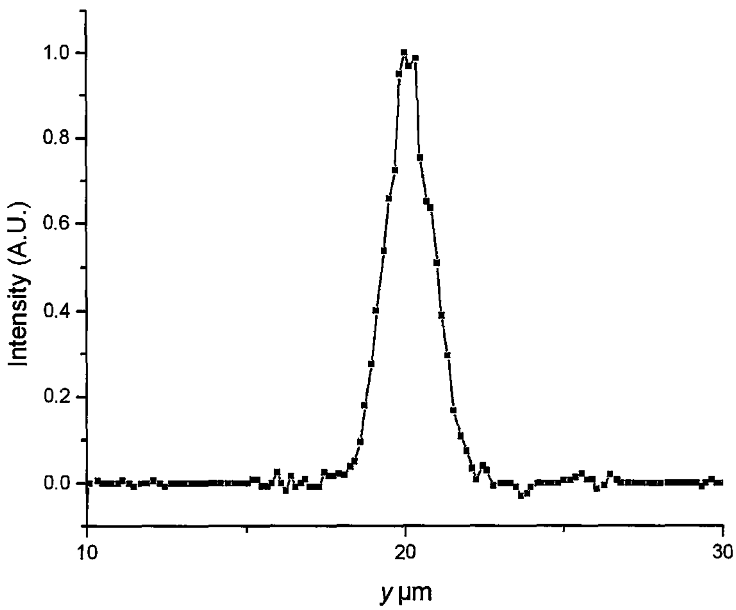

Figure 5-6: Plot of the recovered helium neon laser beam profile in the focus for the lateral dimension. The profile is recovered using the differentiation method. The 1/e² beam diameter, $2w_0$ = 1.50 μm.

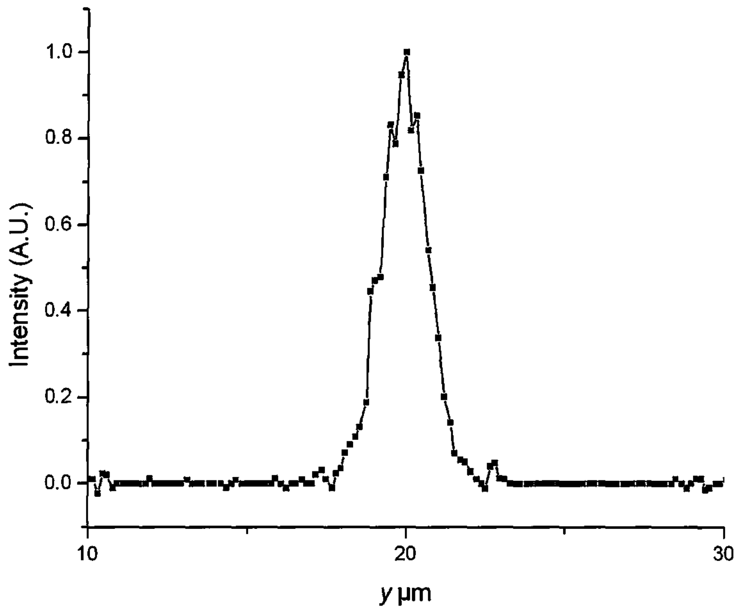

Figure 5-7: Plot of the recovered helium neon laser beam profile in the focus for the transverse dimension. The profile is recovered using the differentiation method. The 1/e^2 beam diameter, $2w_0$ = 1.44 μm.

The helium neon laser generates the most Gaussian beam profile of the tested sources and is therefore best suited to confirm the consistency of the differentiation method with the error function fitting method. Figure 5-8 overlays the lateral beam diameters obtained with the differentiation method with those obtained from fitting the error function to the data. The plot demonstrates very good agreement between the two methods near the focal region, with some divergence away from the beam waist. This is likely due to the increased error in the differentiation method away from the focus. As mentioned earlier, as the slope of the error function is reduced the effective signal-to-noise ratio also decreases, which yields a noisier profile reconstruction and therefore a noisier beam width measurement.

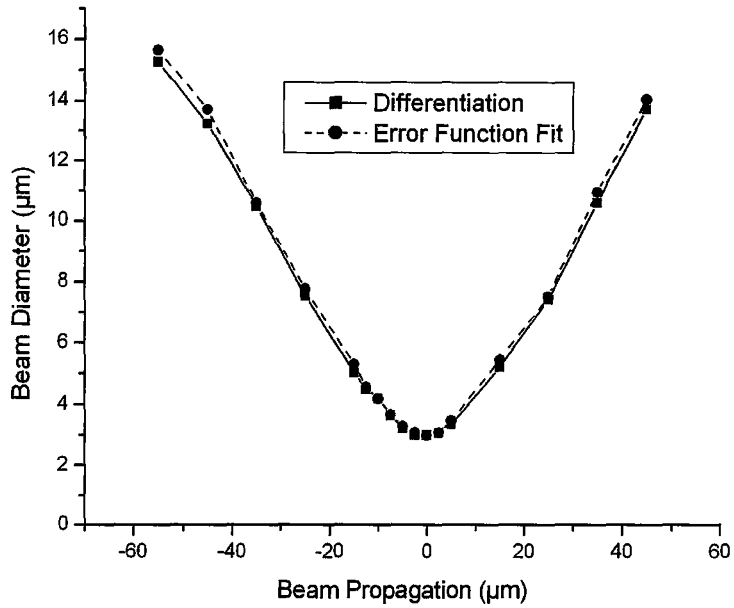

Figure 5-8: Comparison of differentiation and fitting method of determining the beam waist from the knife edge data. Data is from beam diameters in the lateral dimension.

5.5 Ti:Sapphire laser beam waist measurement

The spot size measurements made with the three other lasers/amplifiers were made quite a distance (several metres) from their respective sources. The beams propagated through and reflected off a rather large number of optical elements, so the mode profile experiences some degradation from its initial shape. In the case of the Ti:Sapphire laser, optical elements span three optical tables and a large air gap. The beam path from source to detector was approximately 7 m. An image of the Ti:Sapphire laser beam profile is given in Figure 5-9. The manual for the Tsunami Ti:Sapphire laser indicates that there may be some ellipticity of the beam at the output. This is due to the nature of the folded cavity of the laser.

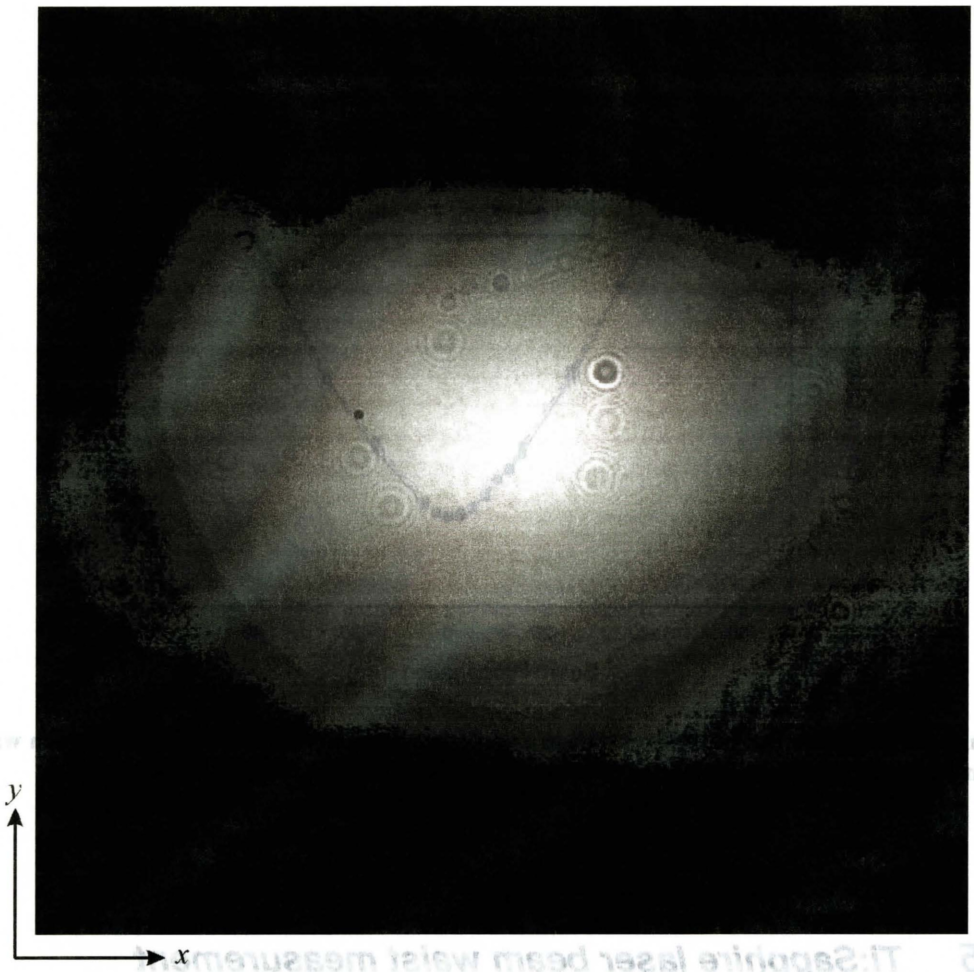

Figure 5-9: Beam profile of titanium sapphire laser approximately 7 m from the laser output aperture. Circular structures are a result of interference originating on the neutral density filters of the profiler.

The small circular artifacts visible on the profile were again caused by defects/interference from the neutral density filters in front of the beam profiler. Cross-sections in the *x*- and *y*-directions are shown with a Gaussian fit in Figures 5-10 and 5-11, respectively The assumption of a Gaussian shape is reasonable despite the noise. The $1/e^2$ diameters of the fits in the lateral and transverse directions are 3.5 and 2.7 mm, respectively

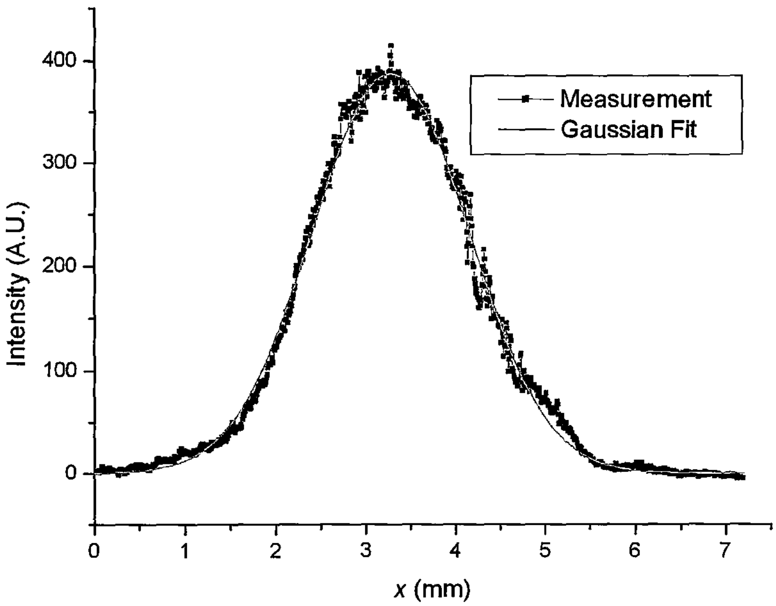

Figure 5-10: Lateral cross-section of the Ti:Sapphire laser beam with a Gaussian fit. The structure seen at about 4.25 mm is a result of the cross-section intersecting with one of the circular artifacts of the beam profile. The beam diameter, $2w$ = 3.5 mm.

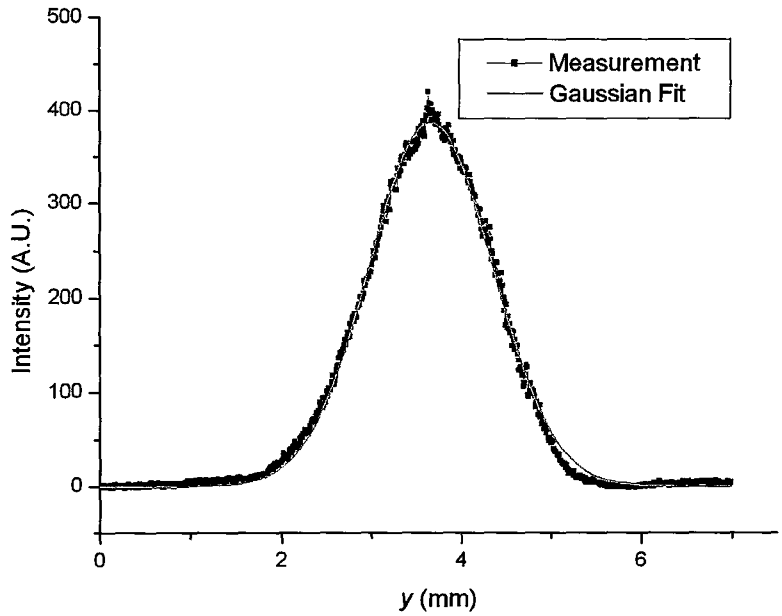

Figure 5-11: Tranverse cross-section of the Ti:Sapphire laser beam with a Gaussian fit. The beam diameter, $2w$ = 2.7 mm.

5.5.1 Estimating truncated beam waist

In the case of the Ti:Sapphire laser a non-negligible proportion of the beam is clipped by the aperture of the lens and therefore it is not entirely valid to assume a Gaussian profile as it was for the helium neon laser. However, it is also not valid to assume a plane wave. Clearly a hybrid approach is necessary. A simple method of estimating the spot size for a partially clipped ideal ($M^2 = 1$) Gaussian beam is given by Urey [90]. The $1/e^2$ diameter of the focal spot for the non-paraxial case (which in this case is considered to be when the $f_{\#} < 2$) is:

$$2w_0 = \frac{K\lambda}{2NA} \tag{5.8}$$

The truncation scaling factor, K, is given by:

$$K = 1.654 - \frac{0.105}{T} + \frac{0.28}{T^2} \tag{5.9}$$

where T is the clipping factor (valid for T > 0.5) given by Equation (5.10), d is the diameter of the lens, and w is the $1/e^2$ radius of the beam at the lens.

$$T = \frac{2w_{aperture}}{d} \tag{5.10}$$

In the x-direction T is 0.703 and in the y-direction T is 0.554. Therefore, the estimated $1/e^2$ beam waists for a pure TEM_{00} beam are 0.76 μm and 0.87 μm in the lateral and transverse directions, respectively. As stated in Section 0, the specified M^2 value of the Spectra-Physics Tsunami Ti:Sapphire laser is ≤ 1.2. This would be expected to translate to an increase of the focal spot size.

The bandwidth of the mode-locked titanium sapphire laser is about 10 nm and this can have an effect on the focal spot size due to chromatic aberration induced by the lens that causes different wavelength components to focus at different positions along the optical axis. The amount of smearing of the focal region due to chromatic aberration is given by Equation (5.11) [91],

$$\Delta f = -\frac{f\lambda^2}{c(n-1)} \frac{0.441}{\tau_p} \frac{dn}{d\lambda} \tag{5.11}$$

where τ_p is the FWHM of the pulse (~95 fs in the transform limited case with a 10 nm bandwidth and a Gaussian pulse shape), f is the focal length of the lens, n is the index of refraction of the lens, c is the speed of light and $dn/d\lambda$ is the dispersion parameter. The type of glass used in the aspheric lens is Corning C0550 which has an index of refraction of approximately 1.60 at 800 nm and a dispersion parameter that is likely greater than that of BK7 glass, which is $-2.0 \times 10^{4}\ m^{-1}$ [92], [93]. The true value of the dispersion could not be found. In the available literature an Abbe number of 50.4 is quoted for the C0550 glass and for BK7 glass it is 64.2 [92]. A larger Abbe number corresponds to a less dispersive material. The index of refraction of the Corning C0550 glass is provided at a number of wavelengths [92]. Interpolating between the two data points nearest 800 nm (707 and 853 nm) yields a dispersion parameter of $-2.8 \times 10^{4}\ m^{-1}$. Evaluating Equation (5.11) yields a focal spread along the optical axis of 2.1 μm. Assuming a small beam waist of 0.75 μm, the theoretical Rayleigh range is about 2.2 μm. This translates into the minimum beam waist being magnified by,

$$w_{\Delta f} = w_0 \sqrt{1 + \left(\frac{\Delta f}{2 z_R} \right)^2} \tag{5.12}$$

where $w_{\Delta f}$ is the beam waist with chromatic aberration taken into account [91]. The beam waist is expected to be about 11% larger due to chromatic aberration than for a CW beam. There was no significant difference in the measured spot size when the Ti:Sapphire laser was operating in the CW mode, however the 10% fluctuation is well within the measurement error. Including the effect of chromatic aberration, the beam waists in the lateral and transverse dimensions are expected to be ~0.84 μm and ~0.95 μm respectively.

Another possible source of increased focal spot size with an ultra-short laser pulse is a spatio-temporal effect called pulse front tilt. Pulse front tilt can be induced for example when a pulse passes through a prism or off a diffraction grating. The different spectral components of the pulse propagate at slightly different angles to one another (also known as angular chirp). This angular chirp can also be interpreted as a tilt of the virtual phase fronts of each of the spectral components. Focusing a pulse of this type can lead to temporal and spatial broadening in the focus. This leads to a reduced focal intensity. The interested reader can learn more about this phenomenon from the paper by Pretzler *et al* [94]. The pulse front tilt of the Ti:Sapphire laser pulses were measured with a Swamp Optics GRENOUILLE 5-20 system and was found to be negligible in both dimensions of the beam.

5.5.2 Measured Spot Size

For the Ti:Sapphire laser, the minimum measured beam waist in the *x*-direction is 0.98 μm and 1.1 μm in the *y*-direction. In both cases this is somewhat larger than the expected values of 0.84 μm and 0.95 μm. There are a number of possible causes for the discrepancy such as: widening of the focal width due to averaging, some smearing of the focal region due to beam position fluctuations, slightly askew alignment of the beam, or the blade not moving fully perpendicular to the optical axis. The M^2 value of the beam was expected to be larger than one. This would also yield a spot size greater than theory predicted for an ideal Gaussian beam. There could also be some other unknown systematic error.

Figure 5-12 illustrates the convergence and divergence of the Ti:Sapphire beam near the focal region. A plot of the recovered profiles in the focal spot for the lateral and transverse directions is given in Figures 5-13 and 5-14. The plot indicates a smooth profile in both dimensions.

Using the beam waist and divergence angle obtained from the knife edge measurements, an estimation of the M^2 value can be made. In the lateral dimension it is estimated to be 1.6, and in the transverse dimension it is estimated to be 1.7. This is noticeably larger than the specified input M^2 value. Focusing a truncated Gaussian beam can be expected to increase the M^2 parameter when compared to the input value [88]. Therefore these measured values do not directly indicate what the quality of the beam was prior to truncation.

To show the agreement between the error function fitting method and the differentiation method the two are plotted together in Figure 5-15 and exhibit the same general characteristics as those found in the helium neon laser beam plot of Figure 5-8.

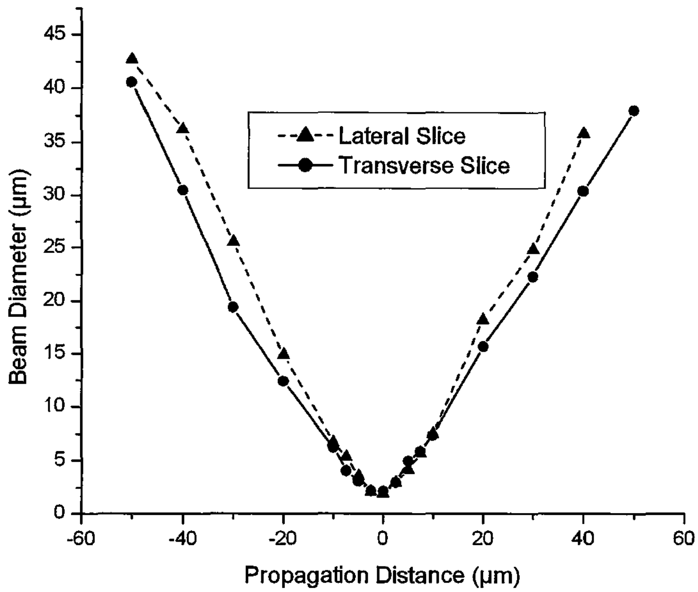

Figure 5-12: Plot of beam waist in the lateral and transverse dimensions of the Ti:Sapphire laser. The fluctuations away from the focal region are likely due to the increased noise of the knife edge data.

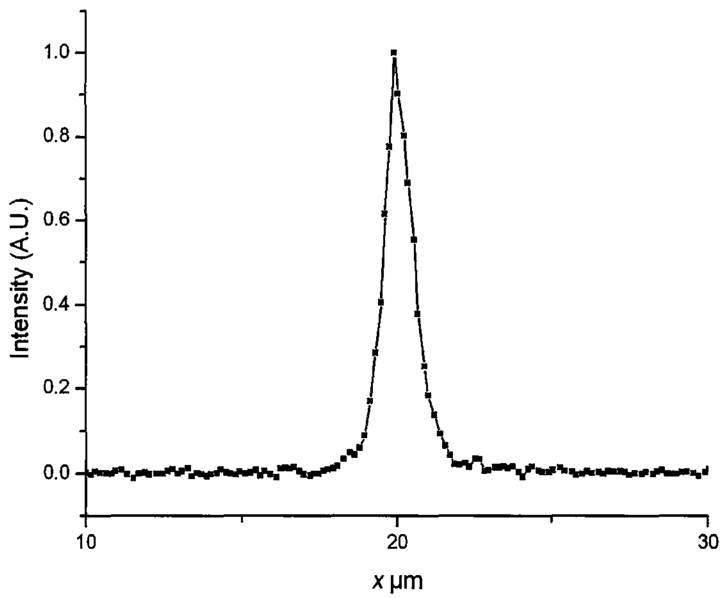

Figure 5-13: Plot of the recovered Ti:Sapphire laser beam profile in the focus for the lateral dimension. Profile recovered using the differentiation method. The 1/e^2 beam diameter, $2w_0$ = 0.98 µm.

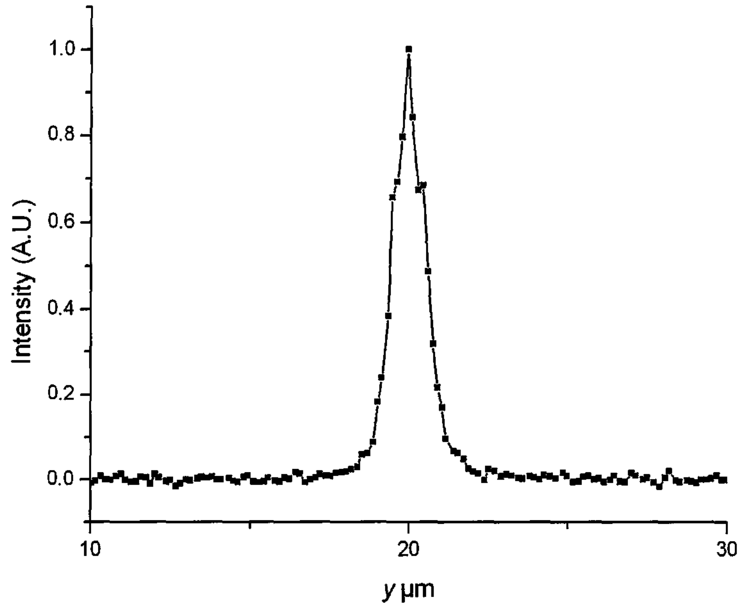

Figure 5-14: Plot of the recovered Ti:Sapphire laser beam profile in the focus for the transverse dimension. Profile recovered using the differentiation method. The 1/e^2 beam diameter, 2w_0 = 1.1 µm.

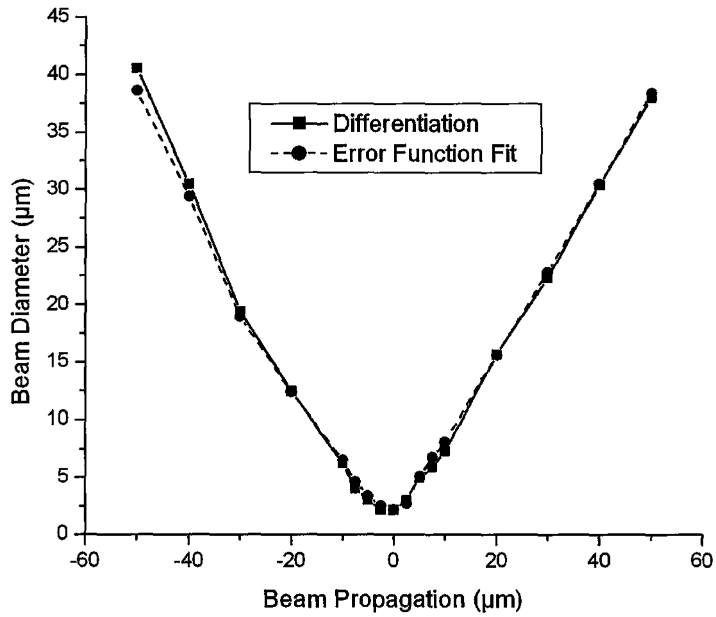

Figure 5-15: Comparison of differentiation and error function fitting method of determining beam waist for the Ti:Sapphire laser. Beam diameters are taken from the transverse dimension.

5.6 Yb-doped fibre amplifier beam waist measurement

A benefit of using the output of the single-mode Yb-doped fibre amplifier is the excellent beam quality The output should be ideal for focusing and for use in microscopy situations An image of the beam profile is given in Figure 5-16 The optical path is approximately 5 m from the facet of the fibre to the beam profiler The beam demonstrates some ellipticity along the diagonal in the x-y plot. This is possibly due to the angled facet of the fibre [101] Circular artifacts are due to interference effects associated with the neutral density filters of the beam profiler

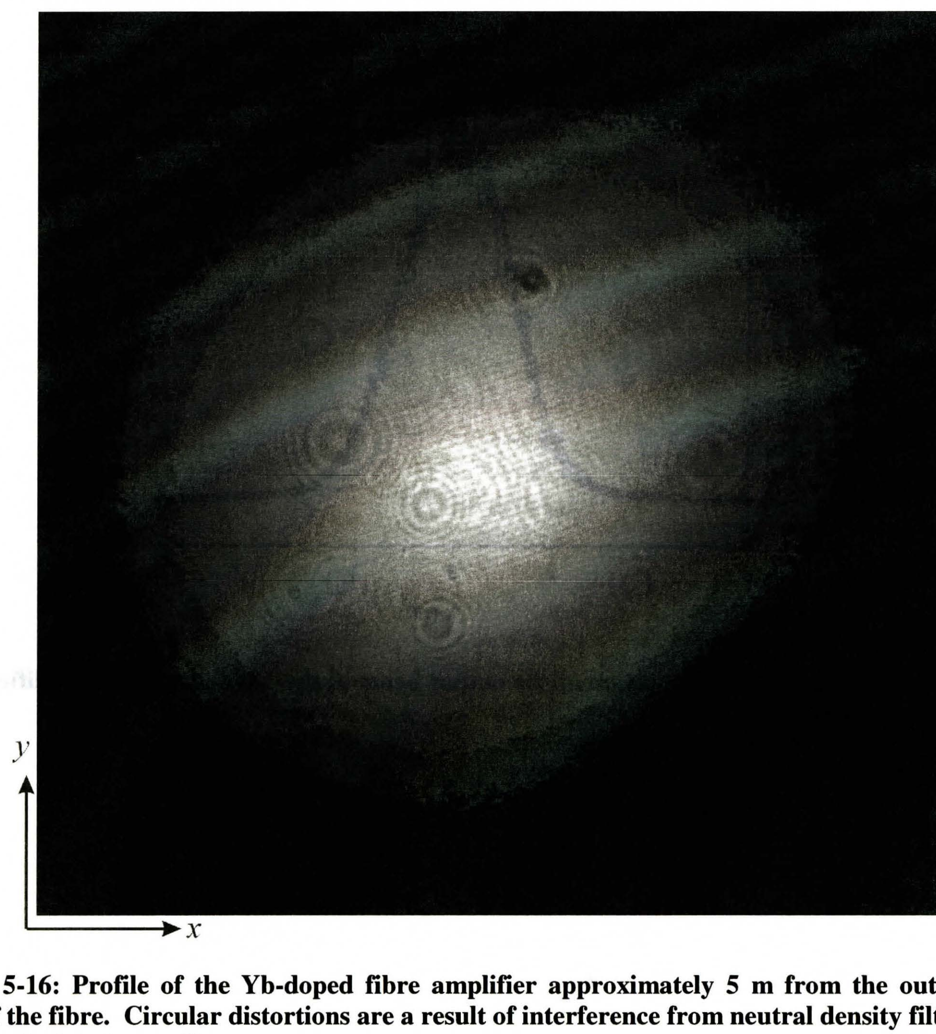

Figure 5-16: Profile of the Yb-doped fibre amplifier approximately 5 m from the output facet of the fibre. Circular distortions are a result of interference from neutral density filters associated with the profiler.

Cross-sections in the x- and y-dimension are shown with a Gaussian fit in Figures 5-17 and 5-18. The $1/e^2$ diameters of the fits are 2.2 mm in both the lateral and transverse dimensions. Again, the noisiness of the signal is a result of the neutral density filters associated with the beam profiler.

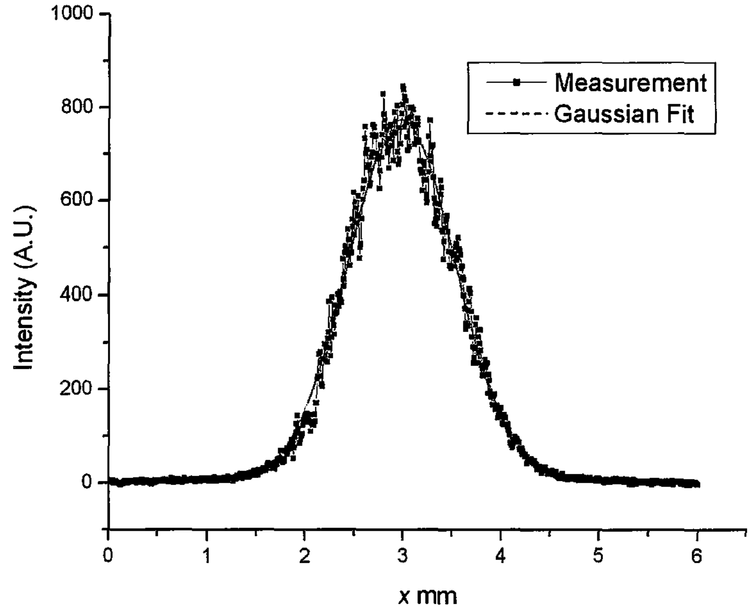

Figure 5-17: Lateral cross-section of the output beam of the Yb-doped fibre amplifier. The $1/e^2$ diameter, 2w = 2.2 mm.

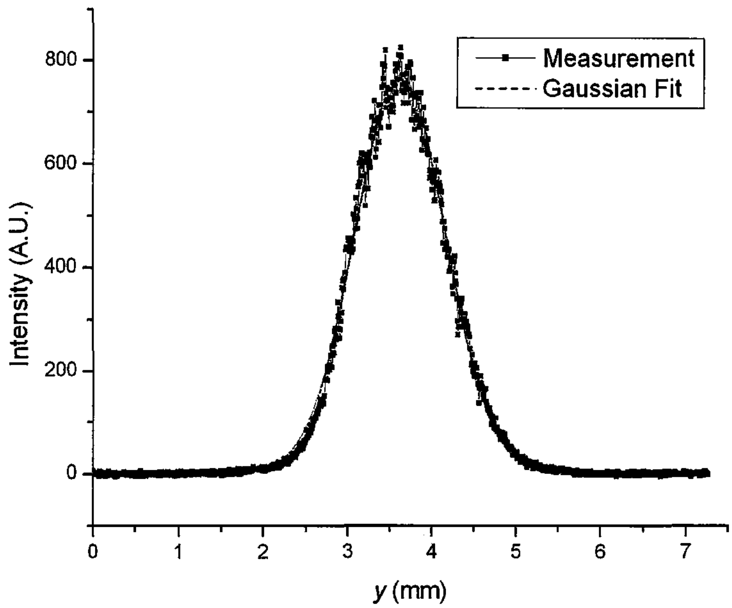

Figure 5-18: Transverse cross-section of the output beam of the Yb-doped fibre amplifier. The $1/e^2$ diameter, 2w = 2.2 mm.

5.6.1 Estimating YDFA beam waist

The diameter of the beam waist in this case is weakly truncated by the lens aperture. The truncation parameter, *T*, defined in Equation (5.10), is 0.44. According to Urey this value is too small to be able to accurately use Equation (5.9) to determine the *K* parameter [90]. For *T* values less that 0.5 he suggests the modified form

$$K = \frac{1.27}{T}. \tag{5.13}$$

Evaluating Equation (5.8) with the measured beam diameter and a wavelength of 1075 nm yields an expected beam waist of 1.4 μm. Given the weak truncation it should also be possible to use Equation (5.5) to a reasonable accuracy. In this case, the M^2 value will be assumed to be 1. For these measurements, the output of the YDFA was converging slightly such that the beam waist was near the spot size measurement setup. A series of measurements were made with the beam profiler in this region to determine the beam waist and its distance from the focusing lens. The minimum obtained waist was ~1.1 mm, approximately 20 cm in front of the focusing lens. These values correspond to a Rayleigh range of ~3.5

m. Using these values to evaluate Equation (5.5) yields an expected beam waist, w_0, of 1.4 μm. The two methods provide remarkably similar predictions of the spot size.

Similar to the Ti:Sapphire laser case, the bandwidth associated with short pulses can cause undesired spreading of the beam waist by chromatic aberration and pulse front tilt. Evaluating Equation (5.11) with values appropriate for the YDFA (λ = 1075 nm, τ_p = 340 fs for a Gaussian transform limited pulse with a bandwidth of 5 nm, and an interpolated dispersion parameter of -1.32 x 10^4 m^{-1} [92]) yields a 0.5 μm spreading of the axial focal length. Assuming a beam waist of 1.4 μm, it is possible to estimate the effect the chromatic dispersion will have on the measured waist. Evaluating Equation (5.12), the measured spot size would be expected to be less than 1% larger due to chromatic aberration. Therefore, in this case chromatic aberration can be neglected.

Given the small bandwidth and the long pulse duration, any pulse front tilt is not expected to have a significant impact on the measured waist. Given that the YDFA is a single-mode fibre any angular chirp that may be present on the input will be lost in the waveguide. The only element that could impart some angular dispersion within the beam path is the 8° angle cleave of the fibre facet. The magnitude of this effect will depend on the wavelength dependence of the index of refraction. Given that the wavelength of light is near the optical resonance (bandgap) of the doped fibre there may be a large change in index of refraction over a small wavelength range. A simple experiment was performed to see if there was significant angular dispersion on the beam. The diode oscillator was set to operate simultaneously at two separate wavelengths ~20 nm apart (~1065 and ~1085 nm) on either side of the gain peak of 1070 nm. After being amplified by the YDFA, the spectrum of the output beam was measured with an optical spectrum analyzer. A razor blade was then used to section a portion of the beam to see if the ratio of the intensities of the two wavelengths changed. This was done in both the lateral and transverse dimension. No significant effect was noted. This suggests that there is not a significant amount of angular dispersion on the beam and hence that the pulse front tilt should be minimal.

5.6.2 Measured spot size

The minimum measured $1/e^2$ waist for the YDFA in the lateral dimension was 1.38 μm, and in the transverse dimension it was 1.54 μm. This agrees well with the expected value of 1.4 μm. A plot of the convergence and divergence near the focus is given in Figure 5-19. Plots of the recovered profiles at the beam waist in the lateral and transverse dimension are given in Figures 5-20 and 5-21.

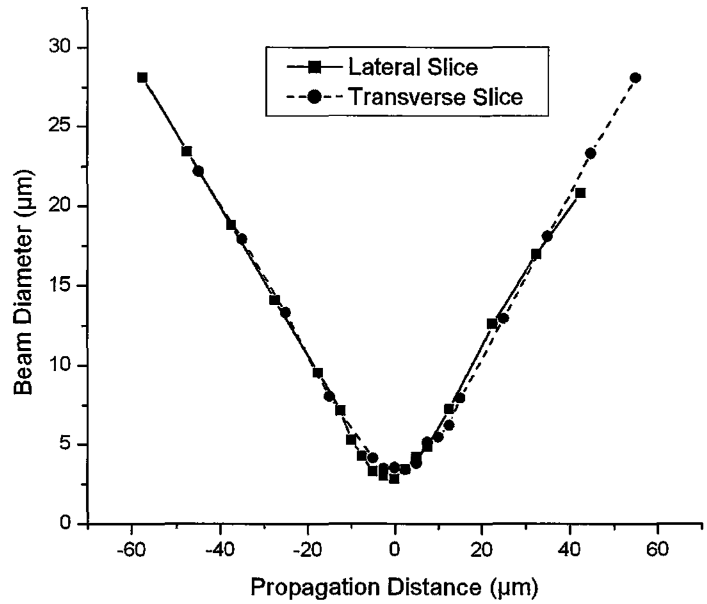

Figure 5-19: Plot of the beam diameters in the lateral and transverse dimension of the Yb-doped fibre amplifier near the focus.

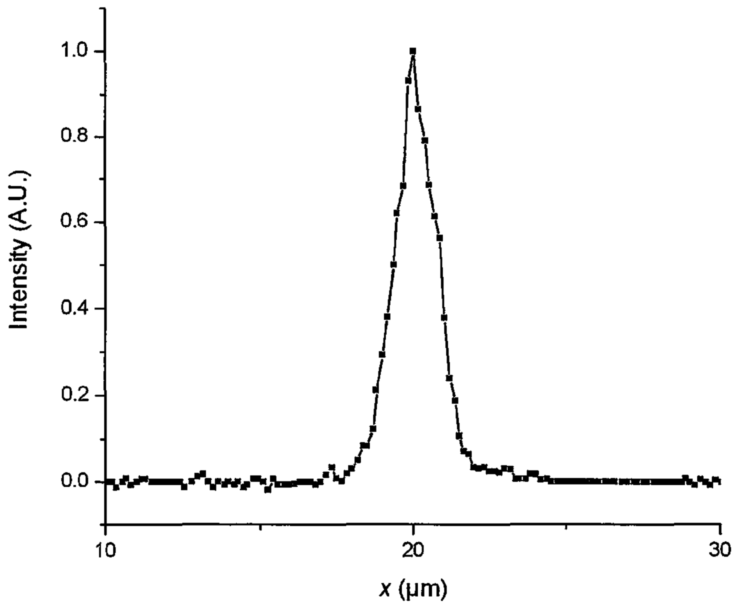

Figure 5-20: Plot of the recovered YDFA beam profile in the focus using the differentiation method for the lateral dimension. The 1/e^2 beam diameter, 2w$_0$ = 1.38 μm.

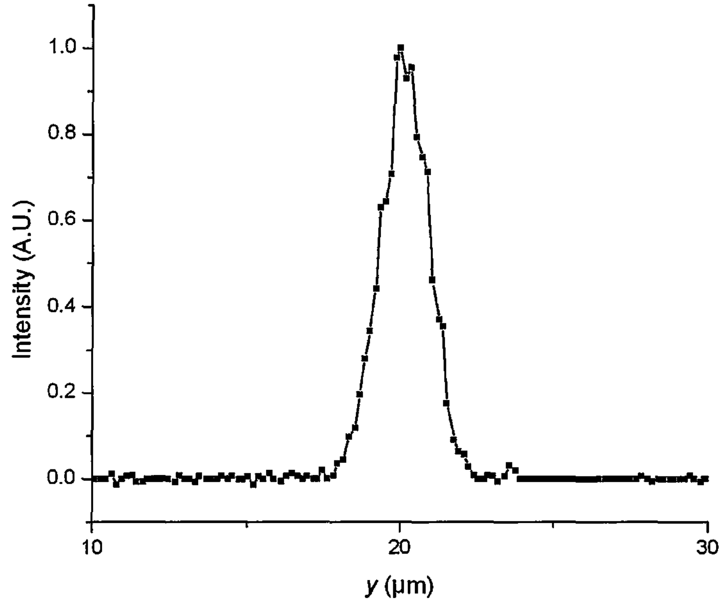

Figure 5-21: Plot of the recovered YDFA beam profile in the focus using the differentiation method for the transverse dimension. The $1/e^2$ beam diameter, $2w_0 = 1.54$ μm.

Using the beam waist and divergence angle obtained from the knife edge measurements, an estimation of the M^2 value can be made. In the lateral dimension it is estimated to be 0.89, and in the transverse dimension it is estimated to be 1.04. Clearly a value less than one is not possible. It does, however, suggest that the beam consists largely of the lowest order Gaussian mode.

To show the agreement between the error function fitting method and the differentiation method the two are plotted together in Figure 5-22 and exhibit good agreement.

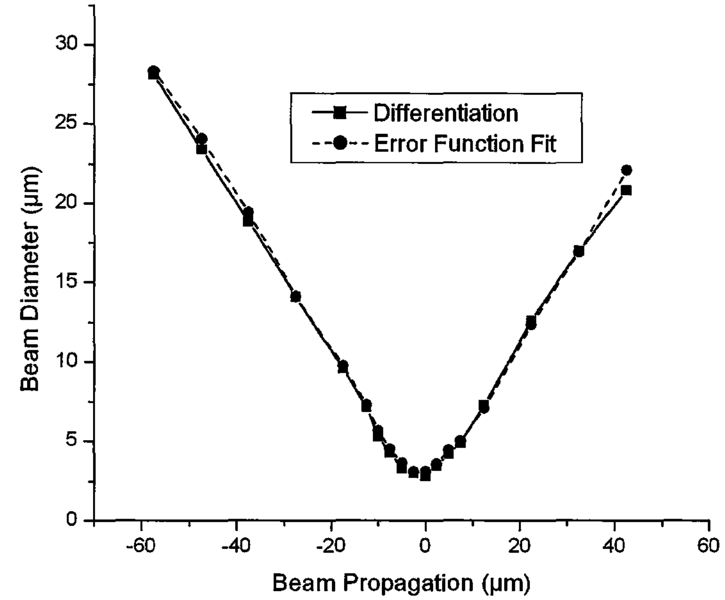

Figure 5-22: Plot of beam diameters obtained from the Yb-doped fibre amplifier near the focus using the differentiation and error function fitting methods.

5.7 SOA beam waist measurement

The beam profile obtained from the semiconductor optical amplifier is significantly worse than that of the helium neon laser, the Ti:Sapphire laser or the Yb-doped fibre amplifier. It consists of a single primary mode in the lateral direction with some smaller side lobes and two primary lobes in the transverse direction. The two-lobed transverse structure has been observed with essentially all the devices fabricated. It is also present in the output of the laser oscillator. The source of the two lobes is not known for certain. However, very recent work in the lab has suggested that it may be diffraction effects associated with the collection lens. If this is the case, then a better choice of lens may remove the two lobe structure. An image of the beam profile is given in Figure 5-23. The measurement system is approximately 3.5 m away from the SOA, spanning two optical tables with a gap between. The beam is also slightly astigmatic; diverging more in the lateral dimension than in the transverse. The beam quality has degraded noticeably by the time the beam has reached the measurement setup. This is a combination of both the large number of mirrors involved, the normal beam divergence as well as the slight astigmatism of the beam that has not been corrected for by the cylindrical lens. Plots of the cross-sections in the x- and y-directions are shown in Figures 5-24 and 5-25. In both cases a Gaussian would be a rather poor fit and it would therefore be unreasonable to characterize the spot size using one of the methods described above.

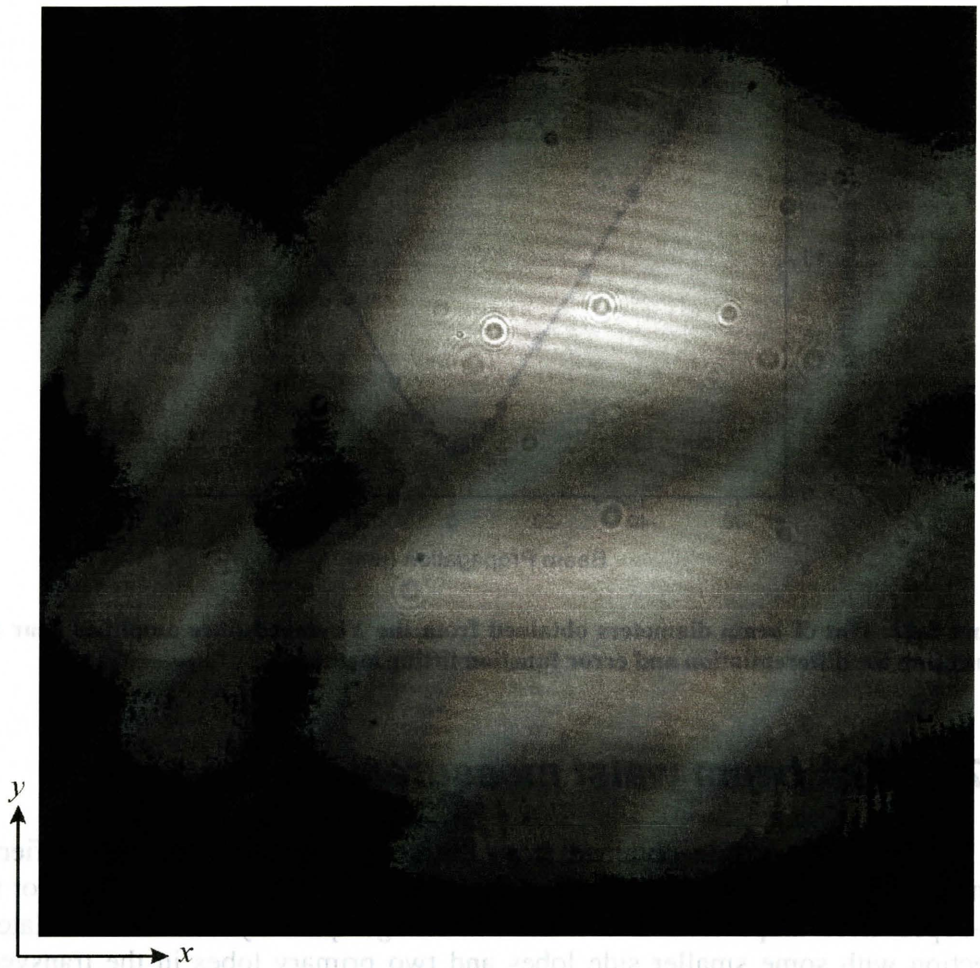

Figure 5-23: Profile of semiconductor optical amplifier beam approximately 4 m from the exit facet. Circular and ribbed structures are an artifact of neutral density filters. The left two lobes are real and not an artifact of the profiler.

In the *x*-direction the $1/e^2$ width is roughly 4.5 mm for the main lobe, and in the *y*-direction it is about 4.75 mm across both primary lobes. In both dimensions the lens is mostly filled and in the transverse direction both of the primary lobes are observed to pass through the lens.

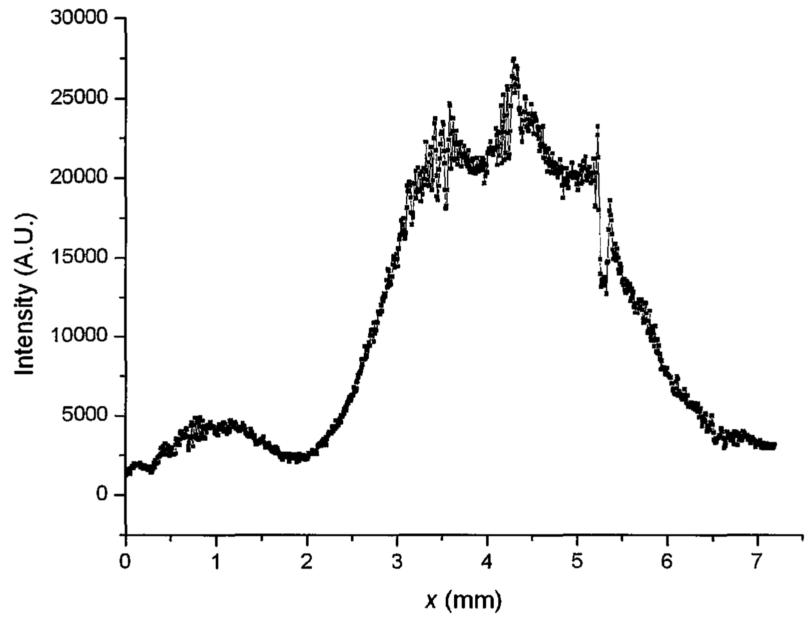

Figure 5-24: Lateral cross-section of SOA output. The large amount of noise is a result of the circular diffraction rings from the beam profiler.

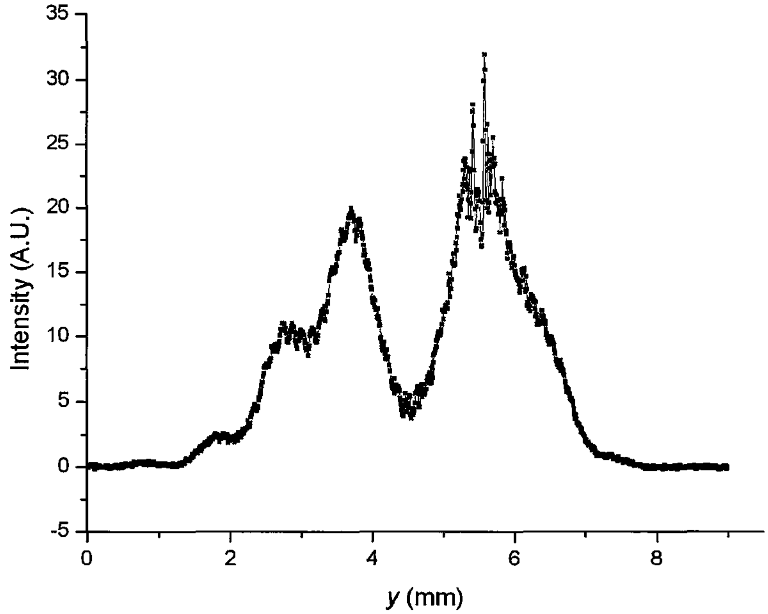

Figure 5-25: Transverse cross-section of the SOA output. The large amount of noise on the right peak is a result of a diffraction ring from the beam profiler.

It is difficult to estimate the size of the focal spot due to the unique beam profile. The diode oscillator has a bandwidth of approximately 2-5 nm when pulsing and amplification in the SOA does not significantly change it. Given the small bandwidth, it will be assumed that neither chromatic dispersion nor pulse front tilt will be an issue. The reasoning for the lack of chromatic dispersion is the same as it was for the Yb-doped fibre, in Section 5.6.1. The angular dispersion out of the SOA was not measured and, therefore, it is possible that pulse front tilt could be an issue in terms of the focal spot.

5.7.1 Measured spot size

In the lateral direction the minimum measured $1/e^2$ beam radius was 1.5 μm and in the transverse direction it was 0.92 μm. The beam width measured in the transverse direction is perhaps the most surprising of all those measured, being the smallest observed. It is possible that there was a confluence of variables that yielded the small dimension such as having measured the absolute minimum, or there being perfect alignment (beam, lens, blade, translation stage) achieved unlike, perhaps, in the other cases. Another possibility is that because the SOA beam fills the lens more than the other sources the full numerical aperture is being used and this results in a smaller spot size. A corroboration of this is that the convergence and divergence angles are greatest in the case of the SOA. The relatively large spot size in the lateral direction may be indicative of a large M^2 value in that dimension. A plot of the convergence and divergence of the beam near the focal region is given in Figure 5-26. Plots of the recovered profiles at the beam waist for both the lateral and transverse directions are given in Figures 5-27 and 5-28. The plots illustrate that the majority of the complex structure of the input beam is essentially not resolved in the focal spot measurement.

An estimation of the M^2 value can be made given the data obtained from the knife edge scans. It is not entirely clear how relevant the value will be given the mode profile. The M^2 parameter is valid for higher order Gaussian mode profiles (Laguerre-Gaussian or Hermite-Gaussian) as well as the fundamental one [86]. As long as the mode can be reduced to a linear combination of Gaussian modes, the parameter does provide relevant information. The overall SOA mode profile does appear to contain elements of higher order terms such as the Hermite-Gaussian TEM_{02} mode [95], [96]. The measured M^2 value in the lateral dimension is found to be 2.0 and in the transverse dimension 1.6. It is surprising that the value in the transverse dimension is so small. However, the beam did focus well in that dimension. Conversely, the M^2 value in the lateral dimension is the largest measured which qualitatively agrees with the large spot size measurement, and this will be further corroborated in Chapter 6.

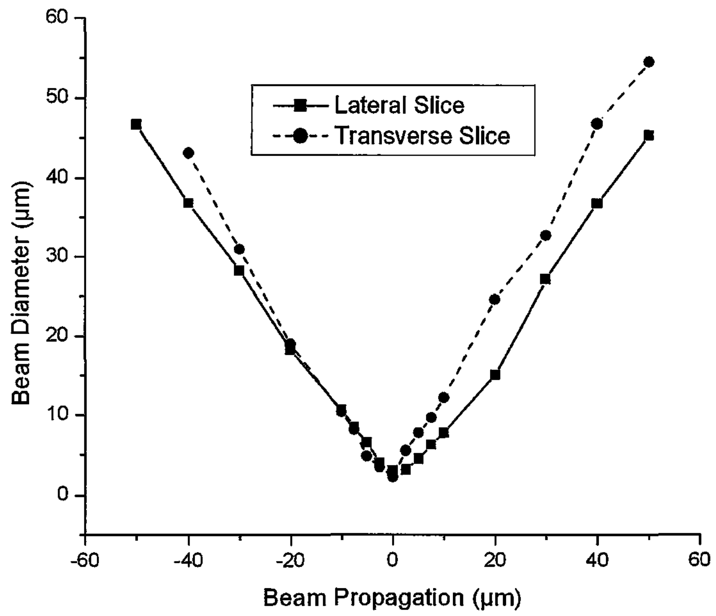

Figure 5-26: Plot of the 1/e^2 beam diameter in the lateral and transverse directions for the SOA.

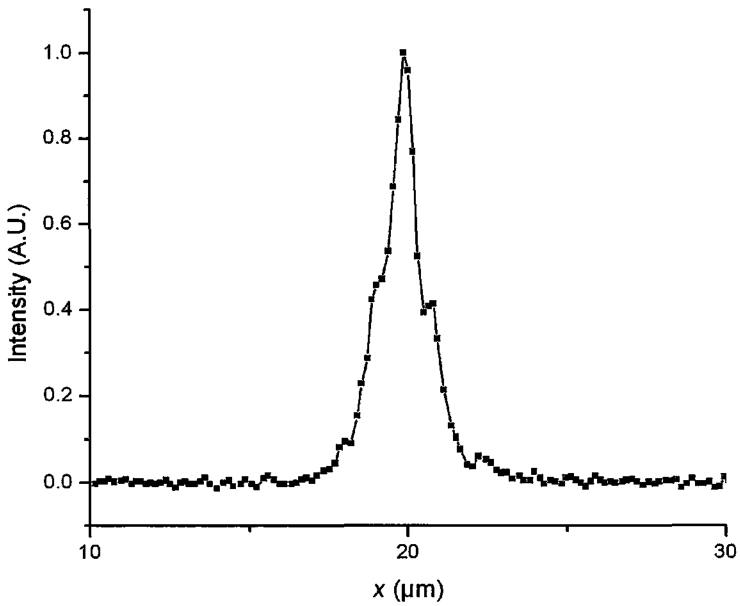

Figure 5-27: Plot of the recovered SOA beam profile in the focus using the differentiation method for the lateral dimension. The 1/e^2 beam diameter = 3.02 μm.

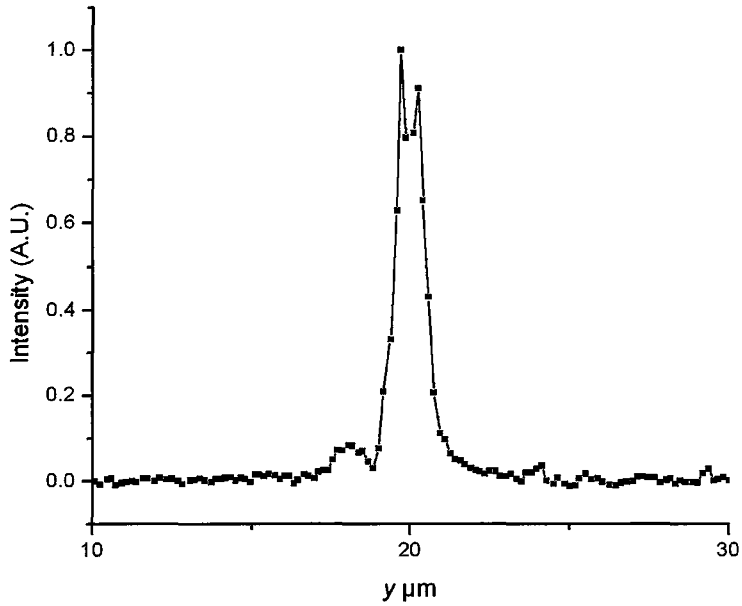

Figure 5-28: Plot of the recovered SOA beam shape in the focus using the differentiation method in the transverse dimension. The $1/e^2$ beam diameter = 1.83 µm.

5.8 Conclusions

The helium neon laser and Yb-doped fibre amplifier focal spot minima were very close to the predicted values while those of the titanium sapphire laser were less so. However, the M^2 value of the laser beam was not explicitly accounted for when predicting the spot size. Including the quality of the mode profile would likely resolve the discrepancy. The results from the SOA were somewhat unexpected. The beam width in the lateral direction of the SOA was somewhat larger than expected given the profile and lens fill factor, while that of the transverse direction (which had the least Gaussian-like profile) yielded the smallest measured spot size. Of the measurements performed the minimum obtained beam waist values are the ones that have been reported in this chapter thus far. This is reasonable because the most obvious sources of error that would confound the measurement would also enlarge the measured spot size, not reduce it. A summary of all of the measured beam waists, when it is believed that the measurement system was functioning adequately, is given in Table 5-1. There are a limited number of values due to time constraints and what were on-going technical issues associated with the beam spot measurements. When the problems were finally resolved, there was time to acquire few sets of data for each source.

Italicized entries indicate that the steps along the z-direction were 10 μm apart. The larger step size reduces the likelihood of having found the true beam waist.

Table 5-1: Table of expected and measured beam waists from knife edge experiments. Italicized entries indicate that measurements near the focus were taken with 10 μm steps along the *z*-axis, not 2.5 μm steps. *"Lat"* refers to the lateral dimension and *"Trans"* refers to the transverse dimension.

	Expected (μm)		***Trial #1 (μm)***		***Trial #2 (μm)***	
Source	**Lat**	**Trans**	**Lat**	**Trans**	**Lat**	**Trans**
HeNe	1.47	1.47	1.50	1.44	*1.46*	*1.57*
Ti:S	0.84	0.95	0.98	1.08	*1.53*	*1.82*
YDFA	1.4	1.4	1.38	1.54	1.41	1.70
SOA	*N/A*	*N/A*	1.51	1.12	*2.0*	*0.92*

The purpose of the above measurements was to determine how much of an impact the beam quality of the SOA would have on its ability to generate two-photon fluorescence as well as the possible resolution in an imaging situation when compared to the standard titanium sapphire laser as well as the better behaved single-mode Yb-doped fibre amplifier beam profile. Given the mode profile, it is difficult to say whether the beam focused as well as expected, given the lack of specific expectations. However, considering the lens fill factor one would reasonably have assumed that the spot size would have been smaller in the lateral dimension than it was measured to be. This is especially true when compared to the measurements obtained in the transverse direction. The data from the SOA suggests that the beam characteristics could be in fact be an issue in terms of a microscopy application. In the lateral dimension, the beam waist and the divergence angle are characteristic of a poorly focused beam. Depending on the dimensions of what is being imaged, this could have a significant impact on both the resolution and the ability to generate fluorescence. Results presented in Chapter 6 also suggest that the beam quality is an issue.

In terms of the Yb-doped fibre, the absolute beam waist that was measured was relatively large, at ~1.5 μm, when compared to the other sources. However, it should be noted that when the measurements were made the beam was slightly converging, resulting in only a partially filled lens. This is in contrast to the SOA which did largely fill the lens. The important point to take from spot size measurement of the YDFA beam is that there was good agreement between the expected beam waist and the measured waist. Also, the measured M^2 value was close to unity. This means that there is no inherent quality of the YDFA output beam that would prevent it from yielding a smaller spot size, which would be ideal for microscopy applications. Filling the back aperture of the lens used in these experiments would reduce the beam waist to below a micron.

It is believed that the ease of matching the expected spot size to the observed one with the helium neon laser was due to its proximity to the measurement setup, its small input waist and its nearly ideal beam shape. The proximity makes the alignment less sensitive to small mirror movements. The smaller input beam width of the HeNe laser greatly reduces the convergence angle making it easier to make a measurement near the minimum. Finally, the visible wavelength and smaller beam size made it easier to ensure that the laser was traveling through the center of the lens to achieve optimal focusing. Some improvements to the measurement setup that were not possible at the time the experiments were performed would be to move the sources closer to the measurement setup (or vice versa), and use a more finely controlled stage in both the scanning direction and the z-propagation direction.

Work could have been done to try to standardize the beam size by enlarging or reducing it by way of a telescope. By overfilling the back of the lens with the laser light the measured spot sizes would be reduced and it would approach the plane wave minimum. In such a case the differences between the beam waists would be essentially due to the different wavelengths of the sources. Ideally this is what would be done in an actual microscope. However, in an attempt to characterize the expected performance of the current SOA in a microscopy situation, it is important to realize that there is insufficient available power to overfill the back aperture of the lens while still being able to generate sufficient fluorescence.

The focal spot measurements were done in air. While the beam waist should remain close to the same value when focusing in a sample [97], it is important to match the index of refraction of the immersion medium (typically air, water or oil fills the gap between the sample and the objective lens) with that of the sample to minimize spherical aberration and other distortions associated with index mismatch [98]-[100].

Chapter 6 Two-Photon Fluorescence Results

6.1 Introduction

In this section the results of the two-photon fluorescence generation from the three excitation sources will be discussed. The purpose of the work here is to determine the suitability of the diode oscillator, semiconductor optical amplifier (SOA) and Yb-doped fibre amplifier (YDFA) as sources for two-photon fluorescence microscopy (TPFM). To determine the suitability it was decided to compare the fluorescence generating efficiency of both amplifiers to the Ti:Sapphire laser standard. The efficiency is defined, essentially, as the α parameter of Equation (6.1).

$$I_f = \alpha P_{exc}^2 \tag{6.1}$$

The I_f term is the time averaged generated fluorescence, and P_{exc} is the average excitation power. Comparing the sources would give an indication of what the costs are of moving to one of either the SOA or YDFA as a two-photon excitation source, and also, where improvements need to be made.

6.2 Experimental setup

The general layout of the setup used to excite the fluorophore and collect the generated fluorescence is given in Figure 6-1. It consists of the two-photon excitation source, a lock-in amplifier, focusing and collection lenses and a photomultiplier tube. Light from one of the excitation sources, SOA, YDFA or Ti:Sapphire laser, is focused using a 0.55 NA Thor Labs C230TM-B AR-coated aspheric lens into a 1 cm x 1 cm x 5 cm quartz cuvette containing the fluorescent dye solution. Generated fluorescence is collected and collimated by a 0.25 NA Thor Labs C220TM-B AR-coated aspheric lens where it passes through a 1 mm thick Schott Glass BG39 short pass filter to remove any scattered excitation light. Light is detected by a Hamamatsu R6358 photomultiplier tube. The signal is amplified by a lock-in amplifier and can be recorded by a data acquisition computer if desired. The excitation intensity is adjusted using a half-waveplate/Glan Thompson polarizer pair placed near the focusing lens. Having the polarizer close to the focusing stage ensures that the polarization of the excitation signal is constant for all three sources.

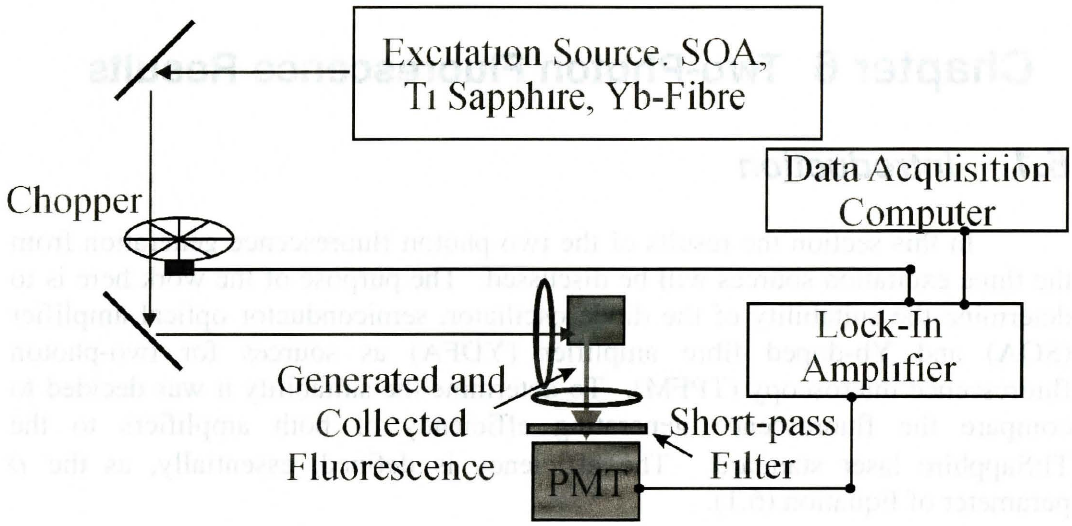

Figure 6-1: Simplified schematic of two-photon fluorescence excitation and collection measurement system. Details of the sources can be found in Chapter 4.

The decision to make the fluorescence collection arm perpendicular to the excitation direction (as opposed to an epi-fluorescence setup) was made to reduce the amount of excitation laser light that would be measured by the PMT and also to eliminate the need for an expensive dichroic mirror to separate the excitation signal from the fluorescence signal. This approach does have some disadvantages, the primary one being alignment. It can be difficult in practice to get the acceptance volume of the collecting lens to overlap with the focal region of the source lens when working with a relatively weak signal. Also, a high NA lens cannot be used to collect the fluorescence due to space constraints near the cuvette. This reduces the collection efficiency of the system which makes detection of weak signals more difficult.

Care needed to be taken to align the excitation beam such that the fluorescence would be generated near the collection-lens side of the cuvette. Doing this reduces the amount of fluorescence re-absorbed or scattered by the dye and hence improves the measured signal.

6.3 Fluorophore properties

The bulk of TPF measurements were made with the common laser dye Rhodamine 590 Chloride (also known as Rhodamine 6G, a well known biological marker) from Exciton. It was chosen because of its relatively low cost, presumed low to moderate toxicity and reasonably high fluorescence efficiency The purchased Rhodamine 590 Chloride was dissolved in methanol to make the final dye solution. A number of different concentrations were attempted in order to find the one that maximized the fluorescent yield. The concentration that yielded the highest signal was found to be 1 x 10^{-2} mol/L.

The laser dye Kiton Red was also tested. However, the fluorescence yield tested at a number of concentrations was lower than that of Rhodamine 6G suggesting that the two-photon cross-section was smaller. Little work was performed with this dye due to the low fluorescence yield.

The fluorescence yield is partly determined by the two-photon excitation cross-section of the dye which is strongly wavelength dependent. It will be important to know the cross-section when comparing the performance of the different excitation sources because the Ti:Sapphire laser operates at 800 nm while the other two operate at around 1075 nm. The most recent published value for Rhodamine 6G at 800 nm is 36 ± 6 GM and 4.0 ± 0.8 GM (units defined in section 2.4.2) at 1064 nm [50], [102], [103]. (Note: The author of the paper that reported the cross-section at 1064 nm uses a slightly different definition of the two-photon cross-section. This leads to a factor of two discrepancy when comparing values. This difference has been accounted for in the values listed here.) The value at 1064 nm is assumed to be close enough to the 1075 nm operating wavelength that there is not a significant difference in the cross-section values.

Two experiments were performed to ensure that photobleaching would not be an issue. Approximately 50 mW of average power from the Ti:Sapphire laser (80 MHz repetition rate, ~200 fs pulse duration) was focused into the cuvette with a dye concentration of 5 x 10^{-4} mol/L for about 5 hours. The 50 mW average power was several times greater than what was typically used in other experiments. The 5 x 10^{-4} mol/L dye concentration was about two orders of magnitude lower than what was used in the majority of the two-photon excitation studies. At the elevated excitation power and reduced concentration any bleaching or saturation effects would be expected to be apparent. There was no evidence of a signal decrease due to bleaching. Measurements were also made to ensure that there were no saturation effects. The expected intensity-squared dependence was observed for excitation powers around 50 mW.

The dye was excited by both the Ti:Sapphire laser (800 nm) and YDFA (1075 nm) to verify that there was no difference in the emission spectrum. This may have been a concern regarding the wavelength response of the PMT. Plots of the spectra are given in Figure 6-2. The noisier data is that from the Yb-doped fibre amplifier which generated a much weaker signal than that of the Ti:Sapphire laser. It can be seen that there is essentially no difference between the two spectra.

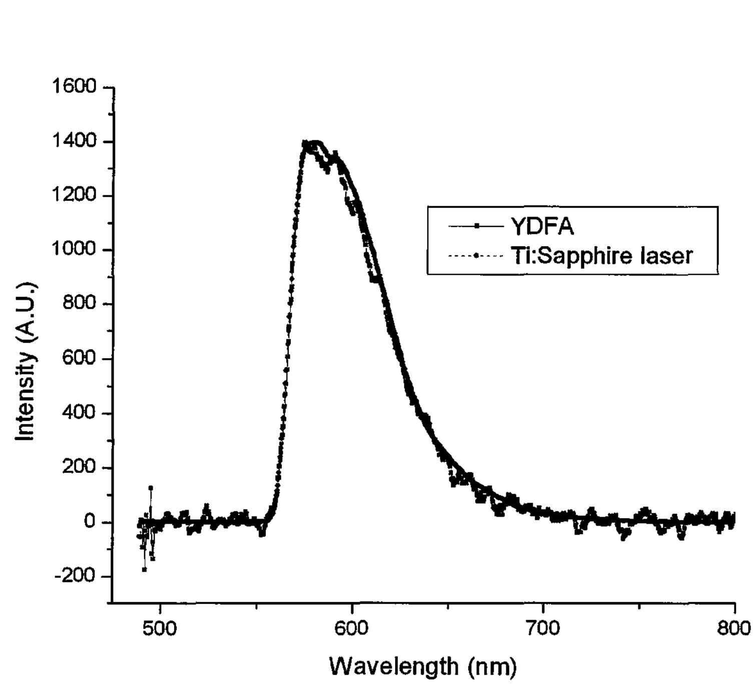

Figure 6-2: Rhodamine 6G (Rhodamine 590 Chloride) emission spectra when excited at 800 nm by the Ti:Sapphire laser and 1075 nm by the ytterbium-doped fibre amplifier.

6.4 Fluorescence Dependence on Intensity

To ensure that the measured signal is truly coming from two-photon generated fluorescence, a squared dependence should be observed with respect to the average input power (known as the I^2 dependence). A less than square dependence suggests that there is some single-photon fluorescence being generated or that excitation photons are being detected by the PMT. It could also indicate a saturation of the dye (though this was experimentally ruled out).

Figures 6-3 to 6-5 illustrate the I^2 dependence of the fluorophore when excited by the Ti:Sapphire laser, Yb-doped fibre amplifier and SOA, respectively. The excellent fits demonstrate that there is no one-photon absorption and that the excitation signal is being effectively blocked.

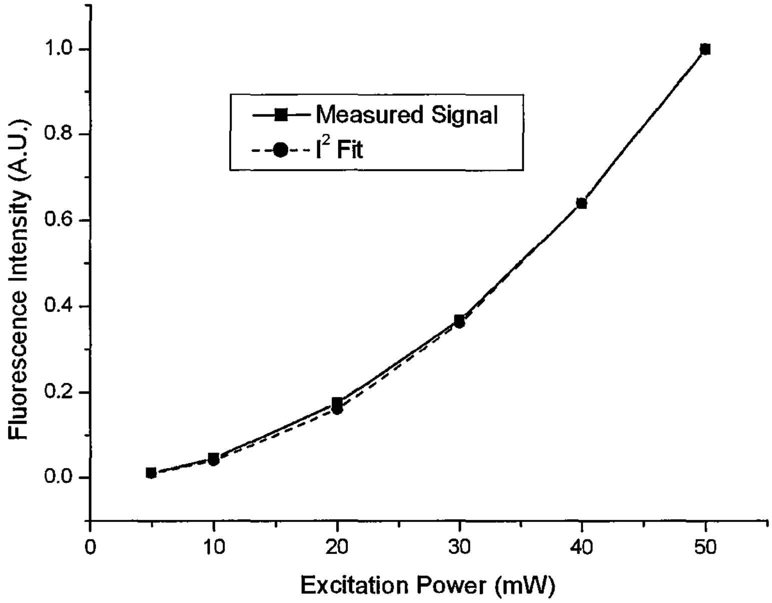

Figure 6-3: Plot of the two-photon fluorescence dependence on intensity for the case of the Rhodamine 6G dye solution being excited by the Ti:Sapphire laser source. The data closely follows the expected square dependence.

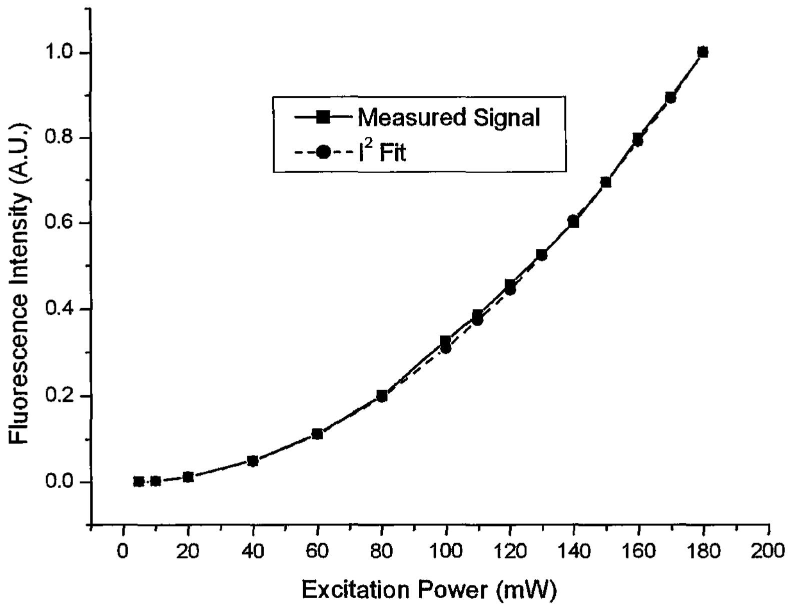

Figure 6-4: Plot of the two-photon fluorescence intensity dependence for the case of the Rhodamine 6G dye solution being excited by the Yb-doped fibre amplifier source. The data closely follows the expected square dependence.

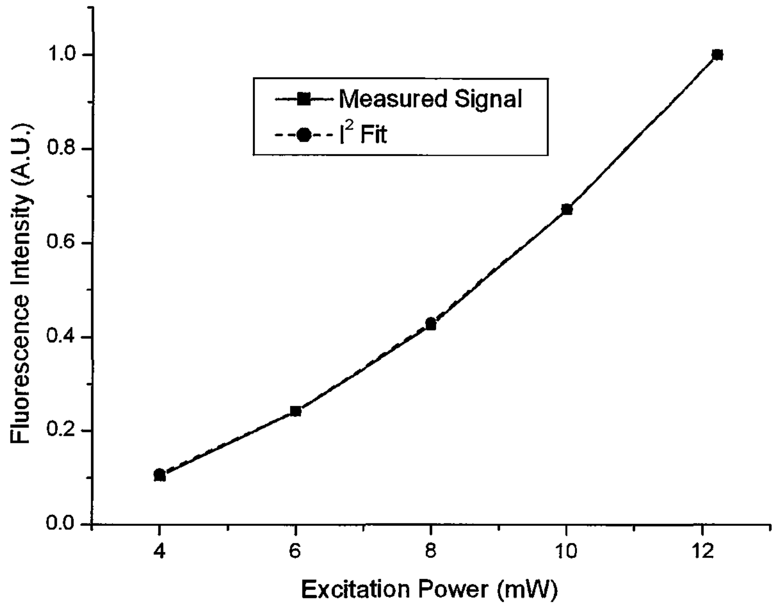

Figure 6-5: Plot of the intensity dependence for the case of the Rhodamine 6G dye solution being excited by the semiconductor optical amplifier source. The data closely follows the expected square dependence.

6.5 Confirmation of expected signal

As mentioned in Section 2.4.2 and described in Equation (2.6) (repeated below for convenience) the fluorescence signal in a bulk sample varies with average input power, pulse duration and repetition rate.

$$\left\langle I_{f,pulse} \right\rangle \propto \frac{g_p \delta_2 n \pi P_{avg}^2}{\tau_p f_p \lambda} \tag{2.6}$$

were changed so that it operated in a number of different regimes. To verify that this relationship provided accurate predictions of fluorescent yield, the operating parameters of the diode oscillator. By adjusting the forward bias, reverse bias and the external cavity of the oscillator it is possible to change the mode-locking conditions relatively easily. The output of the oscillator was amplified with the Yb-doped fibre. The operating conditions of four different regimes are given in Table 2-1. The pulse durations were obtained from an autocorrelation measurement, the temporal pulse shape was assumed to be Gaussian.

Table 6-1: Operating properties of the Yb-doped fibre amplified mode-locked diode laser.

Trial #	Rep Rate (GHz)	Pulse Duration (ps)	Peak Wavelength (nm)
1	2.313	6.8	1073
2	2.883	6.1	1073
3	1.160	8.0	1072
4	0.580	5.9	1072

The analysis was performed by comparing the relative change in the generated fluorescence when the operating conditions were altered (i.e. pulse duration, repetition rate) to what one would expect the change to be. Regime #4 is taken as the reference value. Results and the relative difference between the expected and measured values are given in Table 6-2.

Table 6-2: Ratio of expected and measured fluorescence intensity to a baseline value obtained with the mode-locked diode laser amplified by the Yb-doped fibre amplifier.

Fluor. Inten. Ratio	Expected	Measured	Error
#1/#4	0.219	0.213	2.7%
#2/#4	0.193	0.201	4.1%
#3/#4	0.394	0.370	6.1%

The measured and expected values were essentially the same and indicate that the system behaved as expected. Therefore, observed discrepancies between expected and measured fluorescence signals when comparing different excitation sources can be attributed to variables such as wavelength, cross-section, and alignment among others.

6.6 Comparison of Ti:Sapphire laser and YDFA as two-photon excitation sources

To determine whether the amplified diode oscillator can be expected to be a reasonable replacement for a titanium sapphire laser source it is important to quantify the difference in fluorescence generation efficiency that is observed. The output of the diode oscillator has a longer pulse duration and a higher repetition rate than the Ti:Sapphire laser, both of which lower the fluorescence generation efficiency. When amplification is performed with the Yb-doped fibre the pulse will be temporally stretched due to dispersion. The longer pulse reduces the peak intensity, requiring more average power to generate the equivalent amount of fluorescence. However, if one is willing to add some complexity to the system the pulse can be recompressed to its original duration (or shorter) by a variety of means.

Knowing the fluorophore cross-section, the average power, pulse duration and repetition rate, the Yb-doped fibre amplifier and the Ti:Sapphire laser can be compared to one another. A direct and relatively accurate comparison between the SOA and the Ti:Sapphire laser could not be made because in order to generate enough power from the SOA the oscillator needed to be tweaked in such a manner that mode-locking characteristics such as repetition rate, pulse duration and pulse shape were not easily defined with the devices used (this was much more of an issue toward the end of the experimental work when most of the measurements presented here were made). For example, an autocorrelation trace may not yield the expected smooth curve, but instead one with features (illustrated in Figure A-3). Such a trace indicates a large deviation from the assumed Gaussian temporal pulse shape of the Ti:Sapphire laser pulses. Without knowing the pulse shapes of the sources, for example, there would be little point in pursuing a direct comparison between the Ti:Sapphire laser and the SOA.

As stated in Section 2.4.2, the beam waist does not have an impact on the amount of fluorescence generated if the beam profile is Gaussian and the sample thickness is much larger than the Rayleigh range. However, a large beam spot can impact the amount of fluorescence measured, especially in the collection geometry used (the collection lens at a right angle to the excitation lens). The collection lens used in these experiments has an NA of 0.25, a clear aperture of 5.5 mm and a focal length of 11 mm. The measured beam waists of the Ti:Sapphire laser and YDFA were ~1 μm and ~1.5 μm respectively. The refractive index of methanol is approximately 1.3. In the paraxial approximation the Rayleigh range of a beam in a material is nz_R, where n is the index of refraction and z_R is the Rayleigh range in air [97]. Ashcom shows that the error associated with using the paraxial approximation for a 0.55 NA lens is ~10% [97]. Due to the moderate error, the paraxial approximation will be sufficient here. The Rayleigh range of the YDFA is about 1.7 times larger than that of the Ti:Sapphire laser. The axial extent over which approximately 90% of the fluorescence is generated is about 10 Rayleigh ranges, or ~ 50 μm for the Ti:Sapphire laser and ~ 85 μm for the YDFA in the dye solution. Given the properties of the collection lens, this small change in the length over which the fluorescence is generated will not have a significant impact on the fluorescence collection efficiency. Therefore, the ratio of the fluorescence generated by the Ti:Sapphire laser to the Yb-doped fibre amplifier can be given by

$$\frac{\left\langle I_{f-Ti:S}\right\rangle}{\left\langle I_{f-YDFA}\right\rangle} \propto \frac{\dfrac{g_{p-Ti:S}\delta_{800nm}}{\tau_{Ti:S} f_{Ti:S} \lambda_{Ti:S}}}{\dfrac{g_{p-YDFA}\delta_{1075nm}}{\tau_{YDFA} f_{YDFA} \lambda_{YDFA}}} = \frac{\delta_{800nm}\tau_{YDFA} f_{YDFA} \lambda_{YDFA}}{\delta_{1075nm}\tau_{Ti:S} f_{Ti:S} \lambda_{Ti:S}} = \frac{10\tau_{YDFA} f_{YDFA} \lambda_{YDFA}}{\tau_{Ti:S} f_{Ti:S} \lambda_{Ti:S}} \tag{6.2}$$

where we assume that the temporal pulse shape is the same for both the Ti:Sapphire laser and the Yb-doped fibre amplifier. As stated in Section 6.3 the two-photon cross-section of the Rhodamine 6G is approximately ten times larger at 800 nm than it is at 1064 nm, which is assumed to not be significantly different than it is at 1075 nm. A sample comparison between the YDFA and Ti:Sapphire is made where the FWHM of the pulse duration of the Ti:Sapphire laser is approximately 205 fs. The repetition rate is 80.5 MHz and the wavelength is centered at 800 nm. In a data set taken with the Yb-doped fibre the repetition rate was 575 MHz, wavelength 1073 nm and an autocorrelation FWHM width of 10.2 ps. If we assume a Gaussian pulse shape, the actual pulse width is 7.21 ps. With these values the Ti:Sapphire laser should generate about 3400 times more fluorescence than the Yb-doped fibre for the same average excitation power. The amount of fluorescence generated by Ti:Sapphire laser was found to be ~ 4550 times greater than that obtained from the YDFA source. The discrepancy between the expected and measured values is about 35%.

This result appears to demonstrate good agreement given that there are a number of potential sources of uncertainty. There are questions as to how similar the temporal pulse shapes of the two sources in fact are. Previous work has suggested that the pulse shape out of the Yb-doped fibre amplifier is likely asymmetric and a pulse shape retrieved from the Ti:Sapphire laser revealed structure that deviates from the assumed Gaussian temporal shape [71]. The different pulse structures should affect the fluorescence yield to some degree, though it cannot be easily quantified. It was assumed that the cross-sections at 1064 nm and 1075 nm are the same. This should be reasonable but it was not corroborated. Also, there is variation in the reported values of the two-photon cross-sections and each reported value has a listed uncertainty of about 20%. Both sources demonstrated somewhat large fluctuations in day-to-day fluorescence yield that appeared to be a result of alignment changes. Due to the large distances traveled by the excitation beams a small change in a mirror near the source manifests itself as a large change in the beam position. When trying to maximize the signal, not necessarily the correct mirror will be adjusted. This can lead to different local maxima being used for measurements. Also, the different excitation source beams were not collinear. When switching between sources a number of mirrors needed to be adjusted to maximize the signal. When returning to a previous excitation source it can be very difficult to achieve the exact same alignment. This results in day-to-day variations in apparent fluorescent efficiency even when the pulse properties have remained the same. It is assumed to be an alignment issue because the fluorescence yield with the dye excited by the Ti:Sapphire laser could fluctuate significantly day-to-day, even though the pulse characteristics did not. Nor were there any significant differences in the system layout. Also, as demonstrated in Section 6.5 with the YDFA, the expected fluorescence yield matched the measured yield relatively well when only the mode-locking conditions are changed. When the fluorescence efficiency of the Yb-doped fibre amplifier is compared day to day (taking into account pulsing conditions) the expected and measured values between days do not agree particularly well.

Due to time constraints there are only two sets of data that compare the performance of the Ti:Sapphire laser to the YDFA. One set of data is described above. In the other, the Ti:Sapphire laser would have been expected to generate about 3200 times more fluorescence than the YDFA (for the measured operating conditions, and at a specific average excitation power). The fluorescence signal was measured to be 2100 times greater, a ~35% difference. In this latter case the YDFA outperformed the Ti:Sapphire, opposite of the first data set. Given that the setup and the measurement techniques were essentially the same for these two trials, the range over which the deviation of the expected and measured fluorescence yields varied was quite large. The value of these measurements is essentially to illustrate, to within a factor of two, the degree to which the ability to efficiently generate fluorescence differs between the current Yb-doped fibre amplifier setup and the Ti:Sapphire laser. From the above data, the Ti:Sapphire laser was able to generate more than three orders of magnitude more two-photon fluorescence than the YDFA with the dye and operating conditions available at the time of the experiments. Courses of action to reduce this disparity will be discussed in Chapter 7.

6.7 Comparison of YDFA and SOA as two-photon excitation sources

Comparing the fluorescence generation efficiency of the SOA to the YDFA is easier than comparing it to the Ti:Sapphire laser because both sources are operating at the same wavelength, repetition rate, and the temporal pulse shape should be similar. Essentially the only difference between the two sources is the pulse length and the spatial beam profile. The pulse length of each source is easily measured. As stated in Section 6.6, in order to generate sufficient power from the SOA it is necessary to have at least one mW of average power from the oscillator. At the time these experiments were performed the laser oscillator being used had an average power, when it was mode-locked in a well defined manner, of approximately 300 μW, which was insufficient to saturate the ASE of the SOA (this was a property of the one particular oscillator used toward the end of experimental work, other devices have exhibited good mode-locking parameters with an average power greater than one mW [4]). To generate the desired ≥1 mW of average power the oscillator needed to be tuned to a regime with poorly defined properties of operation. The autocorrelation trace was not well behaved and is given in Figure 6-6. The lack of well defined operating parameters is the same for both the YDFA and the SOA which allows them to be compared to one another on an equal footing. As can be seen the autocorrelation traces contain quite a bit of structure. However, they are essentially the same for both amplifiers except in the fibre case, the pulse is stretched. Measuring the width of each autocorrelation trace will provide an adequate measure of the difference in "pulse length". The difference in pulse width of the Yb-doped fibre amplifier and SOA was measured at a number of places on the autocorrelation trace. The consistent result is that the pulse duration from the YDFA is ~40% longer than from the SOA.

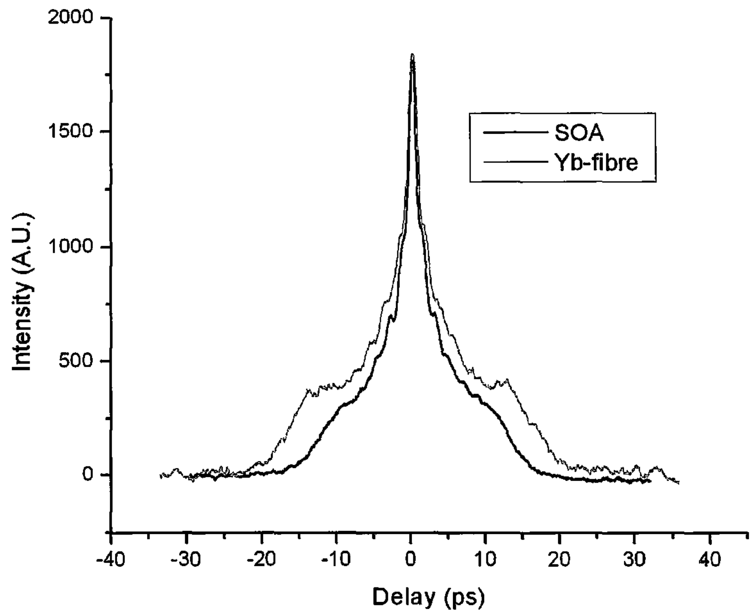

Figure 6-6: Autocorrelation traces of the mode-locked diode oscillator amplified by the semiconductor optical amplifier and the ytterbium-doped fibre amplifier.

The SOA beam waist was found to be small in the transverse direction (0.9 μm) while somewhat larger in the lateral dimension (1.5 μm). The beam waist of the Yb-doped fibre amplifier was to be ~1.5 μm in both dimensions. It should be noted that spot size measurements and fluorescence measurements were made months apart. Therefore there may be a discrepancy in terms of the actual spot size at the two different times. This is most likely true in the case of the Yb-doped fibre. When the spot size measurements were made the beam was converging slightly, resulting in only partial filling of the lens (a $1/e^2$ beam diameter of ~ 4.4 mm). At the time of the fluorescence measurements the beam filled the lens more fully (an estimated $1/e^2$ beam diameter of ~ 5 mm). The greater filling should result in a reduced focal spot size. However, as discussed in Section 2.4.2 the total fluorescence generated in a bulk sample by a focused Gaussian (or plane wave) beam is independent of the beam waist. On the surface this suggests that the mode quality and resultant beam waist of the SOA will have no effect on the measured fluorescence signal in these experiments. That assumption, however, neglects to account for potential problems that may arise from the way the energy is distributed near the focus. It is unclear that the independence of beam waist and fluorescence generation holds for a beam profile such as that of the SOA. A simple, and likely not physical, example of the generated fluorescence being dependent on the beam waist is a uniform intensity distribution. Assume that all of the energy at a given axial cross-section is fully contained within a circle of a certain diameter and is distributed uniformly. Assume also that the diameter, as a function of z, propagates the same way as the $1/e^2$ diameter does in a focused Gaussian beam. If we simulate the generation of two-photon fluorescence and integrate over the entire volume we find that the total fluorescence generated varies as $1/w_0^2$, where w_0 is the minimum radius of the focused beam. In essence, this illustrates that one cannot say that the excitation energy can be distributed randomly within the dye cell and if we integrate over a large enough volume we will always achieve the same amount of two-photon generated fluorescence. A model of the focused SOA beam is beyond the scope of this work and was not attempted. However, some measurements were made that may quantify the effect to a certain degree.

6.7.1 Beam quality effects on fluorescence generation efficiency

In Figure 5-23 (on page 59) it is apparent that the light is propagating in two primary transverse lobes and a primary lateral mode, though a secondary lateral mode is visible. If this light does not focus well it will not contribute to the generation of fluorescence and reduce the apparent efficiency of the SOA. In Section 5.7.1, the measured minimum spot size in the lateral direction is quite a bit larger than in the transverse direction, suggesting that light is not focusing well in that dimension. Experiments, performed before the spot size measurements were taken, explored the effect of spatially filtering the beam in both the transverse and lateral dimensions and measuring the fluorescence generation efficiency. The unfiltered beam is shown in Figure 6-7. Though the profile is somewhat different, the prominent transverse profile is similar to Figure 5-23 as are the partially excited secondary lateral modes. The mode profile is likely different from that of Figure 5-23 due to slightly different coupling of the laser oscillator beam into the SOA and also the aging and degradation of the device over time. By slightly adjusting the coupling of the laser oscillator beam it is possible to more efficiently excite the higher order lateral modes.

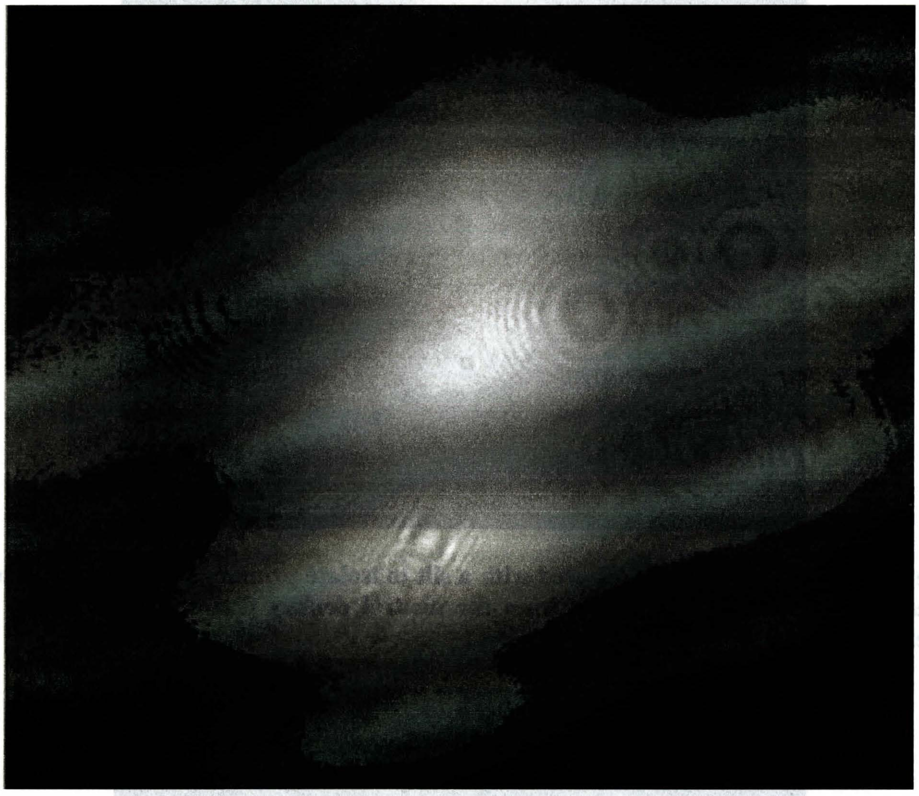

Figure 6-7: Unfiltered beam profile of semiconductor optical amplifier. Circular profiles are a result of interference from the neutral density filters in front of the beam profiler

In these experiments the SOA beam was spatially compressed by a factor of two by using a pair of positive lenses setup as a telescope. The beam was laterally filtered by passing it through a slit to remove the energy outside the main lateral profile. Finally, a single transverse lobe was selected by clipping the laterally filtered beam with a razor blade. The laterally filtered beam is shown in Figure 6-8, while the beam filtered in the lateral and transverse direction is shown in Figure 6-9

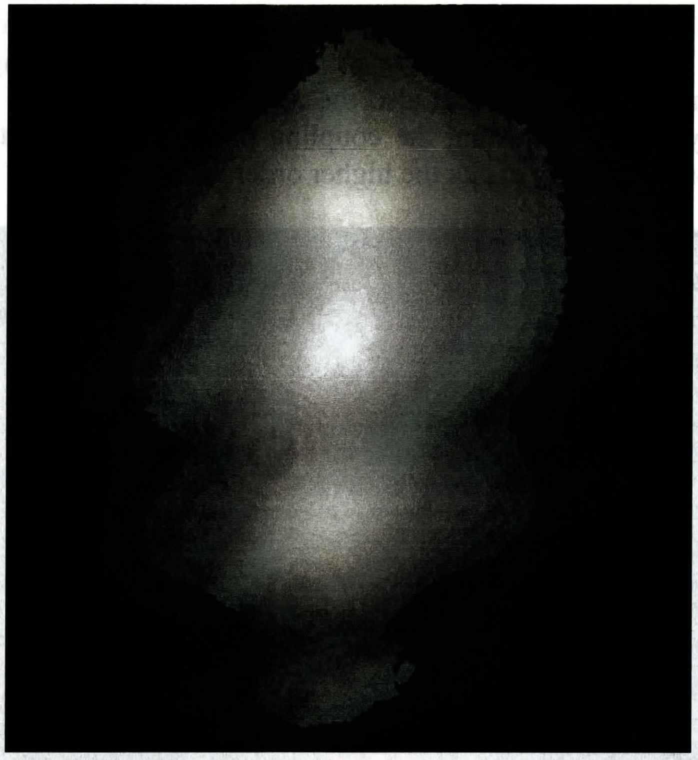

Figure 6-8: SOA beam laterally filtered with a slit to isolate primary lateral mode. Circular profiles are a result of interference from the neutral density filters in front of the beam profiler.

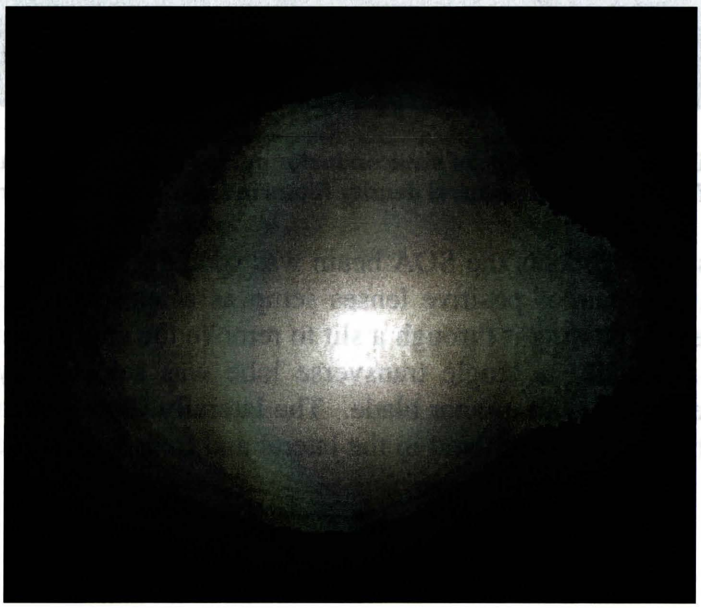

Figure 6-9: SOA beam filtered in the lateral and transverse dimensions to isolate a single lobe. Circular profiles are a result of interference from the neutral density filters in front of the beam profiler

The oscillator operated at 683 MHz at ~1075 nm with a pulse duration of ~1.2 ps (assuming a Gaussian profile). Filtering in the lateral direction removed approximately half of the beam power. The fluorescence generation efficiency after laterally filtering the beam increased by a factor of about 2 when compared to the unfiltered beam. Previous measurements of the SOA, when operating in this regime, have shown that approximately 10% of the power emitted is amplified spontaneous emission (ASE), which would not contribute to TPE. Clearly, it is not simply the removal of spatially distinct ASE from the beam that is resulting in the improved efficiency. Further filtering in the transverse dimension (such that the beam was filtered both laterally and transversally) reduced the power by another factor of 2. The fluorescence generation efficiency of the laterally and transversely filtered beam was about 2.7 times greater than the unfiltered beam. Filtering the lateral profile had a larger effect than filtering in the transverse dimension. This is consistent with the observations from the spot size measurements that the beam does not focus as well in the lateral dimension as in the transverse direction. This suggests that the focal properties in the lateral dimension are quite a bit different than those of a Gaussian beam profile, perhaps more so than in the transverse dimension.

6.7.2 Results of pinhole filtering of the SOA beam

At the very end of in-lab work, some preliminary experiments were performed to try to qualitatively determine what could be expected from filtering the SOA beam by focusing it through a fixed aperture pinhole. In these experiments the beam from the SOA was focused through a 10 μm diameter pinhole with a 5x microscope objective. The light was recollimated by a 0.4 NA aspheric objective. Images of the pre- and post-filtered profiles are given in Figures 6-10 and 6-11, respectively. Approximately 54% of the light is transmitted through the pinhole. After collimating, the overall throughput efficiency is 50%. In Figure 6-11 it can be seen that there is a diffraction halo around the primary mode of the beam (the full extent of the halo is not clear in the black and white figure). An adjustable iris was used to remove the halo; an image is given in Figure 6-12. The total efficiency of the filtering system from power into the lens to the power measured after the adjustable iris is ~37%. Due to limited time and available resources, further experiments were not performed. Lateral and transverse plots of the profile in Figure 6-12 with a Gaussian fit are shown in Figures 6-13 and 6-14, respectively. It can be seen that the profile is much improved.

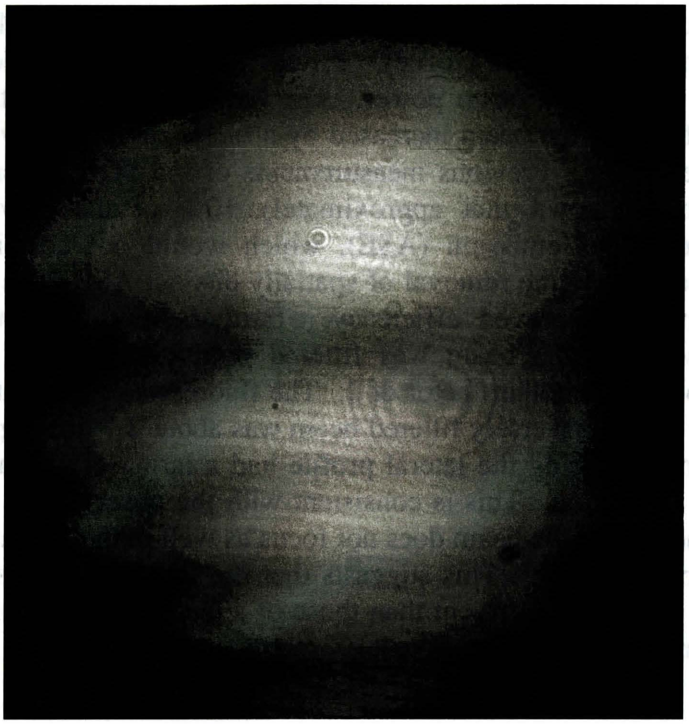

Figure 6-10: SOA beam profile before pinhole spatial filtering.

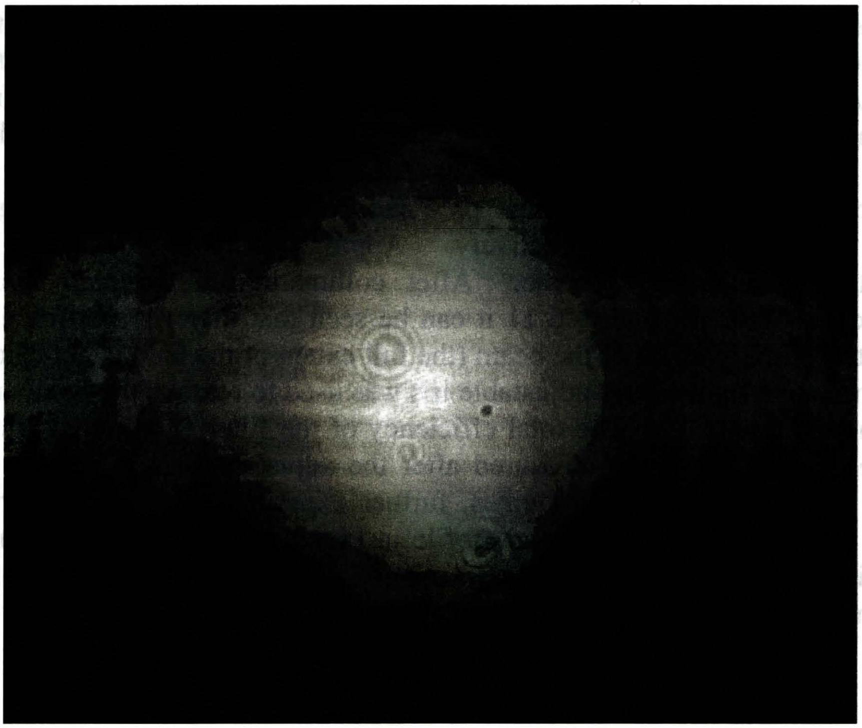

Figure 6-11: SOA beam filtered by focusing through a 10 µm diameter pinhole with a 5x microscope objective.

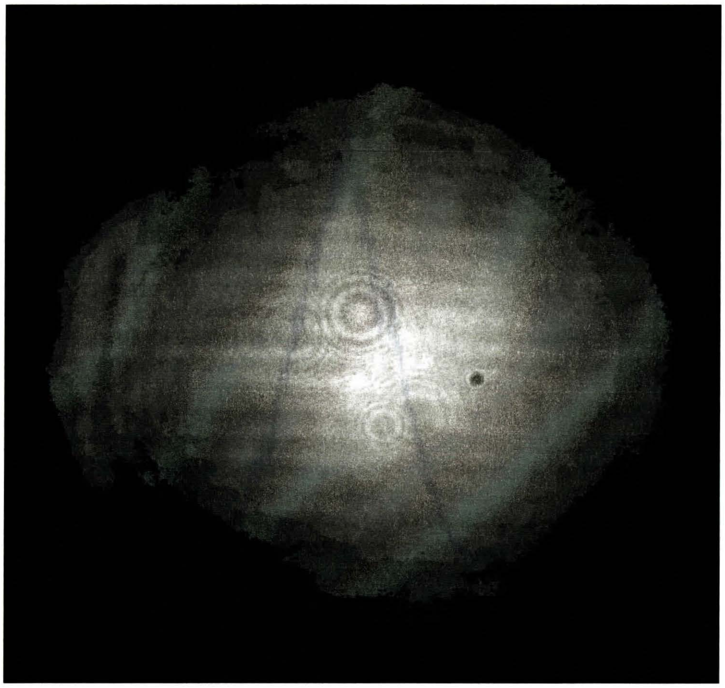

Figure 6-12: SOA beam filtered by focusing through a 10 μm diameter pinhole with a 5x microscope objective and filtering the scattering light with an adjustable iris. The systems demonstrates a throughput of about 37%

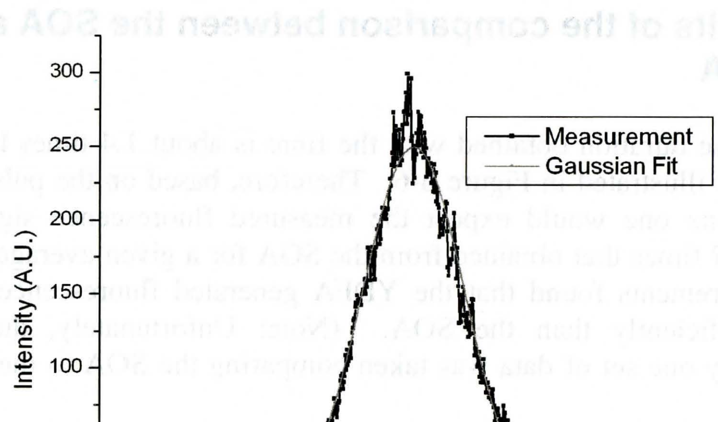

Figure 6-13: Lateral cross-section of the SOA beam focused through a 10 μm aperture with a 5x objective. Included is a Gaussian fit.

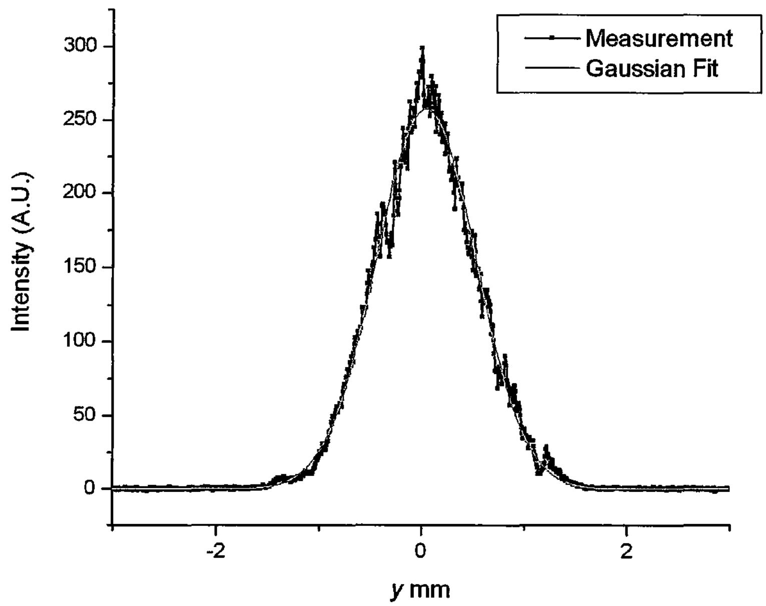

Figure 6-14: Transverse cross-section of the SOA beam focused through a 10 μm aperture with a 5x objective. Included is a Gaussian fit.

6.7.3 Results of the comparison between the SOA and YDFA

The pulse duration obtained with the fibre is about 1.4 times longer than for the SOA, as illustrated in Figure 6-6. Therefore, based on the pulse duration comparison alone one would expect the measured fluorescence signal of the YDFA to be 0.7 times that obtained from the SOA for a given average excitation power. Measurements found that the YDFA generated fluorescence about 1.2 times more efficiently than the SOA. (Note: Unfortunately, due to time constraints, only one set of data was taken comparing the SOA to the Yb-doped fibre.)

The difference between the expected and measured fluorescence efficiencies is somewhat large in this case. There are a number of possible contributors to this discrepancy. There are the same alignment issues that were of concern when comparing the Ti:Sapphire laser to the Yb-doped fibre amplifier. And, as discussed in Section 6.7.1, there appears to be a portion of the SOA beam that does not significantly contribute to the excitation of the fluorescent dye. Though the operating conditions of the oscillator and the mode profile of the SOA in Section 6.7.1 are not the exactly the same as those from the measurement discussed here, they are similar enough to make it reasonable to suggest that the same beam profile may be having an effect on the fluorescence efficiency.

6.8 Conclusion

The measurements in this section give an idea of how much the focusing behaviour and other characteristics of the sources are likely to affect their suitability for two-photon microscopy and other applications. There are a number of parameters that influence the fluorescence yield that are not easily measured such as the precise shape of the temporal pulse envelope, the beam propagation and profile in the sample near the focus, and other characteristics that need to be taken into account to fully describe the generation of fluorescent light. As was stated in Section 6.6, a fair and direct comparison of the SOA to the Ti:Sapphire laser was not possible, but they can be compared indirectly. The Ti:Sapphire laser generated fluorescence with an efficiency three orders of magnitude greater than the YDFA for the same average excitation power (largely as a result of the lower repetition rate, shorter pulse duration and larger two-photon cross-section), while the SOA and YDFA generated fluorescence with roughly the same efficiency (the shorter pulse duration compensating for the poorer mode quality). Therefore, one could conclude that the Ti:Sapphire laser generates fluorescence with an efficiency three orders of magnitude greater than the SOA (again, largely due to the lower repetition rate, shorter pulse duration and greater two-photon cross-section). In the current configuration, the effect of the higher peak power and pulse energy of the Ti:Sapphire laser greatly outweighs the effect of the poor mode profile of the SOA when generating fluorescence in a bulk sample. The impact of the larger beam waist and poor beam quality would likely be larger in a microscopy situation where signal is not integrated over a large volume. This has significant consequences on the feasibility of the SOA being used as a two-photon excitation source in its current configuration. It would seem to be necessary to develop a method to improve the spatial beam quality of SOA without losing too much of the beam power for it to be a practical excitation source. Doing this would ensure adequate resolution and fluorescence generation in a two-photon fluorescence microscope. For the YDFA it would be sufficient to temporally compress the pulse for it to be adequate to for a TPFM

.

Chapter 7 Summary, Analysis and Future Work

7.1 Summary

Two-photon fluorescence microscopy (TPFM) is an established imaging technique that offers advantages over conventional and confocal one-photon fluorescence microscopy as well as other imaging techniques. It has inherent optical sectioning properties, increases imaging depth, reduces photobleaching and toxicity concerns and gives greater access to fluorophores excited by the blue end of the spectrum than its one-photon counterpart. The primary requirement to be able to efficiently perform TPFM is an excitation source that is able to deliver high peak intensities without high average powers, i.e. a short pulse mode-locked laser. The standard source used for TPFM is the titanium sapphire laser, which achieves these requirements easily. The primary drawbacks to a Ti:Sapphire laser source are its large size, high cost and complexity. In this thesis alternatives to the Ti:Sapphire laser are investigated, specifically a mode-locked semiconductor diode laser amplified by alternatively a semiconductor optical amplifier (SOA) and a Yb-doped fibre amplifer (YDFA).

Preliminary work investigating the potential of the hybrid semiconductor-fibre technology was performed. Gain, maximum power output, saturation effects and compression are discussed.

The focal properties in air of the Ti:Sapphire laser, SOA and YDFA (along with a HeNe laser) beams were characterized to a first approximation. These experiments were performed for the purpose of identifying the potential effects that the beam profiles of the SOA and YDFA may have on the fluorescence generation and imaging resolution in a microscopy context.

Results were also presented quantifying the disparity in the ability to generate fluorescence in a bulk sample between the Ti:Sapphire laser and the two amplifiers for a given average excitation power. This was done to illustrate the degree of the obstacles that must be overcome for the two amplifiers to be considered legitimate alternatives to the Ti:Sapphire laser as an excitation source for two-photon fluorescence microscopy.

A summary of the measurement results follows.

7.1.1 Yb-doped fibre amplifier results

Some of the experimental results obtained from the hybrid semiconductor-fibre technology were presented. A mode-locked semiconductor diode laser was amplified by an optically pumped Yb-doped fibre amplifier. It is to the author's knowledge the first attempt at this type of approach. A paper is in the process of being written. A double clad 18 m fibre pumped with a launched power of ~1.4 W at ~971 nm yielded average output powers as great as 790 mW when seeded with 930 μW from the mode-locked diode oscillator resulting in a gain of ~29 dB. Typical post amplification pulse durations were between 4 and 10 ps with a repetition rate of ~580-700 MHz. Compression with a modified grating pair compressor reduced the pulse duration to ~860 fs (assuming a Gaussian temporal profile). Including losses the peak power is ~ 750 W. Measurements indicate that the output power could be scaled up with a more powerful pump diode laser.

7.1.2 Focal spot measurements

The beam waists of a helium neon laser, a titanium sapphire laser, a semiconductor optical amplifier and a Yb-doped fibre amplifier were measured in air. The measurement gives an indication of the ability of the different sources to focus well for the purpose of efficiently exciting two-photon fluorescence in a small volume. It also suggests the relative resolution performance that may be obtained from the different sources in a microscopy application.

The measurements obtained with the helium neon laser were close to the theoretically expected values. This is believed to have been largely the result of the excellent mode quality of a HeNe laser. The M^2 value obtained from the data was ~ 1, which is the expected value for a HeNe laser. It is also believed that the small beam diameter and the proximity of the laser to the measurement system aided these measurements.

The beam waist measured with the Ti:Sapphire laser was about 15% larger than the predicted value. However, the predicted value did not explicitly take into account the M^2 value of the input beam (expected to be ~1.2). The discrepancy was attributed mostly to the quality of the input beam. The M^2 data obtained from the focal spot data was ~1.6, which was higher than the expected input value. However, Sun suggests that truncation of the beam results in an increase of the M^2 value after the aperture [88]. The distance the beam traveled from source to the measurement system was ~7 m with reflections off a number of mirrors (13). It is believed that this hampered the measurement of the beam diameter due to unwanted beam position fluctuations. Distortions from imperfect mirror surfaces may also have contributed to the larger measured beam waist.

Measurement of the focal properties of the Yb-doped fibre amplifier yielded a spot size that was close to the expected value. In this case the input beam was assumed to have an M^2 value of one due to the fibre amplifier being a single-mode waveguide. The quality of the beam and the minor truncation are believed to be the reason for the good agreement between the expected and measured beam waists.

Finally, the beam waist of the semiconductor optical amplifier was measured. The SOA has a complex mode structure that made it difficult to predict the beam size in the focus. The beam, consisting of two primary transverse lobes and one primary lateral mode, largely filled the lens. There was, however, a non-negligible amount of energy propagating in the higher lateral modes. The measured beam waist in the transverse dimension was the smallest measured. In the lateral dimension it was noticeably larger than in the transverse direction despite what appeared to be a better mode profile. This asymmetry is attributed to a larger M^2 value in the lateral dimension than in the transverse, which manifests itself as a larger beam waist. This was corroborated to a degree by two-photon fluorescence measurements performed at a different time.

7.1.3 Two-photon fluorescence measurements

In Chapter 6 the efficiency with which the Ti:Sapphire laser, SOA and YDFA generated two-photon fluorescence in a bulk dye sample was investigated. It was possible to directly compare the efficiency of the Ti:Sapphire laser and the YDFA given that the pulse duration, repetition rate, wavelength and two-photon cross-section of the dye were relatively well known. Measurements were made to compare the predicted efficiency with the measured one. This was done be altering the mode-locking properties of the diode oscillator and measuring the relative change in generated fluorescence. The Ti:Sapphire laser was found to generate fluorescence approximately three orders of magnitude more efficiently. One order of magnitude could be attributed to the difference of the two-photon absorption cross-section at the 800 nm emission wavelength of the Ti:Sapphire laser compared to at the ~1075 nm emission wavelength of the YDFA. The majority of the rest was attributed to the lower peak power and pulse energy of the YDFA, which is a result of the longer pulse duration and higher repetition rate. Because both beams were described relatively well by Gaussian beam propagation theory, the focal mode profile was not expected to have had an impact on the efficiency.

Measurements were also made to compare the two-photon generation efficiency of the SOA to the YDFA. Because both amplifiers were seeded with the same mode-locked diode source the repetition rate, pulse shape and wavelength were considered similar to be considered the same. Measured differences were expected to arise from the longer pulse length of the YDFA (due to GVD) and the poor mode quality of the SOA. If the mode profile were not an issue, the YDFA would be expected to have a lower two-photon fluorescence generation efficiency. However, the opposite was observed. This was largely attributed to the poorer focal properties of the SOA. Two-photon generation efficiency measurements were made on a spatially filtered SOA beam. Results indicated that energy in the higher lateral modes was not generating fluorescence as efficiently as the main mode. This result was consistent with the spot size measurements.

7.2 Analysis

Here the results obtained from the semiconductor optical amplifier and the Yb-doped fibre amplifier will be discussed in the context of their potential as excitation sources for two-photon fluorescence microscopy. Their advantages, disadvantages and prospectives will be considered.

7.2.1 Advantages of SOAs as a TPFM source

A semiconductor optical amplifier is very similar in implementation to the diode oscillator. It is made with the same material structure and is manufactured using the same techniques on the same wafer. Simple modifications are made to the waveguide to make it function as a single pass optical amplifier. As with the oscillator, it is also electrically pumped, which from a complexity and cost standpoint is preferable to optical pumping. Semiconductor devices exhibit high gain which allows them to be very small while still providing relatively high output powers. With the devices used in the experiments average mode-locked powers of ~40 mW were obtained. Other devices fabricated in this lab have yielded average powers of ~90 mW at a wavelength of 980 nm with similar mode-locked characteristics. With greatly increased complexity all-semiconductor mode-locked devices have been shown to provide about ~200 mW of average power with a peak power of over a kilowatt [107]. Indeed two-photon fluorescence imaging has been performed with a CW diode laser source, though sensitive detection equipment (a low noise PMT with a photon counter) and relatively long integration times (three orders of magnitude greater) were required [109].

7.2.2 Potential problems with SOAs as a TPFM source

Assuming that a beam can be efficiently focused, the property of merit for a TPFM excitation source is a high peak power while maintaining modest pulse energies. A high peak power allows for efficient generation of fluorescence. However, if the pulse energy is also high it increases the risk of damage to the sample. The SOA used in these experiments provided peak powers on the order of tens of Watts while having pulse energies in the tens of pJ. An attenuated Ti:Sapphire source (~10 mW when used as an TPF excitation source) generates peak powers on the order of kilowatts while the pulse energy is around 100 pJ. The peak power of the SOA needs to be increased at least two orders of magnitude in order to be considered a possible replacement for the TPFM source.

A potential problem with the use of mode-locked diode sources is the difficulty of mode-locking at arbitrarily low repetition rates. Operating at a reduced repetition rate can increase the pulse energy and reduce the likelihood of saturation effects. Larger pulse energies translate (usually) into higher peak powers, which results in improved two-photon fluorescence excitation efficiency. Fluorescence lifetimes are typically on the order of a nanosecond. This means that repetition rates on the order of a GHz have the potential to saturate a dye. To obtain the strongest fluorescence signal from a sample, it is desirable to have a repetition rate that maximizes the number of excitation-emission transitions per second without saturating the fluorophore. Given the fluorescence lifetime, a repetition rate around a 100 MHz would maximize fluorescence and minimize the likelihood of saturation [127]. (It should be noted that although the mode-locked diode had a repetition rate of ~600 MHz in the performed experiments, saturation effects were not an issue due to the high dye concentration and the modest peak powers of the pulses.) The capability to mode-lock at a low repetition rate is partially a function of the excited state lifetime, which is on the order of a nanosecond in a semiconductor system [118], [129]. This suggests that repetition rates significantly less than a GHz are not readily achievable in a mode-locked semiconductor laser without having ASE problems. Devices in this group have been shown to mode-lock at repetition rates as low as 300 MHz. Essentially, the lower end of achievable repetition rates with our devices is the upper end of desired repetition rates in TPFM. Mike Brennan has done work, as part of his PhD thesis, to determine an optimal regime for the laser diodes to operate in to maximize two-photon fluorescence signal (neglecting saturation effects). With the devices he was working with at the time he determined that the optimal repetition rate was between 1.3 and 1.5 GHz (he tested repetition rates between 600 MHz and 2.2 GHz) [71]. This provided the best balance between pulse energy and pulse duration. Of course these results are only valid for the devices he tested at the time and he also did not amplify the diode output. The result is important in that it indicates that although a lower repetition rate is desirable the achievable pulse duration and pulse energy from the diode laser may not be ideal for TPFM. Gain-switched diodes may provide a method of operating at arbitrary repetition rates. However, pulse durations tend to be longer and the output is strongly chirped.

The SOA beam profile was found to be a potential drawback for any application in the field of microscopy. The larger spot size in the lateral dimension reduces the resolution available in an imaging situation. The larger spot size will also manifest itself in a lower fluorescence signal, especially when imaging a small object. In the bulk dye solution measurements, lower fluorescence in the center of the beam waist is compensated by integration over the entire illuminated volume. However, in the worst case when exciting a small localized spot, such as a single labeled molecule, the measured intensity will drop significantly with an increase in beam waist. For example, assuming a symmetric beam, if the beam waist doubles the intensity at the center of the beam waist decreases by a factor of four and the fluorescence intensity drops by a factor of 16. In most microscopy applications the larger spot size of the SOA has the effect of reducing both resolution and the generated intensity.

7.2.3 Prospective for SOAs as a TPFM source

The devices used in the experiments discussed in this thesis are not ready for use as excitation sources in two-photon fluorescence microscopy. There are a number of aspects of the devices and the accompanying systems that could be reasonably improved upon that would allow the SOAs to be viable TPFM sources.

The average power available near the dye cell was only about 10 mW. This is partially due to losses from the large number of optical elements used to direct the beam from the source to the measurement setup and the beam chopper needed for the lock-in amplifier. A better situation would be to have the source much closer to the measurement setup in order to reduce losses and minimize beam distortion. Also, building a better ambient light rejecting housing around the setup, coupled with a photon counter, would eliminate the need for the lock-in amplifier and the chopper. This would immediately double the available average power.

The devices used in these experiments were 1075 nm single quantum well lasers and SOAs. The group has previously developed lasers operating at 980 nm which produce maximum average powers of about twice what the long wavelength devices are capable of while maintaining similar pulse properties [1]. On this basis alone, switching to the shorter wavelength would improve the fluorescence yield by a factor of four.

The SOAs at both wavelengths suffered from a relatively low current damage threshold. Given the volume of the gain region it was expected that the SOAs would be able to handle more pump current, and therefore achieve greater amplification. The reasons for this limitation have not been fully explored. To a first approximation, the available amplification is expected to scale linearly with the volume of the active region. The 1075 nm devices have only a single quantum well due to concerns about lattice mismatch in the growth [110]. The single well limits the available gain of the device. With the addition of strain compensation layers the number of quantum wells could be increased which would improve the amplification performance. Conversely, more wells could be added to the two-quantum well 980 nm devices with a similar result. Essentially, the full potential of the devices tested to date has not been fully exploited in terms of maximizing output power.

The next generation of SOAs will test a number of modified waveguide structures that should improve the mode quality and the available output power. It is also expected that some of the current limitations experienced in the first generation devices will be reduced allowing for increased power from the current designs. An example of a different waveguide structure to be tested is the 'inverse bow tie' [111]. This type of structure enjoys the increased gain benefits of the flared waveguide design but also maintains the beam quality available from a narrow stripe waveguide. Also, a split contact SOA will be tested which could allow for better control of current injection and thus yield more power. With a single current injection probe applied to the gain section of the SOA there are questions as to the uniformity of the population inversion within the gain section. It is hypothesized that the flared region has a higher inversion than the narrow section. If this is the case then the incoming pulse experiences less gain near the front facet of the SOA and the full potential of the device is not being exploited. By applying a second contact it will be possible to control and maximize the inversion to a certain degree, thus possibly yielding greater average powers.

The pulse durations that were used for these experiments tended to be greater than 5 ps. A longer pulse reduces the peak power. A possibility that was not explored was the use of the modified grating pair compressor available to the setup, which compensates for linear pulse chirp [104]. In previous experiments the compressor has reduced pulse durations to less than a picosecond (as low as 470 fs with the 980 nm devices). As the fluorescence yield is inversely proportional to the pulse duration, an order of magnitude reduction in the pulse duration results in an order of magnitude increase in fluorescence. Also, shorter pulses can reduce the amount of power required to generate adequate fluorescence; which is good for minimizing photodamage in the sample. Unfortunately, there is significant loss (~50%) associated with our compressor in its present state. With the power loss the benefits of compression are reduced (fluorescence scales inversely with pulse duration, but quadratically with power).

However, if a better low loss compressor were to be used the results could significantly improve the peak power. Grating pair compressors can have higher throughput efficiency. Another grating pair compressor in the lab has a maximum throughput efficiency of ~75%. Loss with a grating compressor is inevitable because some power is always coupled into multiple diffraction orders.

Other methods of compression are the use of prism pairs, similar to that used in the Ti:Sapphire laser, optical fibres with different GVD, fibre Bragg gratings and deformable mirrors. The prism pair can be very efficient because no power is lost to higher diffraction orders and reflections at the surfaces can be reduced by operating at Brewster's angle [105]. Compression using optical fibres consists of using different fibres with different group velocity dispersions and adjusting their respective lengths to eliminate the chirp [106]. Fibre Bragg grating compressors have a refractive index grating written into them. The periodicity can be such that the red and blue spectral components of the spectrum are reflected at different distances along the fibre thus compensating for linear chirp [107], [112]. However, coupling into the fibre is a source of loss. The viability of fibre based compressors depends on the ability to efficiently couple light into the fibre. The coupling efficiency of our SOA beam into a single-mode fibre was found to be at best ~35 %, with 20% being a more representative value. Besides reducing the loss there is also room to further shorten the pulses by correcting the non-linear chirp that is typically on a semiconductor mode-locked pulse by including additional compensators. Our compressed pulses, at ~500 fs, are still about twice the transform limit. This indicates that there is sufficient bandwidth to further reduce the pulse duration with a compressor capable of compensating for higher order (non-linear) chirp. Using sets of chirp compensators allows for individual control of the quadratic and cubic phase distortions [105], [108]. A relatively new way to compensate for linear and higher order chirp in a single step is to use a deformable mirror [113], [114]. In this case the beam is spectrally dispersed with a grating and imaged onto a deformable mirror. A search algorithm alters the shape of the mirror such that the distance traveled by each spectral component is set so that upon reflection and recollimation the entire spectrum is in phase. Another approach to improve the chirp performance of the laser is to alter the dispersion characteristics within the external of the laser oscillator [115]-[117]. By properly modifying the dispersion it is possible to ensure that the laser diode output is largely linearly chirped. This permits the use of a simple linear chirp compensator to achieve bandwidth limited pulses. In theory, with a bandwidth of 5 nm (centered at 1075 nm) the shortest pulse possible (assuming Gaussian pulse shape) should be less than ~350 fs. Reducing pulse lengths from 5 ps to ~350 fs without significant losses would greatly improve the prospects of the all-semiconductor source.

Pulses in principle could also be shortened by increasing the bandwidth of the pulse. Currently a 600 lines/mm grating is used in the external cavity to reduce the bandwidth and facilitate mode-locking. Mode-locking with a mirror or less dispersive grating in the external cavity may allow for shorter pulse generation. However, simply adding bandwidth will not necessarily shorten the pulse out of the laser oscillator. Semiconductor lasers tend to not operate close to the transform limit and so to fully exploit the added bandwidth it may be necessary to use a compressor as described above to achieve shorter pulses [118], [119].

The mode profile of the SOA presents a concern in terms of the potential of these devices as excitation sources. Drastic improvement to the mode profile does not appear to be imminent. Were there sufficient power in the beam, it may be possible to spatially filter it to a good quality single mode in both the lateral and transverse dimensions. This single mode could then be expanded to fill the back aperture of the lens. Doing this should improve the beam waist properties and the fluorescence generation efficiency. Scaling up the power to allow spatial filtering may be the most practical solution to the mode profile difficulties. A straightforward method of filtering the beam profile is to couple the laser beam into a single-mode fibre. The output of the beam is near Gaussian, and is ideal for focusing. A problem with this method is the low observed coupling efficiency of the SOA into a single mode fibre. The best achieved efficiency was approximately 35%, with typical efficiencies around 20%. At a 25% coupling efficiency, the loss of excitation power may be too great to make it a practical solution unless significant gains are made in available power. The specific application will determine if it is feasible. The situation was better when coupling the laser oscillator beam into the fibre, with efficiencies of up to 50% observed. It is possible that with alterations to the waveguide of the SOA, so that the SOA beam is more similar to the output of the laser diode, the coupling efficiency will be closer to 50%. Other groups working with flared SOAs have reported coupling efficiencies of 45% in one case and 60% in another with relatively simple bulk optics [120], [121]. However, the coupling efficiency is dependent on the mode properties of the beam and so it may be that the beam profiles in those cases are superior to the ones obtained in our devices. Another drawback of this method is the temporal pulse spreading due to the group velocity dispersion of the fibre.

A different method of spatially filtering a beam is to focus it through a pinhole aperture. This has the effect of filtering out the higher spatial frequencies of the transverse profile of the beam [122]. In preliminary experiments performed here, the throughput efficiency was found to be ~40% with the filtered beam profile looking promising. It is likely that by choosing a different lens and pinhole combination it would be possible to improve the throughput. This method would seem to be easier and more beneficial than filtering with a single-mode fibre as there is no dispersion issue though the mode quality is likely to be not as good. Filling the lens used in the Chapter 5 experiments with a good beam profile should generate a diffraction limited $1/e^2$ spot size diameter of about 800 nm at the

1075 nm operating wavelength. This would be a significant improvement over what was obtained in the measurements.

Other groups using all semiconductor mode-locked sources, in sometimes very different configurations, have succeeded in generating high peak powers that would likely be suitable for two-photon fluorescence microscopy. A relatively straightforward design has been demonstrated to generate 460 fs pulses with a peak power of 70 W [123]. Another straightforward design using the "inverse bow-tie" waveguide structure demonstrated 400 mW average power, with a peak power of 60 W and a good mode profile [124]. A mode-locked diode laser operating in a regime, known as the breathing-mode, has demonstrated pulses of 185 fs, with peak powers as high as 230 W [125]. As mentioned earlier, an elaborate all semiconductor setup has demonstrated pulses as short as 590 fs, with a peak power of 1.4 kW [107]. An optically pumped surface emitting semiconductor device has been shown to be able to generate compressed pulses of 153 fs with a peak power greater than 1 kW [126].

While the devices developed here are not ready to be used as a replacement for the Ti:Sapphire laser in TPFM, their limitations do not appear to rule out that possibility. There is a strong motivation to meet the criteria required for a two-photon excitation source with semiconductor technology. The small size, low cost and all electrical pumping are attractive features when compared to the standard Ti:Sapphire laser. Multiple devices could be included in a single package to provide access to much of the biologically relevant optical spectrum. With some clever device design, improved compression, a scaling up of the power output and spatial filtering, a mode-locked semiconductor laser amplified by an SOA could be a reasonable choice for a two photon fluorescence excitation source.

7.2.4 Advantages of YDFAs as a TPFM source

The ytterbium-doped fibre amplifier is seeded with the same mode-locked diode laser as the SOA and therefore enjoys the same benefits of compact, cheap short pulse generation. However, large amplification of the oscillator output is much easier to achieve with the fibre than with the SOA. With a modest amount of effort it was possible to obtain usable average powers of greater than 600 mW with pulse durations of around 4 ps, which yields peak powers of over a hundred watts and pulse energies in the hundreds of picojoules to nanojoule range. The amount of pulse energy is essentially limited by the amount of power available from the pump diode. In other words this technology is easily scaled up to much higher powers as shown in Figure 3-5. If photodamage is not much of a concern, it is possible to simply generate a sufficiently high power to achieve a strong fluorescence signal without any further modification to the system. However, because power is not a limiting factor, compression becomes more appealing because the losses associated with the temporal pulse compression can be compensated.

Another benefit is the excellent beam quality that comes from a single-mode fibre. With the available power it is also possible to fill the back of the lens and obtain a diffraction limited spot without any beam profile conditioning. The excellent mode profile translates into a high imaging resolution which is critical in microscopy applications.

7.2.5 Potential problems with YDFAs as a TPFM source

As previously stated, the Yb-doped fibre amplifier stretches the pulses to a point where compression would likely be required. While this adds complexity to the system, some sort of compression is required for the other two-photon excitation sources as well.

A disadvantage of the YDFA compared to the conventional Ti:Sapphire laser is the somewhat smaller gain bandwidth which limits the tuning range. The gain bandwidth of the fibre is 970 -1200 nm, with few areas of high gain. Longer fibre lengths must be used to achieve equivalent amplification at the longer wavelength end of the gain spectrum. This compares with the 400 nm bandwidth of a Ti:Sapphire laser. Though accessing the full bandwidth is not trivial, specially coated mirrors must be changed to access different wavelength ranges. The gain bandwidth essentially determines the range of fluorophores that can be used with a given excitation source. In contrast, the semiconductor technology makes it possible to modify the composition of the device to achieve lasing in a broad range of wavelengths. With a limited bandwidth more time would need to be spent selecting and/or designing the appropriate fluorophore for a given application. This type of constraint may not be acceptable for labs where a great diversity of specimens is imaged.

7.2.6 Prospective for YDFA as a TPFM source

The prospective of a hybrid semiconductor-fibre two-photon excitation source is very bright. Generation of the short pulses comes from the relatively simple and cheap passively mode-locked semiconductor diode laser and amplification is readily achieved using the compact doped fibre with a pump diode laser. With available average power not being a limiting factor it is possible to compress the pulse to sub-picosecond durations for high peak powers while simultaneously filling the objective lens of a microscope to ensure maximum resolution and fluorescence generation efficiency (assuming a thin sample, not thick).

Another benefit of the Yb-doped fibre system is the ability to operate at low repetition rates. The capability to mode-lock at a low repetition rate is partially a function of the excited state lifetime, on the order of 1 ms in a doped silicate fibre [77], [128]. In theory this would allow a Yb-doped system to function at repetition rates on the order of a kHz without the generation of significant amounts of spontaneous emission. This is in contrast to the mode-locked diode. Groups have demonstrated amplification with YDFAs of low rep rate systems (tens of kHz) [78], [130]. Yb-doped fibre based lasers are developing into a mature technology capable of generating sub-picosecond pulses at tens of MHz [131]-[134]. While the implementation of these types of lasers can be more involved than a mode-locked semiconductor laser, they are capable of generating higher peak powers (tens of kW), shorter pulses (sub 100 fs) and excellent beam qualities [132]-[134].

Fibre based technology has also been demonstrated to be about as efficient in converting electrical energy into optical energy as semiconductor based sources partly because they exhibit a high slope efficiency (90%) converting pump photons into signal photons [135]. High efficiency has been an advantage of semiconductor sources over other laser systems. In the tuning range of 970-1200 nm, a fiber based laser and amplifier is a very attractive technology that can readily meet the requirements for two-photon fluorescence microscopy.

Using somewhat more exotic technology it may also be possible to greatly increase the tuning range of a YDFA based system by taking advantage of the high peak powers that can be achieved. The high peak power can be used drive non-linear processes to generate a spectral supercontinuum. This has been most effectively demonstrated using a photonic band-gap fibre which has been shown to generate a bandwidth spanning from 500 to 1800 nm with an average output power of 5 W when driven with the output of a Yb-doped fibre amplifier [136]. Supercontinuum generation has also been demonstrated with tapered fibres, doped fibres, narrow core fibres and Q-switched Yb-doped fibre lasers [137]-[140]. The quality of the pulses after the supercontinuum generation would likely need to be improved before it could be used for TPFM [141].

The current state of the YDFA technology within the lab is much closer to what is required of a two-photon excitation source than that of the SOAs. The current limiting factors for the SOAs are the low peak power, low pulse energy and poor mode profile. These issues are either not a problem or are easily fixed in the case of the YDFA. The low pulse energy can be compensated for by increasing the average power, and the peak power can be made higher by compression and the beam profile is already good. The mode quality out of the single-mode doped fibre should allow the investigation of any of the super-resolution techniques that are currently being investigated with Ti:Sapphire lasers, such as two-photon 4pi fluorescence imaging.

7.3 Future work

There is a large amount of work that can be performed to build upon the initial results presented here that would allow the technology developed by the group to be utilized for practical applications. Aside from the continued evolution of the semiconductor sources, some of the more important areas to focus on in the future are listed in separate subsections below.

7.3.1 Measurement setup

A lot of the inconsistency in the measurements performed (especially the fluorescence measurements) is believed to be caused by the distance between the sources and detectors. The large number of optical elements spanning several tables creates a number of places where vibrations, dust, mirror defects and beam misalignment can become issues. It is believed that the inability to achieve co-linearity of the different beams was the largest contributor to the inconsistencies because it required adjustment of a number of mirrors when switching between sources. It proved very difficult to find the same local maximum when subsequently switching back to a source, thus adding inconsistency in day to day measurements. By having fewer optical elements the number of inadvertent beam misalignment issues would be greatly reduced, which would improve the day to day consistency of the setup. Another issue was the optical table on which the measurement system was setup was not a large vibration damped table but instead a bread board mounted on a metal table frame. This opens the possibility of small shifts in the table's position and vibrations leading to further inconsistencies. The entire setup should be moved to the main optics table and the beam path length should be reduced.

The lens being used to focus the light was a 0.55 NA aspheric lens. To reduce the spot size as well as to increase the fluorescence yield in an imaging situation, a higher power microscope objective with an NA of around 1.0 should be used. A better choice would be a water immersion lens (as most imaged biological samples will be in an aqueous solution) to reduce index mismatch which can induce aberration and reduce the available imaging depth [31], [99]. However, with the much smaller working distance that comes with using a high power lens, the fluorescence collection should be done with the same lens, in an epi-fluorescence arrangement. This has the advantage of simplifying alignment while also improving the collection efficiency by having a large NA for light collection. This is in contrast to the current situation where fluorescence is collected with a small NA lens due to space considerations. This arrangement would also more accurately mimic the layout encountered in a real microscope.

A better light tight enclosure should be built around the fluorescence sample. By reducing the amount of ambient light near the sample, the excitation power or the fluorophore concentration could be reduced. The dye concentration was a few orders of magnitude greater than one would typically encounter in practice to maintain a sufficiently high signal level for these preliminary tests.

7.3.2 Compression

In the analysis portion of this chapter it was indicated that for both the SOA and Yb-doped fibre amplifier it would be greatly beneficial to compress the pulse length closer to the transform limit. The current compressor is too lossy (about 50%) to fully achieve the benefits of a shorter pulse in terms of increasing the fluorescence yield. To further explore the prospects of this technology as a TPFM excitation source an improved compressor should be used, as discussed in Section 7.2.3. For these devices to be used in any practical application in the real world the issue of efficient compression will have to be addressed. Prism pairs would seem to be the ideal method of compensating for the linear chirp. Prisms, cut such that they can be used at Brewster's angle, should be very low loss, and have a minimal effect on the beam quality. The addition of higher order chirp compensation would also be readily achievable.

7.3.3 Fluorescent dye

The dye chosen for this work, Rhodamine 6G, had a relatively low two-photon cross-section at the SOA wavelength. In fact it had a two-photon cross-section an order of magnitude greater at 800 nm than it did at 1075 nm, the opposite of what was desired for the experiments. This was not realized until later in the project. The two-photon cross-section at 800 nm is approximately 36 GM. This represents an average cross-section when compared to other common fluorophores. In the future a dye with a two-photon cross-section an order of magnitude greater at the 1075 nm excitation wavelength should be used, such as phycoerythrin which has an estimated cross-section 25 times larger than Rhodamine 6G at 1064 nm (or about 100 GM) [142].

7.3.4 Test imaging

It would be interesting and insightful to explore the performance of the Yb-doped fibre amplifier and perhaps also the SOA when imaging a fluorescent sample as opposed to a homogeneous fluorescent dye solution. With access to the Ti:Sapphire laser and its more than sufficient power levels it would be possible to design, implement and test a simple scanning microscope. In most commercial devices the beam is raster scanned across the sample by a pair of galvanometric mirrors. These are likely too expensive to be purchased for exploratory work. However, an analogous, and cheaper, method would be to move the sample through the focus of the beam using a pair of actuated computer controlled stages. The equipment to perform this experiment is already available in the lab. A standard method of calibrating a microscope is to image a suspension of fluorophore coated microspheres. With the microspheres suspended in a viscous matrix it would be illuminating to try to create a three-dimensional image of them by raster scanning the sample. By changing the diameter of the spheres it would also be possible to determine the resolution of the microscope by finding the minimum resolvable sphere. Using a sufficiently small sphere (~100 nm) it would be possible to map out the intensity profile of the excitation beam near the focus by recording the fluorescence intensity as a function of position [143]. This would ensure an accurate measurement of the beam spot size in the sample. Pulse stretching effects could also be monitored by observation of the generated fluorescence. The Ti:Sapphire laser would be used to ensure the overall quality of the system before attempts were made with the Yb-doped fibre amplifier and eventually the SOA. With the ability to generate high powers with the fibre amplifier the likelihood of success of such an endeavour would be relatively high.

7.4 Concluding remarks

The purpose of the work described in this thesis was to determine whether the semiconductor mode-locked diode lasers and semiconductor optical amplifiers developed by this lab are suitable for use as excitation sources in two-photon fluorescence microscopy as well as other non-linear applications. A corollary of this was also investigating the potential of an ytterbium-doped fibre amplifier seeded with the same semiconductor laser as a source of high power ultra-short optical pulses. Work was done to determine the minimum focal spot size with the various sources in an attempt to quantify the effect the poor beam quality of the SOA might have on both fluorescence generation as well as imaging resolution. Other sources were measured for calibration of the measurement system as well as for comparison purposes. Further, the fluorescence yield was measured from each source and compared to one another. This was done to determine the magnitude of the reduced fluorescence signal when using the SOA and Yb-doped fibre amplifier when compared to the standard the Ti:Sapphire laser. The SOA does not generate sufficient peak power to be a practical excitation source in its current state. With further development and improvement in the setup it should be feasible. The ytterbium-doped fibre amplifier is capable of generating sufficient peak powers for two-photon fluorescence microscopy with the addition of a pulse compressor. A number of suggestions have been made for future work and it is hoped that some will be followed through.

Appendix A Selected Diode Laser Results

During the time spent working with the mode-locked oscillators a number of operating conditions were observed that had not been documented in the lab in the past. They include the shortest pulses observed to date directly from the oscillator as well as the apparent generation of closely spaced double pulses. Typical results from what are considered "good" devices are pulse durations of between 2-3 ps with little structure to them. An example of a good trace is given in Figure A-1.

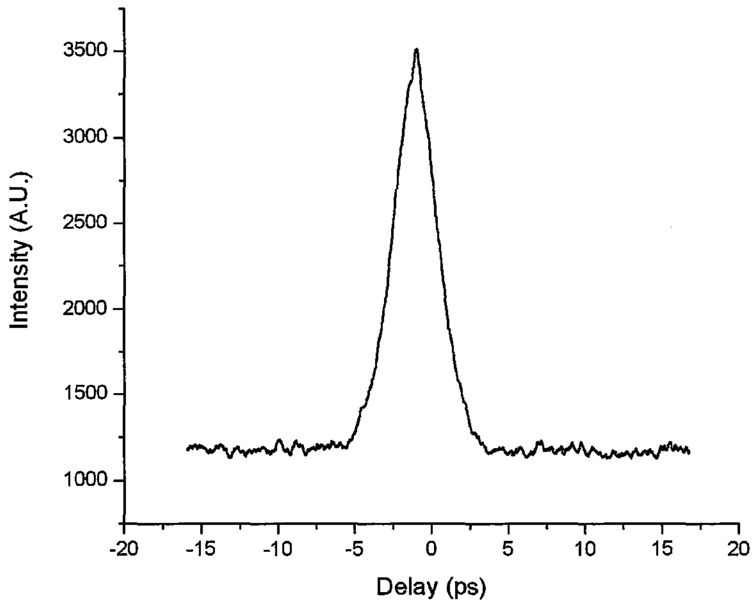

Figure A-1: A "normal" second order autocorrelation trace. The pulse width is 2.1 ps if one assumes a hyperbolic secant squared pulse shape.

The shortest pulse duration obtained directly from the oscillator was measured to be 910 fs if a hyperbolic secant squared pulse shape is assumed. This is in contrast with pulse durations of 2-3 ps that have been typical in our lab in the past. Figure A-2 is a plot of the second order intensity autocorrelation trace pre- and post-amplification by the SOA. It can be seen that in this case the pulse is about 10% longer after amplification. The device was passively mode-locked and operated at a repetition rate of 683 MHz with an average power of ~1 mW. The trace suggests a good quality single pulse.

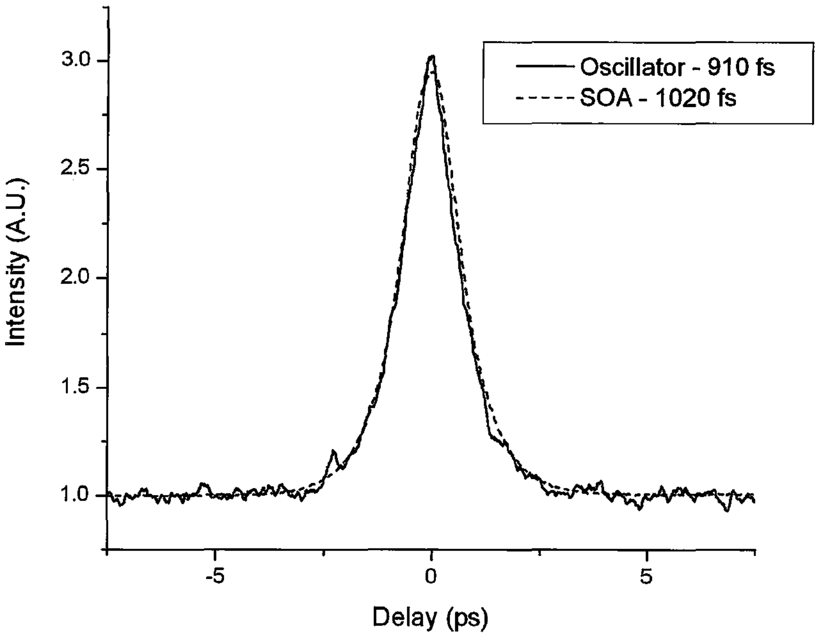

Figure A-2: Second order intensity autocorrelation trace of the pulse before and after amplification with the SOA. Pulse durations assume a hyperbolic secant squared pulse shape.

Over the time that the measurements for this thesis were made a number of "unconventional" autocorrelation traces have been observed. The other diagnostic tools used to characterize the mode-locking conditions indicated a normal and stable output. An example of a repeatedly encountered unconventional autocorrelation trace is given in Figure A-3. An autocorrelation trace is not sufficient to recover a unique pulse shape. In other words different pulse shapes can produce identical autocorrelation traces. There are methods for retrieving the pulse shape; however they are very involved and were not performed in the course of the work done for this thesis. Though a conclusive retrieval of the pulse shape is not possible from the autocorrelation trace, it is possible to make an educated guess.

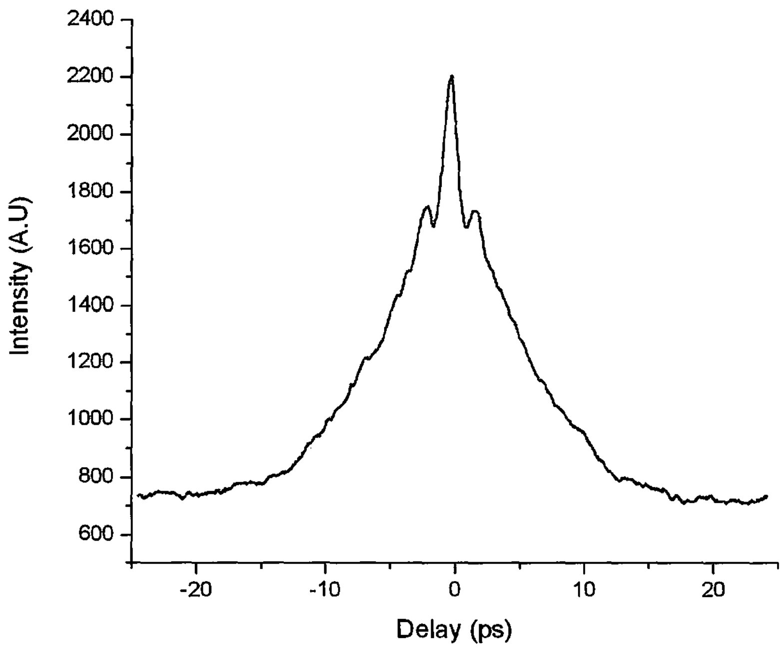

Figure A-3: Second order intensity autocorrelation trace of the mode-locked oscillator. The shape indicates a complex pulse structure.

Software was written that permitted the adjustment of a number of different parameters in an effort to recreate the trace shown in Figure A-3. The program allowed the user to simulate the generation of one or two closely spaced pulses. The time between the two close pulses could be controlled. Each pulse was Gaussian in shape. The width of the leading and trailing edge of each pulse could be adjusted independently. The quality of the pulse could be controlled, by imposing random noise onto the pulse envelope. The relative intensity of the two pulses can be independently controlled. A re-creation of the autocorrelation trace in Figure A-3 was done by computer tested trial and error. A plot of the original and fit autocorrelation and the retrieved pulse shape is given in Figure A-4 and Figure A-5. The two autocorrelation traces are not the same due to some limitations of the written software. However, the most notable feature of Figure A-3 is accurately re-created. A physical explanation of the nature or source of the double pulse is not explored. Again it should be noted that Figure A-5 is likely not the only solution that can create the characteristic humps of Figure A-3. The recovered pulse shape appears to be unphysical. However, it was the solution that most closely fit the measured autocorrelation trace over the available range or pulse durations, pulse separations, etc. Double pulses were observed more directly in some instances of hybrid mode-locking. The RF signal used for mode-locking the oscillator was also used to trigger a Tektronix CSA 803 communication signal analyzer. Light was detected with an avalanche photodiode. The repetition rate was ~700 MHz and the time between the double pulses was approximately 600 ps. A 600 ps separation between the two pulses is much too long to account for the autocorrelation seen in Figure A-3. In fact, a set of two pulses separated by more than 80 ps would likely not be observable using the standard diagnostic tools used in the lab. It is worth noting because a situation such as this would have a detrimental effect on two-photon fluorescence generation because the power would be divided between more pulses, and hence a lower intensity would be available.

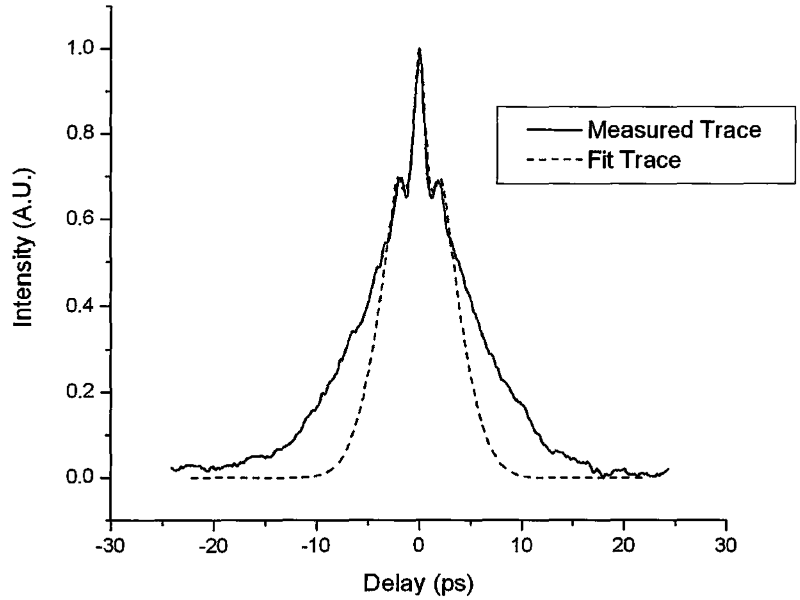

Figure A-4: Measured and best fit autocorrelation trace of a passively mode-locked diode laser.

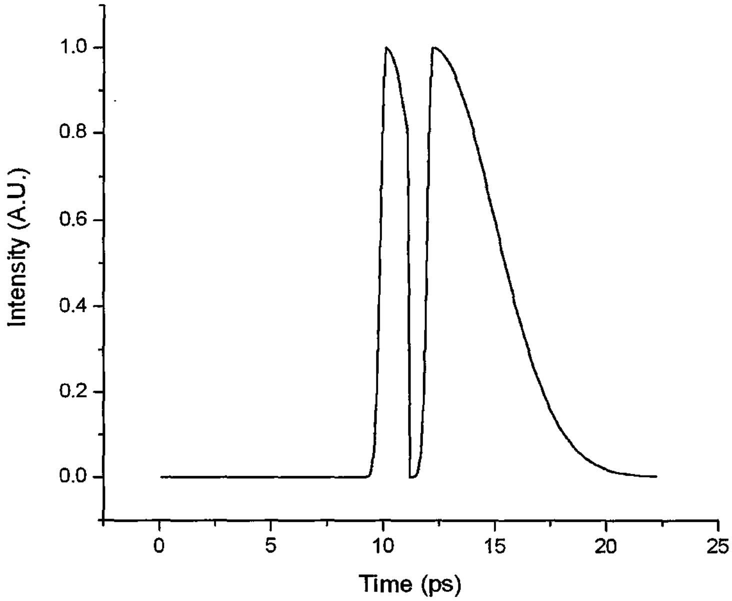

Figure A-5: Pulse shape retrieved from Figure A-3.

Appendix B Selected Two-Photon Fluorescence Results

Included below are some results from the two-photon fluorescence excitation experiments that may be relevant for people following up on the work performed in this thesis. The first data set pertains to atypical results that exhibited an apparent super-squared dependence on excitation power. The second is an unexpected observation, whereby the two-photon fluorescence generation efficiency increased when the semiconductor optical amplifier (SOA) beam was focused into the lens.

To determine the expected squared-dependence on incident power, a half-wave plate and polarizer pair were used to variably attenuate the excitation power. In Figures B-1 to B-3 are data from the Ti:Sapphire laser, Yb-doped fibre amplifier and the SOA based experiments that deviate from the expected I^2 dependence. It is believed that as the half-wave plate was rotated to attenuate the power, it caused a minor change in the beam alignment. Previous experience suggests that the measurement system is rather sensitive to alignment. Therefore, a small change can result in a noticeable discrepancy in the fluorescence signal. The reason the deviation is the same in all cases (measured signal falls faster than I^2) is because the beam path optimization was always done with the half-wave plate – polarizer pair set to maximum transmission. Therefore, as the beam position changed due to the adjustment of the half-wave plate the signal would fall away from the original alignment that maximized the fluorescence signal and result in this apparent super-quadratic dependence. It seems very unlikely that something such as three-photon excitation fluorescence could be occurring given the low power of the SOA.

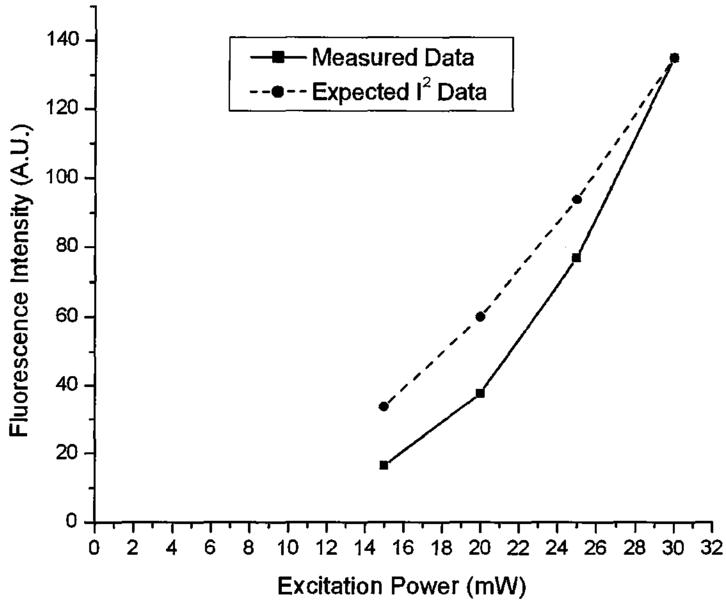

Figure B-1: Plot of the two-photon fluorescence obtained from the Rhodamine 6G dye solution excited by the Ti:Sapphire laser source at 800 nm as a function of excitation power. The data falls away from the expected I^2 dependence.

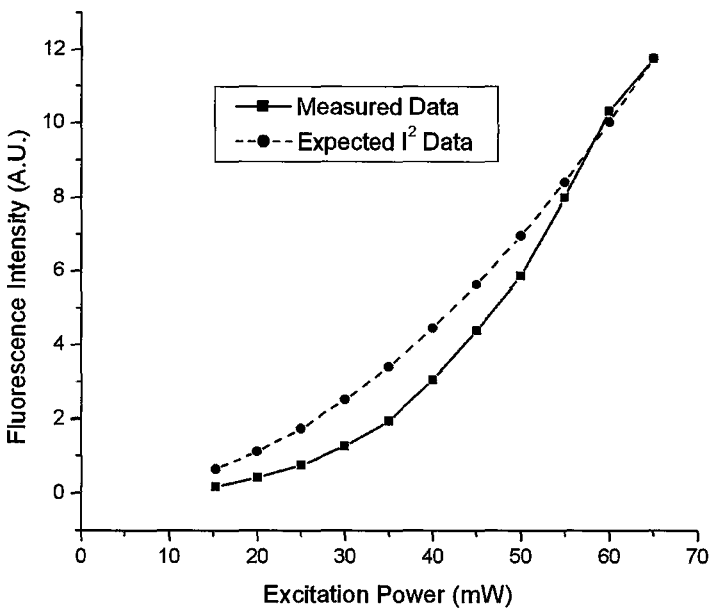

Figure B-2: Plot of the two-photon fluorescence obtained from the Rhodamine 6G dye solution excited by the Yb-doped fibre amplifier source at 1075 nm as a function of excitation power. The data deviates from the expected I^2 dependence.

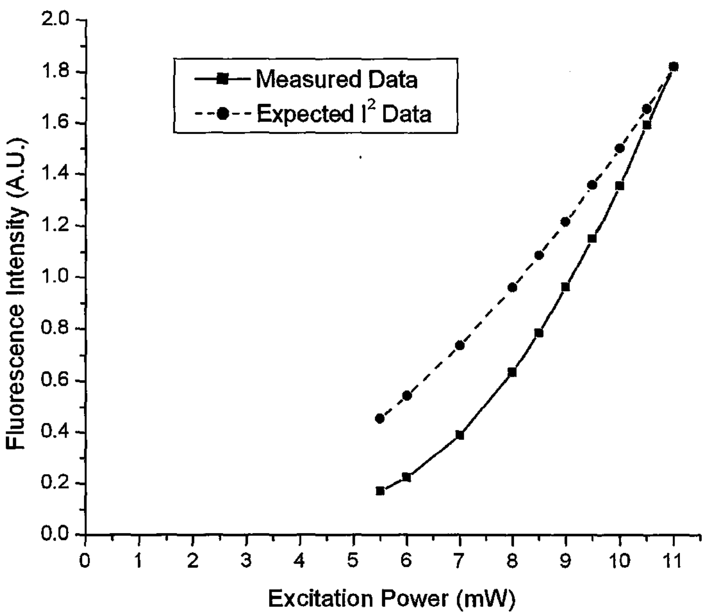

Figure B-3: Plot of the two-photon fluorescence obtained from the Rhodamine 6G dye solution excited by the semiconductor optical amplifier source at 1075 nm as a function of excitation power. The data deviates strongly from the expected I^2 dependence.

Another observation of note is the apparent increase in fluorescence generation efficiency when the SOA beam was focused into the "two-photon" lens (the one that focuses the light into the cuvette containing the fluorophore). By adjusting the position of the output collection lens of the SOA such that the beam appeared to be focused into the "two-photon" lens, the fluorescence efficiency (measured fluorescence power as a function of excitation power) increased by a factor of 2.7. (Interestingly, this is the same factor as was observed when spatially filtering the beam in the lateral and transverse directions with straight edges in Section 6.7.1.) An image of the focused SOA beam is given in Figure B-4. This image was taken at a time much later than the measurement was made, but the profile is qualitatively the same as was observed in earlier experiments. It is not immediately clear why this would improve the efficiency so much. In the unfocused case the transmission efficiency through the "two-photon" lens was ~71% and in the focused case it was ~73%. A similar phenomenon was observed when trying to couple the SOA (or laser oscillator) beam into a single-mode fibre. The coupling efficiency would improve when the beam was converging into the focusing lens. The same effect was not observed when generating fluorescence with the Yb-doped fibre amplifier.

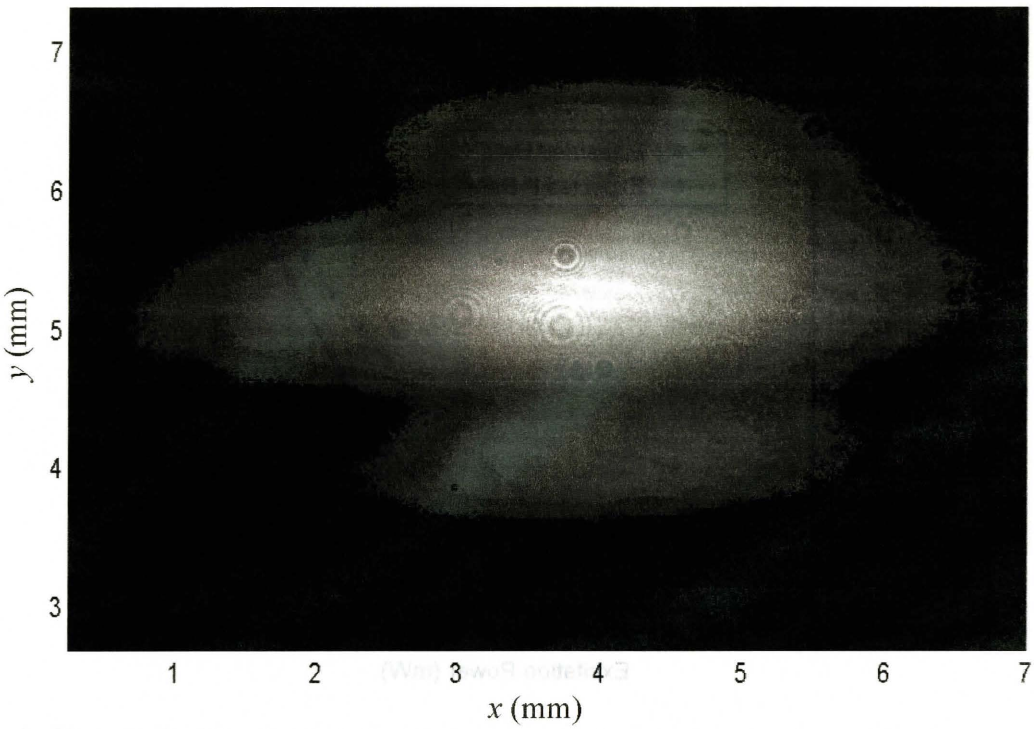

Figure B-4: Beam profile of the "focused" SOA beam. A beam profile such as this as an input to a focusing lens tends to improve fibre coupling and the fluorescence generation efficiency.

Appendix C Calculation of Expected Photon Count

It can be insightful to compare the expected two-photon fluorescence signal to what is actually obtained. As an example, a comparison of the expected and measured signal for the Rhodamine 6G dye emitting at 580 nm, excited by 50 mW of 1075 nm light from the Yb-doped fibre will be made. The pulse duration is 8 ps, the repetition rate is 600 MHz and the concentration is 1 x 10^{-2} mol/L. Assumptions of the collection efficiency of the system will need to be made. Similar to the equation given in Chapter 2, a more detailed version of the time averaged fluorescence in a bulk sample excited with a pulsed source from a diffraction-limited objective lens with uniform Gaussian illumination is

$$\langle F \rangle \approx \frac{1}{2}\phi \eta_2 \delta_2 C \frac{g_p}{\tau_p f_p} \frac{n\pi \langle P \rangle^2}{\lambda} \tag{C-1}$$

where F is the time averaged fluorescence in photons/sec, ϕ is the fluorescence collection efficiency of the system, η_2 is the fluorescence quantum efficiency, δ_2 is the two-photon absorption cross section is cm^{4}s/photon, C is the dye concentration in molecules/cm^{-3}, g_p is the second order temporal coherence, τ_p is the FWHM of the pulse duration in seconds, f_p is the repetition rate in s^{-1}, n is the index of refraction of the dye medium, P is the incident power in photons/s and λ is the wavelength of the excitation light in cm [49]. The collection efficiency is dependent on the solid collection angle of the lens as well as its transmissivity. The NA of the lens is 0.25, which corresponds to a relative solid angle of 8% of the full sphere. The collection lens is AR coated for the 650-1100 nm. The reflectivity at 580 nm is not given. It will be assumed that 90% of the fluorescence is transmitted through the collection lens. The quantum efficiency of Rhodamine 6G is approximately 95% [103]. The two-photon cross-section is ~ 4 x 10^{-50} cm^{4}s/photon at 1064 nm [103]. The dye concentration of 1 x 10^{-2} mol/L is equivalent to 6 x 10^{18} molecules/cm^3. For a Gaussian beam profile the second order temporal coherence parameter is 0.664 [49]. The index of refraction of methanol is approximately 1.3. The incident power of 50 mW is equivalent to 2.7 x 10^{17} photons/s. Using these parameters the time average photon flux that is transmitted through the collection lens is approximately 2.3 x 10^9 photons/s. The transmissivity of the 1 mm BG39 glass filter (to remove stray excitation light) is approximately 70% at 580 nm. Therefore the photon flux impinging on the PMT cathode is 1.6 x 10^9 photons/s. Hamamatsu quotes the R6358 PMT as having a quantum efficiency of ~12% at 580 nm. Therefore, the number of electrons generated at the photocathode is approximately 2 x 10^8 electrons/s assuming all the photons are absorbed by the photocathode. The PMT has a gain of 3.5 x 10^6

with a supply voltage of 1000 V. When measurements were made with the Yb-doped fibre amplifier, the supply voltage was ~ 600 V. The gain of a photomultiplier tube as a function of supply voltage is varies as V^{kn}, where k is a geometry dependent value of the PMT, expected to be ~0.75 (from Hamamatsu) and n is the number of dynodes, which in the case of the R6358 is 9. If the gain at 1000 V is 3.5 x 10^6, then at 600 V it should be approximately 1.1 x 10^5. Therefore, at the PMT anode there should be ~2.2 x 10^{13} electrons/s. Assuming no losses with the electrical connections and the cables, the current at the voltage divider is 3.5 μA. The resistance of the voltage divider is ~ 1000 Ω, which corresponds to an input voltage to the lock-in amplifier of 3.5 mV. This corresponds well with the ~ 20 mV of signal measured with 50 mW of average power from the Yb-doped fibre amplifier.

References

[1] M. J. Brennan, J. N. Milgram, P. Mascher and H. K. Haugen, "Wavelength tunable ultrashort pulse generation from a passively mode-locked asymmetric-quantum-well semiconductor laser", *Appl. Phys. Lett.*, vol. 81, pp. 2502-2504, 2002.

[2] M. J. Brennan, A. J. Budz, B. J. Robinson, P. Mascher and H. K. Haugen, "Ultrashort Optical Pulse Generation With a Mode-locked Long-Wavelength (1075-1085 nm) InGaAs-GaAs Semiconductor Laser", *IEEE Photon. Technol. Lett.*, vol. 16, pp. 1798-1800, 2004.

[3] M. J. Brennan, J. N. Milgram, A. J. Budz, P. Mascher and H. K. Haugen, "Generation and amplification of wavelength tunable short optical pulses from asymmetric quantum well semiconductor devices", *Conference for Lasers and Electro-Optics*, June 2003, paper #CThM10.

[4] A. J. Budz and H. K. Haugen, "Ultrashort Pulse Amplification at 1080 nm with a Long-Wavelength InGaAs Flared Amplifier", *Submitted Oct. 2005 to IEEE Photon. Technol. Lett.*

[5] A. Piper, A. Malinowski, B.C. Thomson, D. J. Richardson, L. M. B. Hickey, M. N. Zervas, "11.1 W average power 20 ps pulses at 1 GHz repetition rate from a fiber amplified gain switched 1.06 μm Fabry-Perot laser diode", *Conference for Lasers and Electro-Optics,* May 2005, paper #CTuCC3.

[6] J. Limpert, T. Clausnitzer, A. Liem, T. Schreiber, H-J. Fuchs, H. Zellmer, E.-B. Kley and A. Tünnermann, "High-average-power femtosecond fiber chirped-pulse amplification system", *Opt. Lett..*, vol. 28, pp. 1984-1986, 2003.

[7] J. Limpert, T.Schreiber, T. Clausnitzer, K. Zöllner, H-J. Fuchs, E.-B. Kley, H. Zellmer and A. Tünnermann, "High-power femtosecond Yb-doped fiber amplifier", *Opt. Express.*, vol. 10, pp. 628-638, 2002.

[8] P. N. Prasad, *Introduction to Biophotonics* (John Wiley & Sons, Hoboken New Jersey, 2003), section 7.11, pp. 232-234.

[9] S. Hell and H. K. Stelzer, "Fundamental improvement of resolution with a 4Pi-confocal fluorescence microscope using two-photon excitation", *Opt. Commun.*, vol. 93, pp. 277-282, 1992.

[10] J. Chen and K. Midorikawa, "Two-color two-photon 4Pi fluorescence microscopy", *Opt. Lett.*, vol. 29., pp. 1354-1356, 2004.

[11] H. Gugel, J. Bewersdorf, S. Jakobs, J. Engelhardt, R. Storz and S. Hell, "Cooperative 4Pi Excitation and Detection Yields Sevenfold Sharper Optical Sections in Live-Cell Microscopy", *Opt. Lett.*, vol. 87, pp. 4146-4152, 2004.

[12] S. W. Hell, "Toward fluorescence nanoscopy", *Nature*, vol. 21, pp. 1347-1355, 2003.

[13] J. S. Ploem, "Laser Scanning Fluorescence Micrsoscopy", *Appl. Opt.*, vol. 26, pp. 3226-3231, 1987.

[14] P. N. Prasad, *Introduction to Biophotonics* (John Wiley & Sons, Hoboken New Jersey, 2003), section 7.5, pp. 220-221.

[15] G. J. Brakenhoff, P. Blom and P. Barends, "Confocal scanning light microscopy with high aperture immersion lenses", *J. Microsc.*, vol. 117, pp. 219-232, 1979.

[16] M. Minsky, Micrsoscopy Apparatus, United States patent 3013467, Decemeber 19, 1961.

[17] M. D. Egger and M. Petran, "New Reflected Light Microscope for Viewing Unstained and Brain and Ganglion Cells", *Science*, vol. 157, pp. 305-307, 1967.
[18] M. Petran, M Hadravsky, M. Egger and R. Galambos, "Tandem-Scanning Reflected-Light Microscope", *J. Opt. Soc. Am.*, vol. 58, pp. 661-664, 1968.
[19] K. König, "Multiphoton Microscopy in Life Sciences", *J. Microsc.*, vol. 200, pp.83-104, 2000.
[20] P. N. Prasad, *Introduction to Biophotonics* (John Wiley & Sons, Hoboken New Jersey, 2003), section 7.7, pp 221-223.
[21] W. Denk, J. H. Strickler and W.W. Webb, "2-Photon Laser Scanning Fluorescence Microscopy", *Science*, vol. 248, pp. 73-76.
[22] A. Diaspro and C. J. R. Sheppard, *Confocal and Two-Photon Microscopy: Foundations, Applications and Advances* (ed. A. Diaspro) (John Wiley & Sons, New York, 2002), Chpt. 1, Sec. 3.1, pp. 43-47.
[23] R. M Williams, D. W. Piston and W. W. Webb, "Two-photon molecular excitation provides intrinsic 3-dimensional resolution for laser-based microscopy and microphotochemistry", *FASEB J.*, vol. 8, pp. 804-813, 1994.
[24] W. Denk and K. Svoboda, "Photon Upmanship: Why Multiphoton Imaging Is More than a Gimmick", *Neuron*, vol. 18, pp. 351-357, 1997.
[25] C. J. de Grauw, P. L. T. M. Frederix and H. C. Gerritsen, *Confocal and Two-Photon Microscopy: Foundations, Applications and Advances* (ed. A. Diaspro) (John Wiley & Sons, New York, 2002) Chpt. 7, Sec. 1, pp. 153-154.
[26] H. J. Koester, D. Baur, R. Uhl and S. W. Hell, "Ca^{2+} Fluorescence Imaging with Pico- and Femtosecond Two-Photon Excitation: Signal and Photodamage", *Biophys. J.*, vol. 77, pp. 2226-2236, 1999.
[27] V. E. Centonze and J. G. White, "Multiphoton Excitation Provides Optical Sections from Deeper within Scattering Specimens than Confocal Imaging", *Biophys. J.*, vol. 75, pp. 2015-2024, 1998.
[28] P. T. C. So, C. Y. Dong, B. R. Masters and K. M. Berland, "Two-Photon Excitation Fluorescence Microscopy", *Annu. Rev. Biomed. Eng.*, vol. 2, pp. 399-429, 2000.
[29] C. J. de Grauw, P. L. T. M. Frederix and H. C. Gerritsen, *Confocal and Two-Photon Microscopy: Foundations, Applications and Advances* (ed. A. Diaspro) (John Wiley & Sons, New York, 2002) Chpt. 7, Sec. 4, pp. 160-162.
[30] V. Daria, O. Nakamura, C. Palmes-Saloma and S. Kawata, "Enhanced Depth Penetration in Imaging Turbid Biological Samples by Two-Photon Fluorescence Microscopy", *Jpn. J. Appl. Phys*, vol. 37, L959-L961, 1998.
[31] C. J. de Grauw, J. M. Vroom, H. T. M. van der Voort and H. C. Gerritsen, "Imaging properties in two-photon excitation microscopy and effects of refractive index mismatch in thick specimen", *Appl. Opt.*, vol. 38, pp. 5995-6003, 1999.
[32] Y. Sako, A. Sekihata, Y. Yanagisawa, M. Yamamoto, Y. Shimada, K. Ozaki and A. Kusumi, "Comparison of two-photon excitation laser scanning microscopy with UV-confocal laser scanning microscopy in three-dimensional calcium imaging using the fluorescence indicator Indo-1", vol. 185, pp. 9-20, 1997.
[33] K. König, P. T. C. So, W. W. Mantulin and E. Gratton, "Cellular response to near-infrared femtosecond laser pulses in two-photon microscopes", *Opt. Lett.*, vol. 22, pp. 135-136, 1997.

[34] G. J. Brakenhoff, M. Müller and R. I. Ghauharali, "Analysis of efficiency of two-photon versus single-photon absorption for fluorescence generation in biological objects", *J. Microsc.*, vol. 183, pp. 140-144, 1996
[35] A. Hopt and E. Neher, "Highly Nonlinear Photodamage in Two-Photon Fluorescence Microscopy", *Biophys. J.*, vol. 80, 2029-2036, 2001.
[36] P. S. Dittrich, P. Schwille, "Photobleaching and stabilization of fluorophores used for single-molecule analysis with one- and two-photon excitation", *Appl. Phys. B*, vol. 73, pp. 829-837, 2001.
[37] S. W. Hell, K. Bahlmann, M. Schrader, A. Soini, H. Malak, I. Gryczynski and J. R. Lakowicz, "Three-Photon Excitation In Fluorescence Microscopy", *J. Biomed. Opt.*, vol. 1, pp. 71-74, 1996.
[38] S. Maiti, J. B. Shear, R. M. Williams, W. R. Zipfel, W. W. Webb, "Measuring Serotonin Distribution in Live Cells with Three-Photon Excitation", *Science*, vol. 275, pp. 530-532, 1997.
[39] J. R. Lakowicz, I. Gryczynski, H. Malak, M. Schrader, P. Engelhardt, H. Kano and S. W. Hell, "Time-Resolved Fluorescence Spectroscopy and Imaging of DNA Labeled with DAPI and Hoechst 33342 Using Three-Photon Excitation", *Biophys. J.*, vol. 72, pp. 567-578, 1997.
[40] M. Gu, "Resolution in three-photon fluorescence scanning microscopy", *Opt. Lett.*, vol. 21, pp. 988-990, 1996.
[41] C. Xu, *Confocal and Two-Photon Microscopy: Foundations, Application and Advances* (ed. A. Diaspro) (John Wiley & Sons, New York, 2002) Chpt. 4, Sec. 2, pp. 76-77.
[42] C. Xu, *Confocal and Two-Photon Microscopy: Foundations, Application and Advances* (ed. A. Diaspro) (John Wiley & Sons, New York, 2002) Chpt. 4, Sec. 8, pp. 96-97.
[43] O. Nakamura, "Fundamental of two-photon microscopy", *Micros. Res. Tech.*, vol. 47, pp. 165-171, 1999.
[44] A. Esposito, F. Federici, C. Usai, F. Cannone, G. Chirico, M. Collini and A. Diaspro, "Notes on Theory and Experimental Conditions Behind Two-Photon Excitation Microscopy", *Micros. Res. Tech.*, vol. 63, pp. 12-17, 2004.
[45] M. Göppert-Mayer, "Über Elementarakte mit zwei Quantensprügen", *Annln. Phys.*, vol. 9, pp. 273-295, 1930.
[46] W. Kaiser and C. G. B. Garrett, "Two-photon excitation in $CaF_2:Eu^{2+}$", *Phys. Rev. Lett.*, vol. 7, pp. 229-231, 1961.
[47] C. Xu, *Confocal and Two-Photon Microscopy: Foundations, Applications and Advances* (ed. A. Diaspro) (John Wiley & Sons, New York, 2002) Chpt. 4, Sec. 1, pp. 75-76.
[48] G. A. Blab, P. H. M. Lommerse, L. Cognet, G. S. Harms and T. Schmidt, "Two-photon excitation action cross-sections of the autofluorescent proteins", *Chem. Phys. Lett.*, vol. 350, pp. 71-77, 2001.
[49] C. Xu and W. W. Webb, "Measurement of two-photon excitation cross sections of molecular fluorophores with data from 690 to 1050 nm", *J. Opt. Soc. Am. B*, vol.13, pp. 481-491, 1996.
[50] M. A. Albota, C. Xu and W. W. Webb, "Two-photon fluorescence excitation cross sections of biomolecular probes from 690 to 960 nm", *Appl. Opt.*, vol. 37, pp. 7352-7356, 1998.

[51] M. Drobizhev, Y. Stepanenko, Y. Dzenis, A. Karotki, A. Rebane, P. Taylor and H. Anderson, "Extremely Strong Near-IR Two-Photon Absorption in Conjugated Porphyrin Dimers: Quantitative Description with Three-Essential-States Model", *J. Phys. Chem. B*, vol. 109, pp. 7223-7236, 2005.
[52] M. Drobizhev, A. Karotki, A. Rebane and C. W. Spangler, "Dendrimer molecules with record large two-photon absorption cross section", *Opt. Lett.*, vol. 26, pp. 1081-1083, 2001.
[53] T. Ha, T. A. Laurence, D. S. Chemla and S. Weiss, "Polarization Spectroscopy of Single Fluorescent Molecules", *J. Phys. Chem. B*, vol. 103, pp. 6839-6850, 1999.
[54] J. R. Lakowicz, I. Gryczynski, Z. Gryczynski and E. Danielsen, "Time-Resolved Fluorescence Intensity and Anisotropy Decays of 2,5-Diphenyloxazole by Two-Photon Excitation and Frequency-Domain Fluorometry", *J. Phys. Chem.*, vol. 96, pp. 3000-3006, 1992.
[55] X. Michalet, A. N. Kapanidis, T. Laurence, F. Pinaud, S. Doose, M. Pflughoefft and S. Weiss, "The Power and Prospects of Fluorescence Microscopies and Spectroscopies", *Annu. Rev. Biophys. Biomol. Struct.*, vol. 32, pp. 161-182, 2003.
[56] D. Magde, G. E. Rojas and P. G. Seybold, "Solvent Dependence of the Fluorescence Lifetimes of Xanthene Dyes, *Photochem. Photobiol.*, vol. 70, pp. 737-744, 1999.
[57] K. König, T. W. Becker, P. Fischer, I. Riemann and K.-J. Halbhuber, "Pulse-length dependence of cellular response to intense near-infrared laser pulses in multiphoton microscopes", *Opt. Lett.*, vol. 24, pp. 113-115, 1999.
[58] J. E. Jonkman, E. H. K. Stelzer, *Confocal and Two-Photon Microscopy: Foundations, Applications and Advances* (ed. A. Diaspro) (John Wiley & Sons, New York, 2002), Chpt. 5, Sec. 2, pp. 101-107.
[59] M. Born and E. Wolf, *Principles of Optics*, (Pergamon of Canada Ltd., Toronto, 1970), Sec. 8.8, pp. 435-449.
[60] M.Gu and C. J. R. Sheppard, "Comparison of three-dimensional imaging properties between two-photon and single-photon fluorescence microscopy", *J. Microsc.*, vol. 177, pp. 128-137, 1995.
[61] J. E. Jonkman, E. H. K. Stelzer, *Confocal and Two-Photon Microscopy: Foundations, Application and Advance* (ed. A. Diaspro) (John Wiley & Sons, New York, 2002), Chpt. 5, Sec. 4, pp. 112-115.
[62] X. S. Gan and M. Gu, "Fluorescence microscopic imaging through tissue-like turbid media", *J. App. Phys.*, vol. 87, pp. 3214-3221, 2000.
[63] R. Gauderon, P. B. Lukins and C. J. R. Sheppard, "Effect of a Confocal Pinhole in Two-Photon Microscopy", *Microsc. Res. Tech.*, vol. 47, pp. 210-214, 1999.
[64] R. Gauderon and C. J. R. Sheppard, "Effect on a finite-size pinhole on noise performance in single-, two-, and three-photon confocal fluorescence microscopy", *App. Opt.*, vol. 38, pp. 3562-3565, 1999.
[65] M. Gu and C. J. R. Sheppard, "Effects of a finite-sized pinhole on 3D image formation in confocal two-photon fluorescence microscopy", *J. Mod. Opt.*, vol. 40, pp. 2009-2024, 1993.
[66] P. J. Delfyett, L. T. Florez, N. Stoffel, T. Gmitter, N. C. Andreadakis, Y. Silberberg, J. P. Heritage and G. A. Alphonse, "High –Power Ultrafast Laser Diodes", *IEEE J. Quant. Electron.*, vol. 28, pp. 2203-2219, 1992.

[67] P. P. Vasil'ev, *Ultrafast Diode Laser: Fundamentals and Applications* (Artech House, Boston, 1995), Sec. 4, pp. 95-96.
[68] B. J. Thedrez, S. E. Saddow, Y. Q. Liu, C. Wood, R. Wilson and C. H. Lee, "Experimental and Theoretical Investigation of Large Output Power Q-Switched AlGaAs Semiconductor Lasers", *IEEE Photon. Technol. Lett.*, vol. 5, pp. 19-22, 1993.
[69] P. P. Vasil'ev, *Ultrafast Diode Laser: Fundamentals and Applications* (Artech House, Boston, 1995), Sec. 4.1.1, pp. 97-100.
[70] P. P. Vasil'ev, *Ultrafast Diode Laser: Fundamentals and Applications* (Artech House, Boston, 1995), Sec. 4.7, pp. 143.
[71] M. J. Brennan, "Broadly Tunable Ultrashort pulse Generation with Mode-locked Semiconductor Lasers", Ph.D. thesis, McMaster University, 2004.
[72] P.Sewell, M. Reed, T. M. Benson and P. C. Kendall, "Full Vector Analysis of Two-Dimensional Angled and Coated Optical Waveguide Facets", *IEEE J. Quantum Electron.*, vol. 33, pp. 2311-2318, 1997.
[73] M. Schell., A. G. Weber, E. Scholl and D. Bimberg, "Fundamental limits of sub-ps pulse generation by active mode-locking of semiconductor lasers: the spectral gain width and the facet reflectivities", *IEEE J. Quantum Electron.*, vol. 27, pp. 1661-1668, 1991.
[74] G. Bendelli, K. Komori, and S. Arai, "Gain saturation and propagation characteristics of index-guided tapered-waveguide traveling-wave semiconductor laser amplifiers (TTW-SLA's)," *IEEE J. Quantum Electron.*, vol. 28, pp. 447-458, Feb. 1992.
[75] H. Ghafouri-Shiraz, P. W. Tan, and T. Aruga, "Picosecond pulse amplification in tapered-waveguide laser-diode amplifiers," *IEEE J. Select. Topics Quantum Electron.*, vol. 3, pp. 210-217, Apr. 1997.
[76] H. M. Pask, R. J. Carman, D. C. Hanna, A. C. Tropper, C. J. Mackechnie, P. R. Barber and J. M. Dawes, "Ytterbium-Doped Silica Fiber Lasers: Versatile Sources for the 1-1.2 μm Region", *IEEE J. Select. Topics Quantum Electron.*, vol. 1, pp. 2-13, 1995.
[77] R. Paschotta, J. Nilsson, A. C. Tropper and D. C. Hanna, "Ytterbium-Doped Fiber Amplifiers", *IEEE J. Quantum Electron.*, vol. 33, pp. 1049-1056, 1997.
[78] J. Limpert, S. Höffer, A. Liem, H. Zellmer, A. Tünnermann, S. Knoke and H. Voelckel, "100-W average power, high energy nanosecond fiber amplifier", *Apl. Phys. B*, vol. 75, pp. 477-479, 2002.
[79] J. P. Koplow, L. Goldberg and D. A. V. Kliner, "Compact 1-W Yb-Doped Double-Cladding Fiber Amplifier Using V-Groove Side-Pumping", *IEEE Photon. Technol. Lett.*, vol. 10, pp. 793-795, 1998.
[80] W. R. Rapoport and C. P. Khattak, "Titanium sapphire laser characteristics", *Appl. Opt.*, vol. 27, pp. 2677-2684, 1988.
[81] I. T. McKinnie, A. L. Oien, D. M. Warrington, P. N. Tonga, L. A. W. Gloster and T. A. King, "Ti^{3+} Ion Concentration and Ti:Sapphire Laser Performance", *IEEE J. Quantum Electron.*, vol. 33, pp. 1221-1230, 1997.
[82] P. F. Moulton, "Spectroscopic and laser characteristics of Ti:Al_2O_3", *J. Opt. Soc. Am. B*, vol. 3, pp. 125-133, 1986.
[83] J. D. Kafka, M. L. Watts and J-W. J. Pieterse, "Picosecond and Femtosecond Pulse Generation in a Regeneratively Mode-Locked Ti:Sapphire Laser", *IEEE J. Quantum. Electron.*, vol. 28, pp. 2151-2162, 1992.

[84] A. Mar, R. Helkey, J. Bowers, D. Mehuys and D. Welch, "Mode-locked Operation of a Master Oscillator Power Amplifier", *IEEE Photon. Technol. Lett.*, vol. 6, pp. 1067-1069, 1994.

[85] P. P. Vasil'ev, *Ultrafast Diode Laser: Fundamentals and Applications* (Artech House, Boston, 1995), Sec. 2.3, pp. 39-50.

[86] M. W. Sasnett, *The Physics and Technology of Laser Resonators* (ed. D. R. Hall and P. E. Jackson) (IOP Publishing, Bristol, 1992), Chpt. 9, pp. 132-142.

[87] Private Communication from E. Yarbrough: Sales Development Engineer, Spectra-Physics.

[88] H. Sun, "Thin lens equation for a real laser beam with weak lens aperture truncation", *Opt. Eng.*, vol. 37, pp. 2906-2913, 1998.

[89] S. A. Self, "Focusing of spherical Gaussian beams", *Appl. Opt.*, vol. 22, pp. 658-661, 1983.

[90] H. Urey, "Spot size, depth-of-focus, and diffraction ring intensity formulas for truncated Gaussian beams", *Appl. Opt.*, vol. 43, pp. 620-625, 2004.

[91] J-C. Diels and W. Rudolph, *Ultrashort Laser Pulse Phenomena* (Academic Press, San Diego, 1996), Sec. 2.5.1, pp. 59-62.

[92] Light Path Technologies: Aspheric Lenses, <http://www.lightpath.com/PDF%20Files/Aspheric%20Lenses.pdf>, 2005.

[93] J-C. Diels and W. Rudolph, *Ultrashort Laser Pulse Phenomena* (Academic Press, San Diego, 1996), Sec. 2.2, pp. 43-50.

[94] G. Pretzler, A. Kasper and K. J. Witte, "Angular chirp and tilted light pulses in CPA lasers", *Appl. Phys. B.*, vol. 70, pp. 1-9, 2000.

[95] P. W. Milonni and J. H Eberly, *Lasers* (John Wiley & Sons, Toronto, 1998), Sec. 24.8, pp. 502-508.

[96] C-L. Chen, *Elements of Optoelectronics & Fiber Optics* (Irwin, Toronto, 1996), Sec. 2.6, pp. 61-64.

[97] J. B. Ashcom, "The role of focusing in the interaction of femtosecond laser pulses with transparent materials", Ph.D. thesis, Harvard University, 2003.

[98] C. J. de Grauw, P. L. T. M. Frederix and H. C. Gerritsen, *Confocal and Two-Photon Microscopy: Foundations, Applications and Advances* (ed. A. Diaspro) (John Wiley & Sons, New York, 2002) Chpt. 7, Sec. 3, pp. 155-157.

[99] H. Jacobsen, P. Hänninen, E. Soini and S. W. Hell, "Refractive-index-induced aberrations in two-photon confocal fluorescence microscopy", *J. Microsc.*, vol. 176, pp. 226-230, 1994.

[100] S. Hell, G. Reiner, C. Cremer and E. H. K. Stelzer, "Aberrations in confocal fluorescence microscopy induced by mismatches in refractive index", *J. Microsc.*, vol. 169, pp. 391-405, 1993.

[101] Z. Wang, B. Mikkelson, B. Pedersen, K. E. Stubkjaer and D. S. Olesen, "Coupling Between Angled-Facet Amplifiers and Tapered Lens-Ended Fibers", *J. Lightwave. Technol.*, vol. 9, pp. 49-55, 1991.

[102] R. Kapoor, C. S. Friend and A. Patra, "Two-photon-excited absolute emission cross-sectional measurements calibrated with a luminance meter", *J. Opt. Soc. Am. B*, vol. 20, pp. 1550-1554.

[103] P. Kaatz, D. P. Shelton, "Two-photon fluorescence cross-section measurement calibrated with hyper-Rayleigh scattering", *J. Opt. Soc. Am. B*, vol. 16, pp. 998-1006.

[104] E. B. Treacy, "Optical Pulse Compression with Diffraction Gratings", *IEEE J. Quantum Electron.*, vol. QE-5, pp. 454-458, 1969.
[105] R. L. Fork, O. E. Martinez and J. P. Gordon, "Negative dispersion using pairs of prisms", *Opt. Lett.*, vol. 9, pp. 150-152, 1984.
[106] S. Arahira, S. Kutsuzawa, Y. Matsui and Y. Ogawa, "Higher Order Chirp Compensation of Femtosecond Mode-Locked Semiconductor Lasers Using Optical Fibers with Different Group-Velocity Dispersions", *IEEE Sel. Top. Quantum Electron.*, vol. 2, pp. 480-486, 1996.
[107] K. Kim, S. Lee and P. J. Delfyett, "1.4kW high peak power generation from an all semiconductor mode-locked master oscillator power amplifier system based on eXtreme Chirped Pulse Amplification(X-CPA)", *Opt. Express*, vol. 13, pp. 4600-4606, 2005.
[108] R. L. Fork, C. H. Brito Cruz, P. C. Becker and C. V. Shank, "Compression of optical pulses to six femtoseconds by using cubic phase compensation", *Opt. Lett.*, vol. 12, pp. 483-485, 1987.
[109] P. E. Hänninen, M. Schrader, E. Soini and S. W. Hell, "Two-photon excitation fluorescence microscopy using a semiconductor laser", *Bioimaging*, vol. 3, pp. 70-75, 1995.
[110] Private Communication from A. Budz: Department of Engineering Physics, McMaster University.
[111] S. Gee, G. Alphonse, J. Connolly and P. J. Delfyett, "High-Power Mode-Locked External Cavity Semiconductor Laser Using Inverse Bow-Tie Semiconductor Optical Amplifier", *IEEE J. Sel. Top. Quantum Electron.*, vol. 4, pp. 209-215, 1998.
[112] J. A. R. Williams, I. Bennion, K. Sugden and N. J. Doran, "Fibre dispersion compensation using a chirped in-fibre Bragg grating", *Electron. Lett.*, vol. 30, pp. 985-987, 1994.
[113] E. Zeek, K. Maginnis, S. Backus, U. Russek, M. Murnane, G. Mourou, H. Kapteyn and G. Vdovin, "Pulse compression by use of deformable mirrors", *Opt. Lett.*, vol. 24, pp. 493-495, 1999.
[114] P. Wnuk, C. Radzewicz and J. S. Krasinski, "Bimorph piezo deformable mirror for femtosecond pulse shaping", *Opt. Express*, vol. 13, pp. 4154-4159, 2005.
[115] J. Yu, M. Schell, M. Schulze and D. Bimberg, "Generation of 290 fs pulses at 1.3 μm by hybrid mode-locking of a semiconductor laser and optimization of the time bandwidth product", *Appl. Phys. Lett.*, vol. 65, pp. 2395-2397, 1994.
[116] P. J. Delfyett, L. Florez, N. Stoffel, T. Gmitter, N. Andreadakis, G. Alphonse and W. Ceislik, "200-fs optical pulse generation and intracavity pulse evolution in a hybrid mode-locked semiconductor diode-laser/amplifier system", *Opt. Lett.*, vol. 17, pp. 670-672, 1992.
[117] S. Gee, G. A. Alphonse, J. C. Connolly, C. Barty and P. J. Delfyett, "Ultrashort Pulse Generation by Intracavity Spectral Shaping and Phase Compensation of External-Cavity Modelocked Semiconductor Lasers", *IEEE J. Quantum Electron.*, vol. 36, pp. 1035-1040, 2000.
[118] D. J. Derickson, R. J. Helkey, A. Mar, J. R. Karin, J. G. Wasserbauer and J. E. Bowers, "Short Pulse Generation Using Multisegment Mode-Locked Semiconductor Lasers", *IEEE J. Quantum Electron.*, vol. 28, pp. 2186-2202.

[119] C. T. A. Brown, M. A. Cataluna, A. A. Lagatsky, E. U. Rafailov, M. B. Agate, C. G. Leburn and W. Sibbett, "Compact laser-diode-based femtosecond sources" *New J. Phys.*, vol. 6, pp. 175, 2004.

[120] J. C. Livas, S. R. Chinn, E. S. Kintzer, J. N. Walpole, C. A. Wang and L. J. Missaggia, " Single-Mode Optical Fiber Coupling of High-Power Tapered Gain Region Devices", *IEEE Photon. Technol. Lett.*, vol. 6, pp. 422-424, 1994.

[121] D. Voigt, E. C. Schilder, R. J. C. Spreeuw and H. B. van Linden van den Heuvell, "Characterization of a high-powered semiconductor amplifier system", vol. 72, pp. 279-284, 2001.

[122] F. L. Pedrotti and L. S. Pedrotti, *Introduction to Optics* (Prentice Hall, Upper Saddle River, New Jersey, 1993), Sec. 25-1, pp. 523-535.

[123] P. J. Delfyett, C-H. Lee, I. T. Florez, N. G. Stoffel, T. J. Gmitter, N. C. Andreadakis, G. A. Alphonse and J. C. Connolly, "Generation of subpicosecond high-power optical pulses from a hybrid mode-locked semiconductor laser", *Opt. Lett.*, vol. 15, pp. 1371-1373, 1990.

[124] S. Gee, G. Alphonse, J. Connolly and P. J. Delfyett, "High-Power Mode-Locked External Cavity Semiconductor Laser Using Inverse Bow-Tie Semiconductor Optical Amplifiers", *IEEE Sel. Top. Quantum Electron.*, vol. 4, pp. 209-215, 1998.

[125] B. Resan, L. Archundia and P. Delfyett, "FROG Measured High-Power 185-fs Pulses Generated by Down-Chirping of the Dispersion-Managed Breathing-Mode Semiconductor Mode-Locked Laser", *IEEE Photon. Technol. Lett.*, vol. 17, pp. 1384-1386, 2005.

[126] W-H Xiang, S. R. Friberg, K. Watanabe, S. Machida, W. Jiang, H. Iwamura and Y. Yamamoto, "Femtosecond external-cavity surface-emitting InGaAs/InP multiple quantum-well laser", *Opt. Lett.*, vol. 16, pp. 1394-1396, 1991.

[127] P. N. Prasad, *Introduction to Biophotonics* (John Wiley & Sons, Hoboken New Jersey, 2003), section 4.3, pp 99-102.

[128] R. Paschotta, J. Nilsson, P. R. Barber, J. E. Caplen, A. C. Tropper and D. C. Hanna, "Lifetime quenching in Yb-doped fibres", *Opt. Commun.*, vol. 136, pp. 375-378, 1997.

[129] M. Dülk, M. Döbeli and H. Melchior, "Fabrication of Saturable Absorbers in InGaAsP-InP Bulk Semiconductor Laser Diodes by Heavy Ion Implantation", *IEEE J. Sel. Top. Quantum Electron.*, vol. 7, pp. 124-134, 2001.

[130] D. Nickel, A. Liem, J. Limpert, H. Zellmer, U. Griebner, S. Unger, G. Korn and A. Tünnermann, "Fiber baser high repetition rate, high energy laser source applying chirped pulse amplification", *Opt. Commun.*, vol. 190, pp. 309-315, 2001.

[131] O. G. Okhotnikoz, L. Gomes, N. Xiang, T. Jouhti and A. B. Grudinin, "Mode-locked ytterbium fiber laser tunable in the 980-1070-nm spectral range", *Opt. Lett.*, vol. 28, pp. 1522-1524.

[132] B. Ortaç, A. Hideur, T. Chartier, M. Brunel, C. Özkul and F. Sanchez, "90-fs stretched-pulse ytterbium-doped double-clad fiber laser", *Opt. Lett.*, vol. 28, pp. 1305-1307, 2003.

[133] F. Ö, Ilday, J. R. Buckley, H. Lim, F. W. Wise and W. G. Clark, "Generation of 50-fs, 5 nJ pulses at 1.03 μm from a wave-breaking-free fiber laser", *Opt. Lett.*, vol. 28. pp. 1365-1367, 2003.

[134] F. Ö, Ilday, J. R. Buckley, L. Kuznetsova and F. W. Wise, "Generation of 36-femtosecond pulses from a ytterbium fiber laser", *Opt. Express*, vol. 11, pp. 3550-3554, 2003.

[135] L. Goldberg, J. P. Koplow and D. A. V. Kliner, "Highly efficient 4-W Yb-doped fiber amplifier pumped by a broad-stripe laser diode", *Opt. Lett.*, vol. 24, pp. 673-675, 1999.

[136] T. Schreiber, J. Limpert, H. Zellmer, A. Tünnermann and K. P. Hansen, "High average power supercontinuum generation in photonic crystal fibers", *Opt. Comm.*, vol. 228, pp. 71-78, 2003.

[137] T. A. Birks, W. J. Wadsworth and P. St. J. Russel, "Supercontinuum generation in tapered fibers", *Opt. Lett.*, vol. 25, pp. 1415-1417, 2000.

[138] G. I. Petrov, V. V. Yakovlev and N. I. Minkovski, "Near-infrared continuum generation of femtosecond and picosecond pulses in doped optical fibers", *Appl. Phys. B*, vol. 77, pp. 219-225, 2003.

[139] D. L. Marks, A. L. Oldenburg, J. J. Reynolds and S. A. Boppart, "Study of ultrahigh-numerical-aperture fiber continuum generation source for optical coherence tomography", *Opt. Lett.*, vol. 27, pp. 2010-2012, 2002.

[140] S. V. Chernikov, Y. Zhu, J. R. Taylor and V. P. Gabontsev, "Supercontinuum self-*Q*-switched ytterbium fiber laser", *Opt. Lett.*, vol. 22, pp. 298-300, 1997.

[141] M. Rusu, A. B. Grudinin and O. G. Okhotnikov, "Slicing the supercontinuum radiation generated in photonic crystal fiber using an all-fiber chirped-pulse amplification system", *Opt. Express*, vol. 13, pp. 6390-6400, 2005.

[142] Z. Chen, D. L. Kaplan, K. Yang, J. Kumar, K. A. Marx and S. K Tripathy, "Two-photon-induced fluorescence from the phycoerythrin protein", *Appl. Opt*, vol. 36, pp. 1655-1659.

[143] M. B. Schneider, W. W. Webb, "Measurement of submicron laser beam radii", *Appl. Opt.*, vol. 20, pp. 1382-1388, 1981.

[144] H. Wang, Z. Li, P. Shao, Y. Liang, H. Wang, J. Qin and Q. Gong, "Synthesis and properties of new two-photon absorption chromophores containing 3,5-dicyano-2,4,6-tristyrylpyridine as the core", *New J. Chem.*, vol. 29, pp. 792-797, 2005.

3966 12